

Ligand-Functionalized Adsorbents for the Extraction and Recovery of Rare Earth Elements

Submitted in partial fulfillment of the requirements for
the degree of

**Doctor of Philosophy
in
Civil and Environmental Engineering**

Jonathan C. Callura

B.S., Environmental Engineering, Georgia Institute of Technology
M.S., Environmental Engineering, Georgia Institute of Technology

Carnegie Mellon University
Pittsburgh, PA

December 2018

© Jonathan C. Callura, 2018

All Rights Reserved

Acknowledgements

This work was initiated with funding provided by the U.S. Department of Energy Office of Energy Efficiency and Renewable Energy under contract DE-EE0006749. Further financial support was provided by National Science Foundation Integrative Graduate Education and Research Traineeship in Nanotechnology-Environmental Effects and Policy (IGERT NEEP) fellowship program (DGE0966227) and a CMU College of Engineering Dean's Fellowship. Any opinions, findings, conclusions, or recommendations expressed in this material are those of the authors and do not necessarily reflect the views of the NSF. The CMU Department of Civil and Environmental Engineering also supported this research via the discretionary funds of Dr. Athanasios Karamalidis and the Hamerschlag University Professor chair.

I am incredibly thankful for the guidance and support of my advisors, Dr. Athanasios Karamalidis and Dr. David Dzombak, who have been a pleasure to work with for the past three years. Thanasis and Dave have been instrumental to the progress of my research and have constantly challenged me to think about questions from new perspectives, while not losing sight of the big picture. I would also like to thank Dr. Gregory Lowry and Dr. Newell Washburn for serving on my thesis committee and providing valuable input which helped to shape this project.

Carnegie Mellon provides a unique environment where intellectual curiosity and ambition are abundant. I have been fortunate to spend time with some extremely intelligent and motivated individuals during my time here. Many people have passed through the 207C offices and CEE labs and I am grateful to each of them: Astrid Avellan, Tim Bartholomew, Alex Bertuccio, Garret Bland, Adam Cadwallader, Nizette Consolazio, Erin Dauson, Will Gao, Stephanie Laughton, Eric McGivney, Joe Moore, Sneha Shanbhag, Eleanor Spielman-Sun, Jiang Xu, Yilin Zhang, and several others that I do not have the space to list individually. I am especially thankful for the help

and patience of Clint Noack, who answered my countless questions about the nuances of research and the R programming language. I would also like to thank colleagues and collaborators who have helped me along the way. John Baltrus (US DOE National Energy Technology Laboratory), Kedar Perkins (CMU Department of Chemistry), and Qingyang Shi (CMU Department of Civil and Environmental Engineering) have each provided valuable contributions to make this project possible.

The CEE faculty and staff have been immensely helpful throughout my candidacy. Ron Ripper, the CEE Laboratory Director, is essential to the continued operation of the CEE labs. Through freezing pipes and flooding offices (multiple times), he has been a constant resource for the many graduate students who rely on him. Maxine Leffard, the CEE Graduate Program Director, is another indispensable member of the CEE department and has been there to make sure that all the correct boxes are checked from start to finish.

Finally, I would like to express my enormous gratitude to my family. My parents (Kathi and Chuck (and Lynn)), siblings (Chris and Nicole), and nephews (Bennett, Connor, and Myles) may be 700 miles away, but they have been in my thoughts every day. My fiancée, Louise McMahon (soon to be Callura), has been so unbelievably supportive of me since the day we met. She deserves an honorary degree for all that she has done to help me, not just over the past three years that we spent in Pittsburgh, but for the entirety of our seven years together. Louise, I look forward to building a life full of love and adventure with you.

Abstract

Rare earth elements (REE) are central components of many developing technologies, but uncertainties surrounding their supply chain have led to concerns about their long-term availability. Recent research has identified new potential sources of REE, including brines and other saline waters, that are abundant though contain high concentrations of other, less valuable, metals which are prohibitively difficult to separate using currently available methods. The development of new, more selective methods for REE recovery from complex aqueous mixtures represents a significant technical challenge and a large potential opportunity to close the growing supply/demand gap for critical materials.

The overall goal of this research was to develop ligand-functionalized adsorbents and evaluate their potential as a method for REE extraction from saline waters. This was accomplished through the following research objectives: **(1)** Investigate adsorption of REE onto functionalized model supports; **(2)** Characterize large-scale functionalized polymer resins and evaluate their REE binding mechanisms; and **(3)** Determine selectivity and study fixed-bed column performance of functionalized adsorbents.

The research related to Objective 1 addressed critical research gaps by studying the performance of silica adsorbents functionalized with three ligands – diethylenetriaminepentaacetic dianhydride (DTPADA) phosphonoacetic acid (PAA), *N,N*-bis(phosphonomethyl)glycine (BPG) – in a range of application-relevant conditions. Attachment of ligands to the surfaces was completed by connection to surface amines using either a ‘Bottom-Up’ (BU-) or ‘Top-Down’ (TD-) approach. ‘Bottom-Up’ materials were synthesized by attaching ligands to pre-silanized silica surfaces, while ‘Top-Down’ materials were made by first combining ligands with aminosilane groups and then attaching the ligand-silane structures to raw silica surfaces. Amine conversion efficiencies were

9-28% for the standard 'Bottom-Up' synthesis method, yielding ligand concentrations of 0.268 mmol/g (BU-DTPADA), 0.15 mmol/g (PAA), and 0.086 mmol/g (BPG). The 'Top-Down' approach yielded improved ligand attachment of 0.463 mmol/g (TD-DTPADA) and better performance in general for the DTPADA ligand. Optimal pH conditions for REE uptake in brine solutions were found for DTPADA- (pH 2.5), PAA- (pH 7), and BPG-functionalized silica (pH 1-3 or >5). The REE adsorption performance of the functionalized adsorbents was largely unimpeded by the presence of competing ions (Ca, Mg, Zn, Fe, Al). Tests with real brines (I ~ 3 M) showed >90% efficiency in REE recovery, which improved at higher temperatures (up to 100 °C). Effective elution of REE was accomplished with 0.7 N HNO₃, and performance of the adsorbents improved with additional usage cycles. The improved performance for cycles two and three was attributed to the washing away of physically deposited ligands (i.e., non-covalently bound) left over from the functionalization process.

This work was advanced by using the same 'Bottom-Up' synthesis method to generate new, large-scale functionalized polymer resins in work performed in relation to Objective 2. Large-scale functionalized adsorbents allow the use of continuous-flow extraction processes, such as fixed-bed adsorption columns. Before continuous-flow systems can be designed, it is necessary to study their properties and performance in batch conditions to gain insight into their adsorption capabilities. Polymeric resin beads, composed of polystyrene-divinylbenzene copolymers containing primary amine surface groups, were functionalized with DTPADA, PAA, and BPG. Their physical and chemical properties (surface area, pore volumes, ligand concentrations, and acidity constants) were investigated, and the REE binding mechanisms were probed using batch experiments and complexation models. Amine concentrations were measured on the non-functionalized supports (4.0 mmol/g) and ligand grafting efficiencies were found for DTPADA- (0.42 mmol/g; 11% amine conversion), PAA- (0.33 mmol/g; 8% amine conversion), and BPG-functionalized resins (0.22 mmol/g; 6% amine conversion). Kinetic studies revealed that the

functionalized resins generally followed pseudo-second order binding kinetics with intraparticle diffusion serving as a rate-limiting step. Capacity estimates for total REE adsorption based on Langmuir q_{Max} were found to be 0.12 mg/g (amine), 0.72 mg/g (PAA), 3.0 mg/g (BPG), and 2.9 mg/g (DTPADA). Addition of ligands to the resin surfaces greatly improved REE adsorption in all cases. Adsorption isotherm results suggest that the observed REE uptake above Langmuir q_{Max} values may be the result of non-selective multilayer physisorption by other chemical groups on the resin surfaces rather than selective chelation by surface-tethered ligands.

The gap between research and practical application was bridged through the research under Objective 3. This portion of the project included the evaluation of resin selectivity and systematic study of mass transport properties in a fixed-bed column system, while determining the parameters required to design and scale up systems. Separation factors were determined for BPG-functionalized large-scale polymer resin beads and non-functionalized aminated resins by conducting multi-element competitive adsorption isotherm experiments, and the BPG-functionalized resins were found to be highly selective for REE, with separation factors for REE over other metals as much as 700 times higher than the non-functionalized aminated resins. Resin performance was measured in fixed-bed adsorption columns and the breakthrough of REE from the column packed with BPG-functionalized resins was influenced by influent concentration and flow rate. Mass transfer zones in the columns were 95% shorter and moved 13% faster with influent REE concentrations of 10 mg/L compared to 0.1 mg/L, leading to more rapid column exhaustion at higher concentrations. The influence of column geometry on REE breakthrough was studied and superficial fluid velocities of 0.4 m/hour were found to be suitable for operation. Reusability of the BPG-functionalized resins was studied through batch and column elution and reuse tests, and performance was found to improve after the first 1-2 cycles and remained stable thereafter. Ligand concentrations were measured on the BPG-functionalized resins and were found to be stable for at least six use cycles after an initial HNO_3 wash.

The data and interpretations offered in this thesis have advanced the understanding of performance characteristics and surface properties of ligand-functionalized adsorbents for REE extraction from saline waters. The materials described and studied in this work have potential for scalable resource recovery schemes due to their selectivity and improved REE binding capacity compared to conventional materials. Outcomes from this research will help advance the development of adsorption systems tailored to a variety of potential feedstocks which allow the recycling and recovery of valuable REE components.

Table of Contents

Acknowledgements	i
Abstract	iii
Table of Contents	vii
List of Tables	x
List of Figures	xii
CHAPTER 1: Introduction	1
1.1. Rare Earth Elements (REE).....	2
1.1.1. REE and their Sources	2
1.1.2. Alternative REE Feedstocks	3
1.1.3. Conventional REE Extraction and Purification Processes	3
1.1.4. Novel Approaches to REE Extraction	4
1.1.5. Opportunity for Targeted SPE with REE-Selective Adsorbents	5
1.2. Research Goals.....	6
1.2.1. Functionalized Model Supports.....	6
1.2.2. Large-Scale Functionalized Polymer Resins	7
1.2.3. Selectivity and Fixed-Bed Column Application of Functionalized Polymer Resins.	7
1.3. Thesis Organization	7
CHAPTER 2: Selective Adsorption of Rare Earth Elements onto Functionalized Silica Particles	9
2.1. Introduction	10
2.2. Materials and Methods	10
2.2.1. Chemicals.....	10
2.2.2. Analytical Instrumentation.....	12
2.2.3. Functionalization and Characterization	12
2.2.4. REE Adsorption Experiments	14
2.2.4.1. Batch Equilibrium Adsorption Experiments.....	14
2.2.4.2. Competitive Adsorption Experiments	15
2.2.4.3. Adsorbent Elution and Reuse Studies.....	16
2.3. Results and Discussion	17
2.3.1. Batch Adsorption Experiments with Synthetic Brine.....	17
2.3.2. Batch Adsorption Experiments with Great Salt Lake (GSL) Brine	23
2.3.3. Adsorbent Elution and Reuse	27

2.4. Summary and Conclusions.....	30
CHAPTER 3: Adsorption Kinetics, Thermodynamics, and Isotherm Studies for Functionalized Lanthanide Chelating Resins	32
3.1. Introduction	33
3.2. Materials and Methods	33
3.2.1. Functionalization.....	33
3.2.2. Characterization	35
3.2.2.1. XPS for Quantification of Ligand Loadings.....	35
3.2.2.2. BET for Determination of Specific Surface Area.....	35
3.2.2.3. Adsorbent Titrations for Acid/Base Characteristics.....	36
3.2.3. REE Adsorption Experiments	36
3.2.4. Modeling of REE Complexation by Solution-Phase Ligands	37
3.3. Results and Discussion	38
3.3.1. Characterization	38
3.3.1.1. Ligand Loading and Specific Surface Area.....	38
3.3.1.2. Acid/Base Titrations	40
3.3.2. REE Adsorption Results	42
3.3.2.1. Kinetics	42
3.3.2.2. Thermodynamic Studies	46
3.3.2.3. Equilibrium Adsorption Isotherms.....	49
3.3.2.4. Comparison of Surface-Tethered or Solution-Phase Ligands.....	52
3.3.2.5. Effect of pH on REE Binding Capacity	53
3.4. Summary and Conclusions.....	55
CHAPTER 4: Recovery of Rare Earth Elements with Ligand-Functionalized Polymers in Fixed-Bed Adsorption Columns	57
4.1. Introduction	58
4.2. Materials and Methods	59
4.2.1. Adsorbent Synthesis and Characterization	59
4.2.2. Column Experiments	59
4.2.3. REE Selectivity Experiments	61
4.2.4. Adsorbent Regeneration and Reuse Experiments	62
4.3. Results and Discussion	63
4.3.1. Fixed-Bed Column Experiments	64
4.3.2. REE Selectivity Experiments	72
4.3.2.1. Batch Competitive Isotherms	72
4.3.2.2. Fixed-Bed Adsorption of REE from Multi-element Feedstock.....	74

4.3.3. Adsorbent Regeneration and Reuse	78
4.3.3.1. Batch Reuse Experiments.....	78
4.3.3.2. Column Regeneration and Reuse	78
4.3.4. Surface Ligand Concentrations and Their Durability	81
4.4. Summary and Conclusions.....	81
CHAPTER 5: Conclusions	83
5.1. Research Goals.....	84
5.2. Summary of Major Findings.....	84
5.2.1. Major Findings from Objective 1	84
5.2.2. Major Findings from Objective 2	85
5.2.3. Major Findings from Objective 3	86
5.3. Summary of Novel Contributions	86
5.4. Recommendations for Future Work.....	87
REFERENCES	89
APPENDIX A: Supporting Information for Chapter 2	97
APPENDIX B: Supporting Information for Chapter 3	109
APPENDIX C: Supporting Information for Chapter 4	129

List of Tables

CHAPTER 2

Table 2.1. Adsorbent Characterization Results.....	14
---	----

CHAPTER 3

Table 3.1. Summary of resin characterization results. Ligand loadings were calculated from XPS measurements, BET surface area and BJH pore volumes were determined from nitrogen adsorption tests.....	38
---	----

Table 3.2. Acidity constants for each functionalized resin derived from base (OH ⁻) or acid (H ⁺) titrations. Reference values are provided to show pK _A for each ligand in solution phase.....	42
---	----

Table 3.3. Kinetic modeling parameters for adsorption on functionalized resins	45
---	----

Table 3.4. Thermodynamic parameters for adsorption of REE mixtures (Nd, Gd, and Ho) from 0.5M NaCl solutions onto functionalized resins. (pH = 6.5 for Amine, PAA, and BPG or 2.5 for DTPADA).....	48
---	----

Table 3.5. Isotherm model parameters for REE adsorption (mixture of Nd, Gd, and Ho in 0.5M NaCl) on functionalized resins.....	51
---	----

CHAPTER 4

Table 4.1. Geometry and flow characteristics for adsorption columns used in this study.	65
---	----

Table 4.2. Element groupings for selectivity experiments.	73
---	----

APPENDIX A

Table A.1. Standard instrument settings for Agilent 7700x ICP-MS measurements. Oxygen-free grade argon was used as the carrier and dilution gas. Ultra high-purity helium was used in the reaction cell. Tuning solutions purchased from Agilent were diluted 1000:1. Table adapted from Noack, et al. (2016).....	98
---	----

Table A.2. Elemental composition of Great Salt Lake brine. Data provided by the Idaho National Laboratory (sampling location: 40.735287, -112.212512).....	99
---	----

Table A.3. Separation factors for REE/U from experiments performed in Great Salt Lake brines.	100
---	-----

Table A.4. Separation factors for REE and competing ions from the competitive isotherm study. Adsorbent These results are based on elution data from the sorption study.....	108
---	-----

APPENDIX B

Table B.1. Elemental composition of functionalized adsorbents and aminated support.111

Table B.2. Summary of ligand concentration calculations using two different methods.....112

Table B.3. Ligand concentrations from varied functionalization parameters (calculated using bulk concentration method).114

APPENDIX C

Table C.1. Separation factors for REE (average of Nd, Gd, and Ho) over other metals from the Group D competitive isotherm. Calculated from adsorption and elution data. Values highlighted in red indicate selectivity for the competing metal over REE, while blue or white cells show favorable REE separation (darker blue = greater REE selectivity relative to the competing metal).132

Table C.2. Summary of adsorption results for each metal in the multi-element column test with Group D from Figure 4.10 of the main text. Values for the REE are highlighted in yellow.....132

Table C.3. Fixed-bed adsorption column sizing table for BPG-functionalized resins. Assumes 0.4 m/hour superficial velocity and Langmuir adsorption parameters for the resin ($q_{Max} = 3$ mg/g; $K_L = 4.657$ L/g).....136

List of Figures

CHAPTER 2

- Figure 2.1.** Chemical structures for ligands used to functionalize silica particles.11
- Figure 2.2.** Summary of ‘Bottom-Up’ (top) and ‘Top-Down’ (bottom) synthesis reactions (Noack et al. 2016).13
- Figure 2.3.** Adsorption of REE from 100 µg/L lanthanide mixtures in 0.5 M NaCl as a function of pH. Results are grouped according to the starting support used to make each material: (A) pre-aminated silica, or (B) raw silica gel. (Solids = 10 g/L; T ~ 20°C)18
- Figure 2.4.** Adsorption of 100 µg/L REE mixtures (Nd, Gd, Ho; total REE = 300 µg/L) from 0.5 M NaCl solution onto functionalized silica in the presence of varied concentrations (from 0-1,000 mg/L) of competing ions (Ca, Mg, Zn, Al, and Fe). Dashed lines represent average uptake of REE from control samples (REE+NaCl, no other competing ions), and shaded regions denote the range in which adsorbate concentrations exceeded the available surface binding sites on the adsorbents. Equilibrium pH for each sample is indicated by the data point shading; darker data points are more acidic (pH 1-8; T ~ 20°C). Results are grouped according to the starting support used to make each material: (A) pre-aminated silica, or (B) raw silica gel.21
- Figure 2.5.** Adsorption of elements from Great Salt Lake brine onto silica particles as a function of pH. (A) Aminated silica and bottom-up functionalized adsorbents; (B) Raw silica and top-down functionalized DTPADA silica. Equilibrium pH for each sample is indicated by the data point shading; darker data points are more acidic (pH 1-8; T ~ 20°C). Initial concentrations for each element shown in the mixture were approximately 60 µg/L; full composition of the brine is shown in Table A.2 in Appendix A.24
- Figure 2.6.** Impact of solution temperature on elemental adsorption from Great Salt Lake brine onto functionalized silica particles at fixed pH. Initial concentrations for each element shown in the mixture were approximately 60 µg/L.26
- Figure 2.7.** REE elution efficiency for DTPADA on silica as a function of nitric acid strength after one use cycle. Adsorption cycle was performed at pH ~ 1.8.28
- Figure 2.8.** (A) Adsorption of 100 µg/L REE mixture from 0.5 M NaCl onto functionalized silica particles through three adsorption and elution cycles; (B) Elution data for BPG functionalized silica.29

CHAPTER 3

- Figure 3.1.** Expected configurations of surface-tethered REE-chelating ligands shown with residual unreacted primary amines.35
- Figure 3.2.** (A) Acid-base titration results for amine and functionalized resins. Yellow diamonds and solid horizontal lines indicate pK_A values. (B) Comparison of slope from panel A with sample pH.41

Figure 3.3. Summary of adsorbate transport processes.44

Figure 3.4. (A) Kinetics data for adsorption of total REE (Nd, Gd, Ho) on functionalized resins, fit with first- and second-order models. (B) Weber-Morris plots for intraparticle diffusion modeling of the kinetics data. ($C_0 = 100 \mu\text{g/L}$ each Nd, Gd, Ho, $300 \mu\text{g/L}$ total REE; $\text{NaCl} = 0.5\text{M}$; Resins = 10g/L ; Temperature = 20°C ; $\text{pH} = 5.3$ (Amine), 5.4 (PAA), 5.6 (BPG), 2.3 (DTPADA))45

Figure 3.5. Isotherm plots for equilibrium adsorption of total REE (Nd, Gd, and Ho spiked at equal concentrations) on functionalized resins. (A) Log-log plot overlaid with isotherm models (Strong Sites = Langmuir model for ligand binding; Weak Sites = Freundlich model for uptake by aminated support; Combined = Strong Sites + Weak Sites). (B) Semi-log plot of total REE removal efficiency vs. spiked concentration. Gray shaded region shows approximate site saturation based on ligand loading for PAA, BPG, and DTPADA. ($\text{NaCl} = 0.5\text{M}$; Resins = 10g/L ; $\text{pH} = 6.5$ (Amine, PAA, BPG), 2.5 (DTPADA); Temperature = 20°C ; Time = 24 hours).....51

Figure 3.6. (A) Adsorption pH edges with varied adsorbate concentrations. Initial concentrations represent total REE (Nd, Gd, Ho spiked at equal concentrations on mass basis). Dashed lines indicate 100% removal of spiked REE. (B) Isotherm results for DTPADA resins at different fixed pH values. Results are shown as removal efficiency vs. total spiked concentration; gray shaded region indicated expected saturation of surface DTPADA. ($\text{NaCl} = 0.5\text{M}$; Resins = 10g/L ; Temperature = 20°C ; Time = 24 hrs).....55

CHAPTER 4

Figure 4.1. Illustration of experimental setup for fixed-bed column tests.....60

Figure 4.2. SEM images of aminated and BPG-functionalized polymeric resin adsorbents.64

Figure 4.3. Breakthrough curves for REE mixtures in columns packed with aminated support or BPG-functionalized resins. ($C_i = 0.1 \text{mg/L}$ each for Nd, Gd, and Ho; $I = 0.5\text{M NaCl}$; $\text{pH} = 7.0 \pm 0.3$ for amine, 6.7 ± 0.1 for BPG; $Q = 37 \text{BVH}$; Aspect Ratio = 11:1).....66

Figure 4.4. Column results for BPG-functionalized resins with intermittent operation. The system was shut off for 12 hours each after ~ 150 and ~ 550 bed volumes, before resuming the experiment. ($C_i = 0.1 \text{mg/L}$ each for Nd, Gd, and Ho; $I = 0.5\text{M NaCl}$; $\text{pH} = 6.4 \pm 0.5$; $Q = 37 \text{BVH}$; Aspect Ratio = 11:1)67

Figure 4.5. Effect of volumetric flow rate on REE breakthrough for BPG-functionalized resins. ($C_i = 1 \text{mg/L}$ each for Nd, Gd, and Ho; $I = 0.5\text{M NaCl}$; $\text{pH} = 5.8 \pm 0.2$ for both series; $Q = 7$ or 37BVH ; Aspect Ratio = 11:1)68

Figure 4.6. Effect of column aspect ratio (column depth:diameter) on total REE (sum of Nd, Gd, and Ho) C/C_i slope within mass transfer zone. Values on the x-axis indicate the number of bed volumes treated after 10% breakthrough. ($C_i = 1 \text{mg/L}$ each for Nd, Gd, and Ho; $I = 0.5\text{M NaCl}$; $\text{pH} = 5.8 \pm 0.2$ for 11:1 aspect ratio, 6.1 ± 0.1 for 1:2 aspect ratio; $Q = 7 \text{BVH}$; Aspect Ratio = 11:1 or 1:2)70

Figure 4.7. Effect of influent concentration of REE breakthrough for BPG-functionalized resins. ($I = 0.5\text{M NaCl}$; $\text{pH} = 6.1 \pm 0.4$ for 0.1mg/L , 5.8 ± 0.2 for 1mg/L , 5.5 ± 0.4 for 10mg/L ; $Q = 7 \text{BVH}$; Aspect Ratio = 11:1)72

Figure 4.8. Analysis of C/C_i slope within column mass transfer zone. Data from Figure 4.7 were converted to total REE values (sum of Nd, Gd, and Ho) and truncated to show C/C_i trends from 10-90% breakthrough for each influent concentration. Values on the x-axis indicate the number of bed volumes treated after 10% breakthrough.....72

Figure 4.9. Adsorption isotherm results for total REE (sum of Nd, Gd, and Ho) from solutions containing different mixtures of metals spiked at equal concentrations on a mass basis ($C_i = 0.1$ - 100 mg/L each). (A) Isotherm data organized by element groupings (listed in Table 4.2) to show comparison between ligands. (B) Organized by ligand to show competition effects of different mixtures. ($[NaCl] = 0.5M$; $pH = 7.3 \pm 0.3$ for amine, 6.5 ± 0.1 for BPG; Adsorbent Loading = 10 g/L; Time = 24 hours).....74

Figure 4.10. Adsorption (top) and elution (bottom) results for column tests with mixture of metals (Group D shown in Table 4.2) in $0.5M$ NaCl solution. ($C_i = 1$ mg/L of each metal; $I = 0.5M$ NaCl; $pH = 5.9 \pm 0.2$ for amine, 5.4 ± 0.3 for BPG; $Q = 7$ BVH; Aspect Ratio = $11:1$)77

Figure 4.11. Mixed-element adsorption pH edges for aminated or BPG-functionalized resins through 2 use cycles. Resins were rinsed with deionized water, dried, and eluted with $0.75N$ HNO_3 between adsorption cycles. ($C_i = 100$ $\mu g/L$ each for Nd, Gd, Ho, 300 $\mu g/L$ total REE; $NaCl = 0.5M$; Adsorbents = 10 g/L; Temperature = $20^\circ C$; Time = 24 hours)78

Figure 4.12. Breakthrough curves for total REE (sum of Nd, Gd, and Ho) on column reused for 5 cycles. Column was eluted with $0.75N$ HNO_3 , rinsed with deionized water, and reconditioned with $0.5M$ NaCl between each adsorption cycle. ($C_i = 1$ mg/L each for Nd, Gd, Ho; $I = 0.5M$ NaCl; $pH = 6.1 \pm 0.1$ for cycle 1, 5.9 ± 0.2 for cycle 2, 6.0 ± 0.2 for cycle 3, 5.8 ± 0.2 for cycle 4, and 6.0 ± 0.1 for cycle 5; $Q = 37$ BVH; Aspect Ratio = $11:1$).....79

Figure 4.13. Adsorption and elution plots for Figure 4.12 data showing material reuse through 5 cycles. (A) Mass of REE adsorbed onto BPG-functionalized resins shown as a function of bed volumes treated. Sharp decreases in 'q' values indicate recovery of adsorbed REE from the resins via elution with $0.75N$ HNO_3 . (B) Elution data for each cycle showing effluent REE concentrations in the eluate.80

Figure 4.14. Ligand concentration on BPG-functionalized resins after multiple use-cycles.81

APPENDIX A

Figure A.1. Full pH edge adsorption dataset for 100 $\mu g/L$ mixtures of Nd, Gd, and Ho in $0.5M$ NaCl. Adsorption reactions were performed for 3 hours at $T = 20^\circ C$, using adsorbent loadings of 10 g/L.....101

Figure A.2. Adsorption pH trends for 100 $\mu g/L$ mixtures of Nd, Gd, and Ho in $0.5M$ NaCl with and without iron. Iron concentrations are denoted by the color of the data points. A single pH value was targeted for each solid for all samples containing Fe, though high concentrations of iron lead to decreased equilibrium pH. Adsorption reactions were performed for 3 hours at $T = 20^\circ C$, using adsorbent loadings of 10 g/L.102

Figure A.3. REE elution efficiency for DTPADA and BPG on silica as a function of nitric acid strength after one use cycle. Adsorption cycles were performed at $pH \sim 1.8$104

Figure A.4. Ratio of mass eluted to mass spiked for each element eluted from TD-DTPADA particles after competitive adsorption study. Adsorption was conducted at pH ~ 2 and room temperature. 105

Figure A.5. Enrichment factors for REE relative to competing ions shown as a function of molar ratios of spiked adsorbate concentrations (i.e., x-axis = $[\text{Competing Ion}]_i / [\text{REE}]_i$; adsorbent = TD-DTPADA). 106

Figure A.6. Competitive isotherm results TD-DTPADA functionalized adsorbents with a mixture of 10 elements (7 competing ions and 3 REE) spiked at equal concentrations on a mass basis. Equilibrium solution-phase concentrations are shown on the x-axis, while the y-axis shows adsorbed concentrations for each element (pH = 2.5, T ~ 20°C). 107

APPENDIX B

Figure B.1. Lanthanide complex coordination by solution phase and surface-tethered DTPA molecules. Structures for surface complexed REE inferred from literature-reported conformations of REE-DTPA complexes in solution phase (Thakur et al. 2013). 110

Figure B.2. Effect of molar ratio of ligand to surface amines used in synthesis on adsorbent performance (Ligand = BPG; $[\text{NaCl}] = 0.5\text{M}$; $[\text{REE}] = 0.1 \text{ mg/L}$ each; Reaction Time = 24 hours; Reaction Temperature = 20°C). 114

Figure B.3. Calculated equilibrium speciation of lanthanides (Nd, Gd, and Ho at 0.1-1,000 mg/L each) in pure water ($I = 0$) across the pH range of interest for this study. Grey shaded regions indicate potential precipitation of REE. 116

Figure B.4. Calculated equilibrium speciation of lanthanides in solutions containing REE (Nd, Gd, and Ho at 0.1-1,000 mg/L each) and 0.5M NaCl. Note that the species listed are different from Figure B.3 due to the presence of chlorides. Grey shaded regions indicate potential precipitation of REE. 117

Figure B.5. Calculated equilibrium speciation of DTPA, PAA, and BPG ligands as a function of pH in solution with $I = 0.5\text{M}$ 118

Figure B.6. Modeled complexation of lanthanides (Nd, Gd, and Ho at 0.1-1,000 mg/L each) by solution phase DTPA (4.4 mmol/L) in 0.5M NaCl. Note that colors and shapes for species are different in 1,000 mg/L plots. 120

Figure B.7. Modeled complexation of lanthanides (Nd, Gd, and Ho at 0.1-1,000 mg/L each) by solution phase PAA (3.3 mmol/L) in 0.5M NaCl. Note that colors and shapes for species are different in 1,000 mg/L plots. 121

Figure B.8. Summary of modeled complexation by DTPA (4.4 mmol/L) or PAA (3.3 mmol/L) as a function of solution pH in 0.5M NaCl solutions assuming liquid phase ligand behavior. 122

Figure B.9. Linearized Freundlich and Langmuir isotherm model fitting to experimental results for total REE equilibrium adsorption on functionalized adsorbents and aminated resin supports ($I = 0.5\text{M NaCl}$). 123

Figure B.10. Log-log isotherm plot for total REE (Nd, Gd, and Ho) adsorption on functionalized silica particles ($d \sim 0.1\text{mm}$) and polymer resins ($d \sim 0.6\text{mm}$). 123

Figure B.11. Total REE (Nd, Gd, and Ho) adsorption (y-axis) as a function of initial total concentration (x-axis). Experimental adsorption data from isotherms are compared to solution-phase ligand binding models using a variety of ligand concentrations (0.01-0.44 mmol/L) for 0.5M NaCl solutions..... 124

Figure B.12. Comparison of solution-phase model predictions for total REE (Nd, Gd, and Ho) complexation with experimental data for adsorption of REE on functionalized adsorbents. Solid black lines indicate 1:1 correspondence of experimental adsorption data to the solution-phase model predictions for REE complexation. Points are shown as experimentally measured $q_{\text{Experimental}}$ or calculated q_{Model} using a solution-phase model for an equivalent ligand concentration (i.e., [ligand in solution] = [ligand on resins]; [PAA] = 0.33 mmol/g; [DTPA] = 0.44 mmol/g)..... 124

Figure B.13. Individual REE element data from Figure 3.6.B of the main text. Shown as adsorbed concentration vs. spiked concentration for each REE, with the shaded regions indicating likely saturation of surface DTPA. 125

Figure B.14. Thermodynamic model fitting of REE equilibrium adsorption data which shows $\ln(q/C_e)$ [L/g] vs. q [mg/g]. Results are organized by ligand (columns) and reaction temperature/element (rows, temperature units = °C). Y-intercepts from this plot were used to calculate $\ln(K_0)$ and ΔG° values presented in Table 3.4 of the main text..... 126

Figure B.15. Van't Hoff plot used to calculate entropy and enthalpy values for adsorption of REE mixtures in sodium chloride solutions (0.5M NaCl) at different temperatures. Results are organized by ligand (columns) and element (rows). Data points shown here represent the y-intercepts from Figure B.14. Error bars show standard error for each series..... 127

Figure B.16. Potential structures of surface-bound DTPA ligands, shown with and without electrostatic interference from amines. Note that amines will be protonated (i.e., NH_3^+) below pH ~9.3..... 128

APPENDIX C

Figure C.1. Speciation of metals in complex mixture used in batch and column experiments calculated with PHREEQC. Metals are separated by valence of the predominant species. Gray shaded regions show potential pH regions of precipitation, and the yellow bar indicates the experimental pH used in this research. (Metal concentrations = 1 mg/L each; I = 0.5M NaCl) 130

Figure C.2. Metal recovery for each metal in Group D from Figure 4.9 of the main text. Y-axes are different for each plot. 131

CHAPTER 1

Introduction

1.1. Rare Earth Elements (REE)

1.1.1. REE and their Sources

Rare earth elements (REE) are a group of 15 metals – comprised of the lanthanide series plus scandium and yttrium – which have been identified as critical materials due to their importance to developing technologies as well as their supply chain risks (Van Gosen et al. 2017; United States Department of Energy 2010). Unique physical and electromagnetic properties make REE particularly useful for consumer and industrial products. For example, neodymium is used to make strong magnets that are central to the operation of many consumer products, while scandium is used to make strong and lightweight metal alloys for airplane components and gadolinium is used as a contrast agent for magnetic resonance imaging in the healthcare sector (United States Environmental Protection Agency 2012).

Conventional mining processes historically employed for REE production are highly resource-intensive, with gross energy requirements of approximately 2,430 GJ per tonne of total rare earth oxide, and global warming potentials are estimated to be 230 tonnes CO₂-equivalent per tonne of total rare earth oxide (Weng et al. 2016). Energy requirements and greenhouse gas emissions more than an order of magnitude higher for REE production when compared to equal masses of other common metals, such as steel (Zaines et al. 2015). Furthermore, mining operations are geographically limited to regions where high-quality ores are abundant and require large up-front capital investments. It can take up to 17 years for a mine to begin REE production from the time of initial investigation (United States Environmental Protection Agency 2012). These factors translate to a production process which may not be economically or environmentally sustainable to meet long-term global REE demand (Wall et al. 2017).

Mineral ores remain the primary source of REE, though alternative sources and recycling could be used to augment supplies and mitigate price volatility (Kumari et al. 2016). International

efforts to identify potential REE sources have accelerated dramatically since China, the world's leading producer, began limiting exports around 2009 (Paulick and Machacek 2017). Many industrial wastes contain REE at trace levels (Liu and Naidu 2014; Stewart et al. 2017; Taggart et al. 2016), but other metals present at much higher concentrations make the separation and recovery of dissolved lanthanides from these complex mixtures challenging.

1.1.2. Alternative REE Feedstocks

Much attention has been directed towards identifying and leveraging new or recycled sources of REE – such as electronics scrap (Sun et al. 2017), coal fly ash (Dutta et al. 2016; Taggart et al. 2016), brines (Noack et al. 2016), and various industrial wastes (Davris et al. 2016; Liu and Naidu 2014) – to meet surging demand. However, these sources often contain impurities and have relatively low REE concentrations when compared to common REE source ores. Studies investigating REE in brines and other environmental media have reported a wide range of concentrations, from the low parts-per-trillion to hundreds of parts-per-million, though most brines fall in the parts-per-billion range ($\mu\text{g/L}$) for lanthanides (Lewis et al. 1997; Noack et al. 2014; Sanada et al. 2006; Wood 2006; Wood and Shannon 2003). In contrast, other cations are abundant at much higher concentrations, including: Na^+ (~1,600 mg/L), Ca^{2+} (~200 mg/L), Mg^{2+} (~70 mg/L), Al^{3+} (~10 mg/L), Fe^{2+} (~20 mg/L), and Zn^{2+} (~10 mg/L) (Clark et al. 2010).

1.1.3. Conventional REE Extraction and Purification Processes

Traditional REE extraction processes can be summarized by 4 primary steps: mining, physical beneficiation, chemical treatment, and final separation (Krishnamurthy and Gupta 2004). Each of these steps includes numerous sub-processes which are tailored to the site-specific mineral composition. Beneficiation includes the grinding and physical separation of minerals, primarily by flotation or gravity separation. Chemical methods are then used to break down the ores further through the addition of acids/bases or chlorination. The resulting rare earth complexes are finally separated from one-another using either solvent extraction or ion exchange.

Liquid-liquid extractions (LLE) utilizing solvents can require thousands of cycles to reach sufficient levels of purity, so ion exchange may be used where >99.9% purity is required (Krishnamurthy and Gupta 2004). However, conventional ion exchange resins are limited by a lack of selectivity for REE over other metal species, which makes their use in complex mixtures problematic (Krishnamurthy and Gupta 2004). Therefore, solvent extraction has been the dominant method for commercial-scale REE separation since its advent in the 1960s (Xie et al. 2014).

1.1.4. Novel Approaches to REE Extraction

There is a growing body of research devoted to the production of new materials and processes that could alter the economic viability of resource recovery from waste streams by improving upon the selectivity of conventional REE separation processes. Methods are being developed for improved LLE (Hoogerstraete et al. 2013; Wang and Cheng 2011), biological processes (Park et al. 2016) and hybrid membrane/solvent systems (Kim et al. 2015) for REE purification. Solid-phase extraction (SPE) has the potential to circumvent many of the issues associated with LLE processes – such as their requirement for complicated engineering designs and hundreds of extraction stages to reach sufficient quality (Xie et al. 2014) – and yield high-purity rare earth supplies with relatively simple operations and low cost.

Researchers have generated SPE materials which target metals using a variety of ligand-functionalized adsorbent supports, including chitosan (Galhoum et al. 2015; Inoue et al. 1997; Mahfouz et al. 2015; Nagib et al. 1999; Repo et al. 2010; Roosen and Binnemans 2014; Zhao et al. 2015a), silica (Ashour et al. 2018; Callura et al. 2018; Dupont et al. 2014; Fryxell et al. 2004, 2007; Hossain and Mercier 2002; Hu et al. 2017; Juere et al. 2016; Noack et al. 2016; Polido Legaria et al. 2017; Ramasamy et al. 2017; Yantasee et al. 2009), activated carbon (Babu et al. 2018; Yantasee et al. 2004), diatomite (Zhou et al. 2016), magnetite (Almeida and Toma 2016; Dupont et al. 2014), and β -cyclodextrin (Zhao et al. 2015b, 2016) and their extraction performance was summarized in recent reviews (Anastopoulos et al. 2016; Hu et al. 2018; Iftekhhar et al. 2018).

Most SPE studies with novel materials involve nano- or micro-scale materials. Nanomaterials have some desirable properties, such as their high surface area to volume ratio, but they are typically limited to batch applications and present problems with respect to process scaling. These issues could be circumvented by attaching functionalized nanoparticles to larger supports, though additional work would be required to address the viability and robustness of this approach. More work is needed to address scale-up and associated costs, operational challenges, and durability/reusability of the adsorbent materials before SPE will be able to compete with traditional solvent-based processes for REE recovery.

1.1.5. Opportunity for Targeted SPE with REE-Selective Adsorbents

Extraction of lanthanides from aqueous solutions containing many elements presents a significant technical challenge. Separation processes need to have high selectivity to remove dilute ions and high throughput to treat large volumes of fluid. To address these requirements, metal chelating aminocarboxylate ligands (e.g., ethylenediaminetetraacetic acid (EDTA) and diethylenetriaminepentaacetic acid (DTPA)) have been introduced into conventional ion exchange systems to enhance the separation efficiency of REE during elution from ion exchange resins (Krishnamurthy and Gupta 2004). Similarly, phospho-ligands have been used for liquid phase separations in large scale systems due to the strength of their interactions with REE (Xie et al. 2014). The chelators bind to REE in solution, allowing separations of target elements based on their affinity towards the ligands. The ligand-containing fluid may be collected and recycled after use, but large-scale implementation of this approach is hindered by the high maintenance requirements involved with recycling and regeneration of the ligands in solution. By chemically immobilizing the chelating ligands onto adsorbent particle surfaces, it would become possible to retain the extractants for rapid recovery and reuse (i.e., within an adsorption column).

Selective extraction of REE from aqueous sources using ligand-functionalized adsorbents would allow for effective pre-concentration of targeted components present at low concentrations,

and the elimination of problematic bulk ions, which possess little value but require extensive processing for removal with associated generation of large volumes of concentrated liquid waste under current practices (Lee and Wen 2016). This, in turn, could valorize waste streams which have historically been viewed as a nuisance, such as acid mine drainage, bauxite residue, produced waters from oil and gas operations, or leachates from coal fly ash. The scalability of adsorption columns could provide operators with the flexibility to easily add or remove REE production capacity in response to rapidly changing market conditions.

1.2. Research Goals

The overall goal of this research was to develop ligand-functionalized adsorbents and evaluate their potential as a method for REE extraction from saline waters. This study was designed to advance the understanding of interactions between REE and functionalized adsorbents using batch and continuous-flow adsorption experiments. Specific research objectives were as follows: **(1)** Investigate adsorption of REE onto functionalized model supports; **(2)** Characterize large-scale functionalized polymer resins and evaluate their REE binding mechanisms; and **(3)** Determine selectivity and study fixed-bed column performance of functionalized adsorbents.

1.2.1. Functionalized Model Supports

Adsorption dynamics are highly dependent on solution chemistry and operating conditions (Iftekhar et al. 2018). Therefore, it is necessary to develop a better understanding of how functionalized adsorbents perform with dilute feedstocks containing problematic competing ions at relevant concentrations. This objective studied the performance of ligand-functionalized silica adsorbents in a range of matrices and conditions. Critical variables, such as pH and competing ion concentrations were experimentally evaluated, and adsorbent durability was determined through elution and reuse studies.

1.2.2. Large-Scale Functionalized Polymer Resins

While much is known about the behavior of REE and ligands in solution, there are many unanswered questions regarding their interactions once the ligands are tethered to a surface. Immobilization of ligands is achieved by forming a chemical bond with surface groups, which alters both the ligand and surface. This objective investigated the physical properties (e.g., surface area, ligand loadings, and acid/base properties) of large-scale functionalized adsorbents. Adsorption kinetics and capacity were determined, and the influence of temperature on REE affinity was studied. The relative influence of different surface functional groups was quantified, and solution-phase REE/ligand complexation models were used to analyze experimental adsorption results and evaluate difference between surface-tethered and unbound ligands.

1.2.3. Selectivity and Fixed-Bed Column Application of Functionalized Polymer Resins

Large adsorbents facilitate the use of flow-through systems, which are not feasible with frequently-studied nanoparticles, unless the nanoparticles are supported on larger particles or other immobile supports (e.g., membranes). While kinetic parameters determined through batch experiments provide useful information about adsorbent performance, small-scale column experiments are critical to understanding the transport of adsorbate molecules in flow-through systems, a process which is highly sensitive to operating conditions. Objective 3 explored the influence of REE concentration, flow rate, and column geometry on adsorbate breakthrough curves. The selectivity and reusability of functionalized adsorbents was evaluated in batch and column experiments.

1.3. Thesis Organization

The remainder of this thesis includes three chapters corresponding to the three major objectives, and a summary chapter. The first chapter provides an overview of the importance of REE, including details regarding conventional and novel REE extraction/purification methods.

Chapters 2-4 detail the experimental and modeling results generated in support of Objectives 1-3, respectively. The fifth and final chapter provides overall conclusions from this body of work, summarizes its novel contributions, and provides recommendations for future work. Appendices A-C provide additional data and analysis in support of Chapters 2-4.

CHAPTER 2

Selective Adsorption of Rare Earth Elements onto Functionalized Silica Particles

Contents of this chapter have been published in the following journal article:

J. C. Callura, K. M. Perkins, C. W. Noack, N. R. Washburn, D. A. Dzombak, A. K. Karamalidis, 'Selective Adsorption of Rare Earth Elements onto Functionalized Silica Particles,' *Green Chemistry* **2018**, 20 (7), 1515-1526.

2.1. Introduction

Separation of rare earth elements from dilute feedstocks remains a challenging unsolved problem. The efficacy of REE extraction processes may be influenced by a range of variables, including feedstock composition and process parameters. It is crucial to understand the impact of these variables before REE recovery schemes can be designed.

The primary objective of this research was to quantify the ability of ligand-functionalized silica particles to adsorb REE selectively from chemically complex synthetic- and real brine solutions, and to evaluate the impact of competing ions on REE adsorption. Three ligands were selected for study based on their high affinity for chelating REE and their favorable performance during pre-screening tests. The ability of the ligand-functionalized silica adsorbents to extract REE from brine mixtures was evaluated under a range of conditions. Adsorption of various ions was compared to identify species that may interfere with REE adsorption by competing for binding sites. This study aims to provide new insight into the performance of REE-selective functionalized adsorbents for extraction of REE in operationally-relevant conditions.

2.2. Materials and Methods

2.2.1. Chemicals

Adsorbents were functionalized using either 3-aminopropyl silica particles (d: 75–150 μm ; TCI America) or high-purity silica particles (d: 150–250 μm ; Sigma-Aldrich, 60Å pore size) as starting supports. The ligands tested in this study were diethylenetriaminepentaacetic dianhydride (DTPADA), phosphonoacetic acid (PAA), and *N,N*-bis(phosphonomethyl)glycine (BPG). Ligand structures are shown in Figure 2.1.

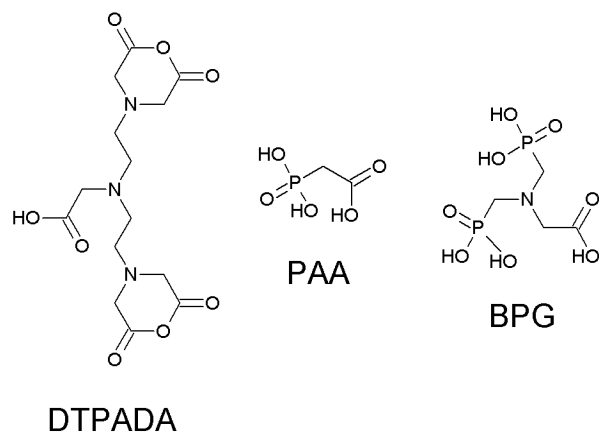


Figure 2.1. Chemical structures for ligands used to functionalize silica particles.

Propylphosphonic anhydride (T3P) and *N,N'*-dicyclohexylcarbodiimide (DCC) were used to facilitate the formation of the amide bond, by which the chosen ligands are attached to the silica supports. The chemicals activated carboxyl groups for room temperature amide formation and are common reagents in peptide synthesis (Valeur et al. 2009). In the case of DTPADA, this allows preferential attachment of the ligand at the free carboxyl group, as opposed to uncontrolled attachment via ring-opening reactions in the cyclic anhydrides; this targeted approach showed superior performance compared to functionalization with free DTPA (Noack et al. 2016).

Nitric acid (HNO_3 ; BDH ARISTAR Plus, VWR) was used to acidify and preserve samples for inductively coupled plasma mass spectrometry (ICP-MS) analysis. Hydrochloric acid (HCl; BDH ARISTAR Plus, VWR) and sodium hydroxide (NaOH; Fischer Scientific) were used for pH adjustments. Background electrolyte solutions were prepared by dissolving NaCl (Sigma-Aldrich; $\geq 99\%$ purity) in ultrapure water (ASTM Type I, $18.2 \text{ M}\Omega/\text{cm}$), prepared using a Barnstead NANOpure water purification system.

REE spike solutions were prepared by dissolving hexahydrated $\text{Ln}(\text{NO}_3)_3$ salts (Sigma-Aldrich or Alfa Aesar) in ultrapure water. Single element standard solutions ($1000 \mu\text{g/L}$) of REE were obtained from Inorganic Ventures and used to prepare the calibration curve for ICP-MS

analysis. Standards were prepared with a 0.5M NaCl background to match sample matrices. Batch adsorption experiments were prepared and reacted in 12 mL Teflon tubes (Sallivex). Metal spike solutions for the competing ion studies were prepared by dissolving chloride (CaCl_2 , MgCl_2 , FeCl_2 , AlCl_3) or nitrate ($\text{Zn}(\text{NO}_3)_2$) salts in ultrapure water.

2.2.2. Analytical Instrumentation

Total dissolved REE concentrations were determined using an Agilent 7700x ICP-MS with HEHe-mode octopole reaction cell. Operating parameters were optimized daily via the autotune function of the Agilent MassHunter software using 1000:1 diluted Agilent tuning solutions. Concentrations were determined from a six-point calibration curve (0, 1, 5, 10, 50, and 100 ppb) containing each REE. Typical instrument operating parameters are provided in Table A.1 of Appendix A. Analytical error was estimated to be ± 5 ppb, based on repeated measurements of standard samples. Detection limits for this study were <1 ppb.

An Orion 8165BNWP ROSS Sure-Flow pH electrode (Thermo Scientific), coupled to an Accumet XL600 m (Fisher Scientific), was used for pH measurements of high-total dissolved solid (TDS) solutions. The pH meter was calibrated with pH 1.7, 4.0, 7.0, and 10.0 standards daily. All samples were prepared gravimetrically using an analytical balance with 0.01 mg precision (Adam Equipment). Chemicals and instrumentation used for this study were consistent with our previous work (Noack et al. 2016).

2.2.3. Functionalization and Characterization

Synthesis of the functionalized materials was completed using either a “bottom-up” or “top-down” approach, as detailed previously (Noack et al. 2016). For the bottom-up materials, pre-aminated silica particles were mixed in a dimethylformamide (DMF) solution containing the ligand (PAA, BPG, or DTPADA), 4-dimethylaminopyridine, and T3P overnight at room temperature. Sorbents modified with the DTPADA ligand were functionalized using both top-down and bottom-

up methods; the materials are labelled as TD-DTPADA or BU-DTPADA, respectively (Figure 2.2). The mixture was then centrifuged, decanted, rinsed with fresh DMF five times, rinsed with fresh warm water ($\sim 70^{\circ}\text{C}$) three times, then dried in a vacuum oven. Top-down materials were prepared by first mixing DTPADA with DCC under N_2 gas, followed by the addition of dichloromethane (DCM) and 3-aminopropyltriethoxysilane (APTES). Contents were stirred overnight, filtered, and concentrated under vacuum. The resulting dried mixture was then added to silica particles in dry toluene and stirred overnight under N_2 gas. Finally, the top-down materials were rinsed with toluene (5x), tetrahydrofuran (5x), warm water (3x), and dried in a vacuum oven. The functionalization methods are included in pending patent US 20170101698 A1 (Karamalidis et al. 2017).

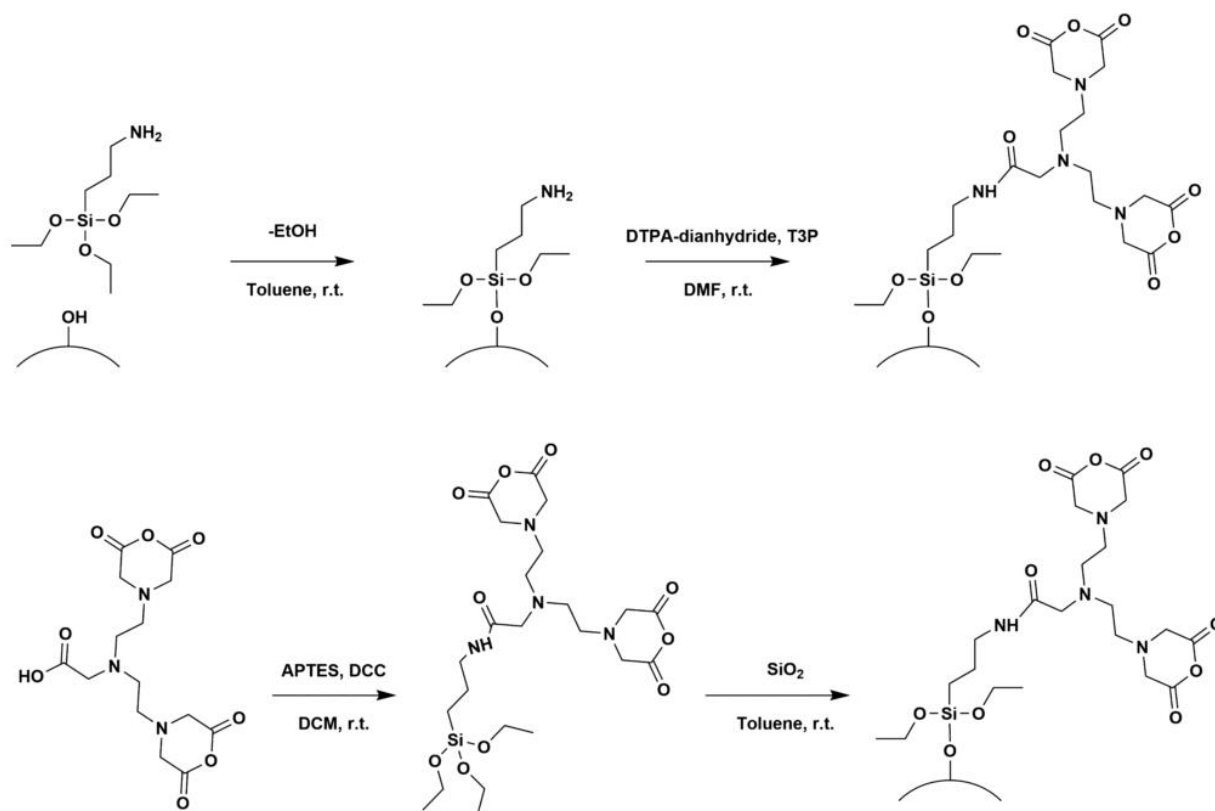


Figure 2.2. Summary of 'Bottom-Up' (top) and 'Top-Down' (bottom) synthesis reactions (Noack et al. 2016).

Characterization methods for the functionalized adsorbents included thermogravimetric analysis (TGA), attenuated total reflectance-Fourier transform infrared spectroscopy (ATR-FTIR), electrophoretic mobility (EPM), and rapid acid-base titrations to confirm and quantify the presence of the ligands on the adsorbent surfaces. Results from adsorbent characterization have been reported previously (Noack et al. 2016). Key characterization findings and a list of molecular volumes for each ligand-APTES unit are summarized in Table 2.1.

Table 2.1. Adsorbent Characterization Results

Adsorbent	Ligand Loading (mmol/g)	Ligand Density (mmol/m²)	Amine Conversion (%)	pH_{PZC}	Molar Volume^a (Ligand+APTES, cm³)
Aminated	0.96	1.9x10 ⁻³	-	6-9	236
PAA	0.15	3.0x10 ⁻⁴	16%	6-7	311
BPG	0.086	1.7x10 ⁻⁴	9%	4-5	371
BU-DTPADA	0.268	5.4x10 ⁻⁴	28%	3	481
TD-DTPADA	≤0.463	≤9.3x10 ⁻⁴	≤48%	N.R.	481

N.R. = Not Reported

^a(United States Environmental Protection Agency 2017)

2.2.4. REE Adsorption Experiments

2.2.4.1. Batch Equilibrium Adsorption Experiments

Batch equilibrium adsorption experiments were conducted in either synthetic (0.5 M NaCl + 100 µg/L each Nd, Gd, and Ho) or real brines (I ~ 3M; composition shown in Table A.2 in Appendix A), using a solid loading of 10 g/L (100 mg adsorbent particles in 10 mL solution). Samples were mixed end-over-end at 30 rpm for 3 hours until equilibrium was reached – kinetics tests showed rapid equilibration for these adsorbents (t < 30 minutes) (Noack et al. 2016). Solids were allowed to settle via gravity sedimentation for approximately 10 minutes after the 3 hour reaction period, and the supernatant solution was sampled, acidified, and analyzed for REE content via ICP-MS. Adsorption efficiencies were calculated by comparing the spiked and equilibrium solution concentrations (Equation 2.1; C_e = equilibrium concentration, C_i = spiked concentration). Measurements

for pH were made on the remaining supernatant after sampling. Samples were reacted at room temperature (T ~ 20°C), unless otherwise noted.

$$Removal (\%) = \left(1 - \frac{C_e}{C_i}\right) \times 100\% \quad (\text{Equation 2.1})$$

Samples for adsorption measurements at different temperatures were prepared at the optimal pH condition for each material, as determined by adsorption pH-edge tests, and placed on a heated stir plate at the prescribed temperature and mixed using a magnetic stir bar set to 250 RPM for 3 hours.

2.2.4.2. Competitive Adsorption Experiments

Samples for competitive adsorption studies were prepared by spiking prescribed concentrations (0-1,000 mg/L) of competing ions (Ca, Mg, Zn, Al, or Fe) into 0.5 M NaCl solutions containing 100 µg/L of Nd, Gd, and Ho. Tests were also conducted using real brine solutions to evaluate adsorbent material performance for REE removal in with water from the Great Salt Lake (GSL) near Salt Lake City, Utah, USA. Brine samples containing approximately 2.3M NaCl were filtered through 0.45 µm fiber filters, diluted 2x, and spiked with 55.56 µg/L of Sc, Y, Th, U, and each lanthanide prior to receipt. The filtered and diluted brines were tested as-received (see composition in Table A.2 in Appendix A). Separation factors (α) were calculated for elements present in the Great Salt Lake brines. The α values indicate the selectivity of the adsorbents for element 'A' over element 'B' (Equation 2.2; D = distribution coefficient, M_{ads} = mass adsorbed, M_e = mass remaining in solution).

$$Separation Factor (\alpha_{A,B}) = \frac{D_A}{D_B} = \frac{M_{ads,A}/M_{e,A}}{M_{ads,B}/M_{e,B}} = \frac{\left[\frac{(C_i - C_e)}{C_e}\right]_A}{\left[\frac{(C_i - C_e)}{C_e}\right]_B} \quad (\text{Equation 2.2})$$

2.2.4.3. Adsorbent Elution and Reuse Studies

Tests were conducted to determine the concentration of nitric acid required for successful elution of adsorbed REE. Adsorbent suspensions (100 mg solids in 10 mL total solutions) were equilibrated with 10 ppm mixtures of Nd, Gd, and Ho in 0.5 M NaCl at pH ~ 1.8, rinsed with deionized (DI) water, decanted, dried overnight at 100°C, then mixed with pre-determined concentrations of nitric acid (0.01-6.55 N). The resulting eluates were spiked with varying amounts of HNO₃ to normalize acid concentrations and eliminate the effects of matrix differences prior to analysis with ICP-MS. Results were corrected for any dilution that occurred during the matrix-matching process. Elution efficiencies were calculated as shown in Equation 2.3 (M_{elu} = mass eluted, M_{ads} = mass adsorbed, C_{elu} = elution concentration, V = 10 mL).

$$\text{Elution Efficiency (\%)} = \frac{M_{\text{elu}}}{M_{\text{ads}}} = \frac{C_{\text{elu}}V}{(C_i - C_e)V} \quad (\text{Equation 2.3})$$

Material reusability was evaluated by first reacting functionalized silica particles (10 g/L) with 100 ppb mixtures of Nd, Gd, and Ho in 0.5 M NaCl. Supernatant fluids were sampled and acidified after a 3-hour reaction period, pH measurements were taken, then the remaining fluid was decanted. The solids were retained and rinsed with DI water, then dried overnight at 100°C. Dried solids were then mixed with 10 mL HNO₃ (0.75 N) solutions for 3 hours, and the solution phase was collected for later analysis. The eluted solids were then rinsed with DI, decanted, and dried overnight again. This adsorption/elution cycle was repeated three times for each type of adsorbent, and the samples from each cycle were analyzed for their REE content using ICP-MS.

2.3. Results and Discussion

2.3.1. Batch Adsorption Experiments with Synthetic Brine

Adsorption pH-edge tests with 100 ppb REE mixtures in 0.5 M NaCl solutions revealed that uptake onto the functionalized materials was strongly pH-dependent, as shown in Figure 2.3. The results are grouped by the type of support used. Figure 2.3.A shows the results for adsorbents synthesized with pre-aminated silica and materials generated using the bottom-up method, while Figure 2.3.B shows the results for the raw silica particles and DTPADA-functionalized silica particles made with the top-down method. Results were truncated at pH 8 to eliminate the potential influence of lanthanide precipitation, which may occur under alkaline conditions as hydroxyl complexes become more prevalent (the complete data set is provided in Figure A.1 in the SI). In both cases, the non-functionalized supports (aminated silica, Figure 2.3.A; raw silica, Figure 2.3.B) showed little-to-no REE uptake below pH 5, while adsorption onto the raw silica peaked at pH 7. The point of zero charge for silica is approximately 2.0 (Benjamin 2010), so interactions between cationic REE and the negatively charged raw particle surfaces are expected to be stronger in circumneutral to basic conditions. It is important to note, however, that this type of adsorption is not selective (i.e. demonstrates no preference for REE over other metals) since it is based solely on non-site-specific electrostatic attraction. In contrast, adsorption onto the functionalized materials was attributed mostly to the ligand-REE attractions since the selected ligands are known to strongly form stable complexes with the REE.

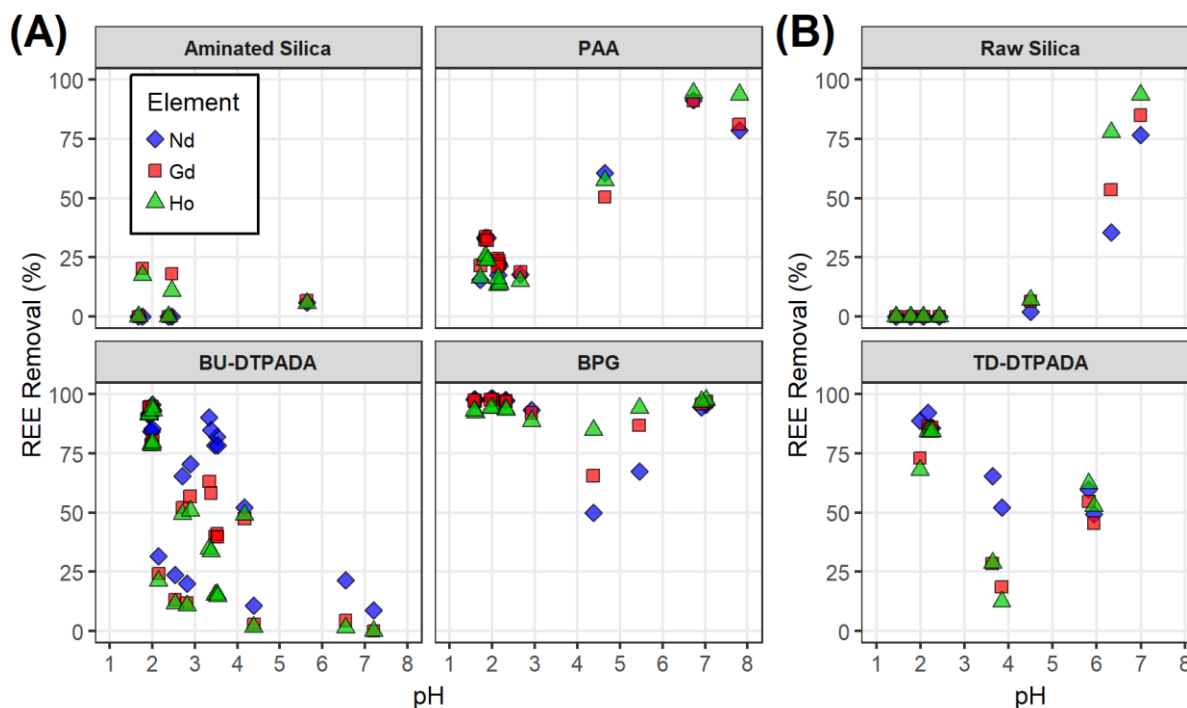


Figure 2.3. Adsorption of REE from 100 µg/L lanthanide mixtures in 0.5 M NaCl as a function of pH. Results are grouped according to the starting support used to make each material: (A) pre-aminated silica, or (B) raw silica gel. (Solids = 10 g/L; T ~ 20°C)

PAA, the smallest ligand tested, was expected to achieve high grafting densities due to its low molecular volume and the limited effect of steric hindrance compared to larger molecules. Attachment of PAA to pre-aminated silica particles allowed for nearly complete REE adsorption (95% removal) at pH 6.7. These results represent equilibrium conditions, as confirmed by kinetic studies, and are indicative of the net impacts of particle surface charge, ligand protonation states, and REE speciation. Additional characterization and performance data for these materials have been reported in detail previously (Noack et al. 2016).

BPG and DTPADA-functionalized materials showed a high degree of REE uptake (>95%) under acidic conditions, providing further confirmation of successful ligand attachment since the raw supports were ineffective in this range prior to functionalization. DTPADA contains two cyclic anhydride moieties which undergo hydrolysis upon exposure to water. As a result, the chemical structure for DTPADA becomes nearly identical to DTPA when immersed in aqueous solution.

DTPA has five acid dissociation constants (pK_A), ranging approximately from 2 to 10, which describe the protonation states of the carboxyl groups (Grimes and Nash 2014). The ligand's pK_A values shift when the carboxyls are conjugated (Sherry et al. 1988), as occurs upon attachment to the surface, and they also change as a function of the solution's ionic strength (Grimes and Nash 2014). At lower pH, more of the carboxyl groups are expected to become protonated, causing the ionic attraction between DTPA and the positively charged REE to be diminished in solution. While thermodynamic modeling would suggest improved complexation of REE by DTPA with increasing pH, experimental results revealed the opposite trend. This observation was also noted in our previous work and is hypothesized to be the result of electrostatic attraction between ligands and the silica surfaces at higher pH values (Noack et al. 2016). Uptake data for BU-DTPADA were particularly variable since the plot is comprised of results from materials synthesized and analyzed at different times. While the functionalization chemistry is well-documented and robust, some variability exists between different material batches, introducing a degree of uncertainty in interpreting the results. Still, multiple batches for each material yielded results with similar trends as those shown here.

Adsorption trends were similar for both the bottom-up and top-down DTPADA materials, though the top-down material yielded greater REE adsorption through the circumneutral pH range. This may be due to a higher ligand grafting density on the top-down materials, as shown in Table 2.1, which could result in reduced attraction between unreacted surface amines and deprotonated carboxyl groups of the surface-bound ligands. Other research on functionalized mesoporous silica has shown that a two-step synthesis (i.e. top-down method) yields approximately three times higher ligand grafting efficiency, and improved metal adsorption, when compared to a single-step method (i.e. bottom-up) (Pérez-Quintanilla et al. 2006). BPG materials performed well throughout the entire range tested, except for a lower level of adsorption at pH ~4.5. This local minimum was more pronounced for light REE (Nd) than heavy REE (Ho).

Electron-rich oxygen and nitrogen moieties within the BPG and DTPADA ligands appear to play an important role in coordinating and binding lanthanides, allowing adsorption at lower pH despite the contrary influence of electrostatics.

Figure 2.4 shows the results of a set of REE adsorption experiments conducted in the presence of 0.5 M NaCl and varied amounts of competing ions. Brines contain numerous dissolved chemical species that will compete for the finite number of binding sites on an adsorbent surface, so it is important to compare the affinity of each ligand for REE vs. bulk ions. Results for the competing ions spiked (Ca, Mg, Zn, Al, Fe) are listed by column, and the different adsorbent materials tested are listed by row. Competing ion concentrations were varied from 0 to 1,000 mg/L, while REE concentrations were held constant at 100 $\mu\text{g/L}$ each for Nd, Gd, and Ho. Concentrations for the competing cations were in excess of the estimated total reactive sites present on the functionalized particles for samples spiked at 100-1,000 mg/L.

Specific pH values were targeted for the adsorption experiments with each material based on adsorbent peak performance for REE removal as determined from Figure 2.3: pH 6.5-7.0 for raw silica, aminated silica, and PAA, or pH 2.0-2.5 for TD-DTPADA and BPG. Equilibrium pH values for each sample are depicted by the amount of shading (darker points represent more acidic conditions). Variation from target pH at higher competing ion concentrations was attributed to precipitation of the competing ions; the aqueous samples were not pH buffered due to the potential for complications from reactions with buffer compounds.

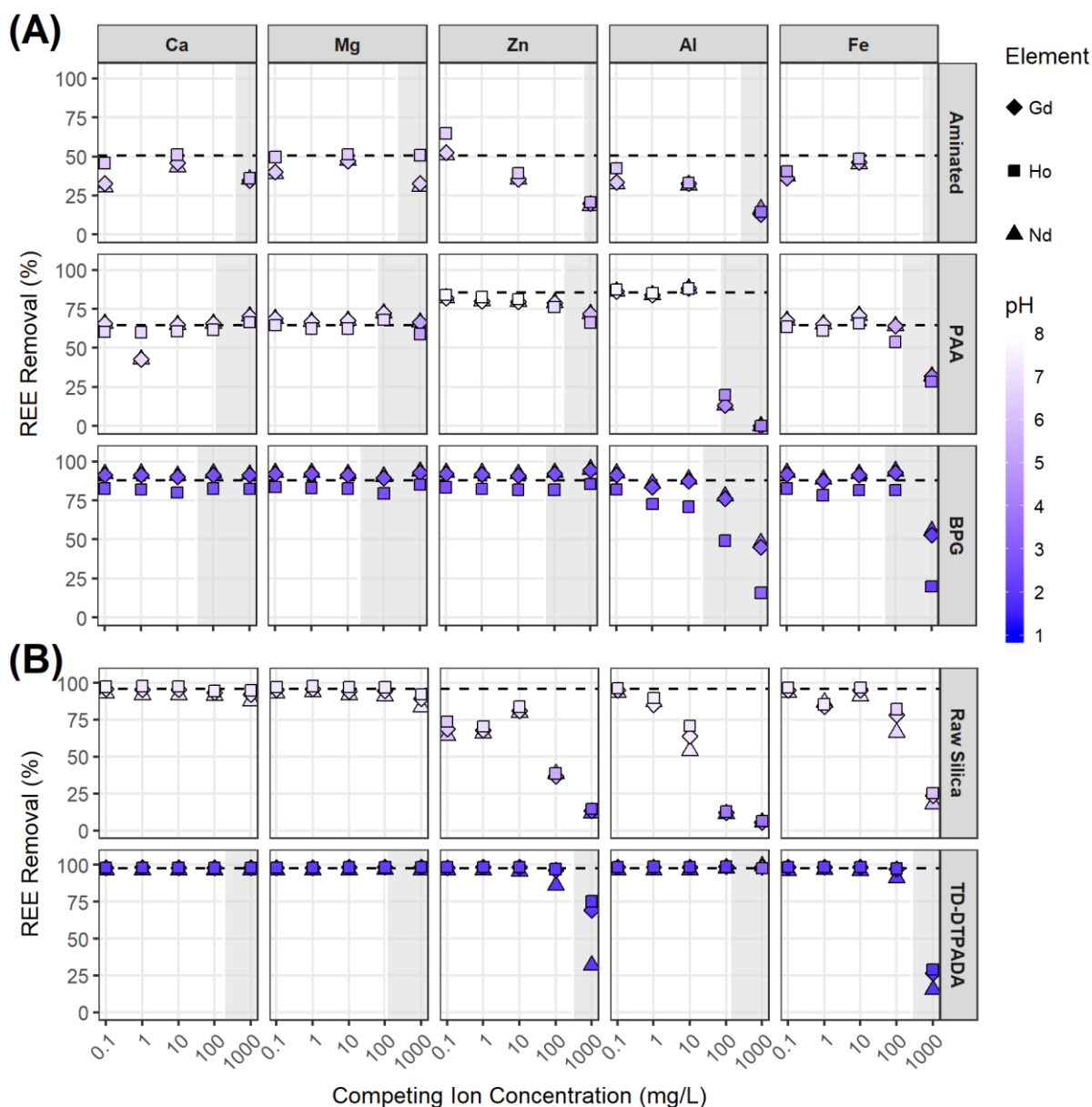


Figure 2.4. Adsorption of 100 µg/L REE mixtures (Nd, Gd, Ho; total REE = 300 µg/L) from 0.5 M NaCl solution onto functionalized silica in the presence of varied concentrations (from 0-1,000 mg/L) of competing ions (Ca, Mg, Zn, Al, and Fe). Dashed lines represent average uptake of REE from control samples (REE+NaCl, no other competing ions), and shaded regions denote the range in which adsorbate concentrations exceeded the available surface binding sites on the adsorbents. Equilibrium pH for each sample is indicated by the data point shading; darker data points are more acidic (pH 1-8; T ~ 20°C). Results are grouped according to the starting support used to make each material: (A) pre-aminated silica, or (B) raw silica gel.

Dashed lines in Figure 2.4 represent average uptake results for Nd/Gd/Ho from control samples containing only 0.5 M NaCl + REE + adsorbents. Grey shaded regions on the plot show where competing ion concentrations exceeded estimated available reactive sites on the

adsorbent surfaces (i.e. potential site saturation, assuming 1:1 ligand-ion complexation). Calculations for available reactive sites on the adsorbent surfaces were based on ligand grafting efficiencies reported in Table 2.1. Data points that align with the dashed control line indicate no reduction in REE adsorption caused by the increased competing ion concentration, while points below the dashed lines indicate reduced uptake of REE in the presence of the competing ion. Calcium showed no impact on the ability of functionalized materials to adsorb REE. Similarly, magnesium showed little competition with REE binding to the functionalized surfaces. Adsorption was reduced in the presence of competing ions for both of the non-functionalized adsorbents (aminated silica and raw silica).

Functionalized adsorbents with BPG showed constant high performance of REE uptake in the presence of Zn at concentrations 0.1-1000 mg/L. Uptake of REE was diminished in the presence of Zn for TD-DTPADA adsorbent and, to a lesser degree, the PAA adsorbent. The competing ion effects were observed at concentrations ≥ 100 mg/L Zn^{2+} for these functionalized adsorbents, but at concentrations ≥ 0.1 mg/L Zn for the raw and aminated silica. Aluminum was expected to be among the most problematic competing ions in acidic conditions, since its trivalent state is the same as lanthanides in solution. Above pH 5, however, hydroxylated species of Al predominate. TD-DTPADA functionalized adsorbents showed high uptake (>97%), even at high Al concentrations (1,000 mg/L, Figure 2.4.B). At Al concentrations of 100 to 1,000 mg/L, the adsorbents functionalized with PAA and BPG exhibited somewhat reduced uptake of REE, while uptake onto aminated and raw silica was reduced at much lower Al concentrations.

Fe (II) reduced REE uptake for all of the solids tested at concentrations of 1,000 mg/L. Iron concentrations this high, though, are unlikely to be encountered in most environmental media, and the reduced REE adsorption may be the result of complications from iron precipitation as the Fe (II) is expected to be oxidized to the less soluble Fe (III) form. This Fe precipitation was evidenced by decreasing equilibrium pH, as well as appearance of a reddish-brown layer at the

bottom of the Teflon sample tubes as Fe concentrations were increased. While the pH drop associated with Fe precipitation appears partially responsible for the diminished REE uptake (see Figure A.2 in the SI), it is also possible that very high levels of iron coat and passivate the adsorbent surfaces, preventing the ligands from interacting with REE in solution through either precipitation of ferric hydroxide onto the adsorbents or direct adsorption of dissolved iron species.

After completion of adsorption reactions for the competition study, TD-DTPADA adsorbents were separated from solution, rinsed with deionized water, dried overnight, then adsorbed elements were eluted using 0.75N HNO₃. The elution data (shown in Figure A.4 and summarized in Figure A.5 of the SI) confirm the adsorption phase results shown here. Approximately 100% of the spiked REE mass was recovered during elution, except for the 1,000 mg/L Zn and Fe samples, where diminished REE uptake was observed. In contrast, very low ratios of mass eluted to mass spiked were observed for the competing ions, particularly at higher spiked concentrations. These results provide further evidence for the specificity of the functionalized adsorbents towards REE over competing ions.

Additionally, a competitive isotherm study was conducted using TD-DTPADA to determine the combined effects of multiple competing ions on REE adsorption (presented in Figure A.6 and summarized in Table A.4 of Appendix A). This test revealed that separation factors (α) – a measure of selectivity defined by the ratio of distribution coefficients (D) of two elements – for REE/Competing Ions were greater than 1 for all samples, with some α values approaching 200, confirming the selectivity of the functionalized adsorbents.

2.3.2. Batch Adsorption Experiments with Great Salt Lake (GSL) Brine

REE uptake trends in the GSL brine are shown in Figure 2.5 for individual elements labeled on the x-axes in order of increasing molecular weight. Results were consistent with the synthetic brine results presented in Figure 2.3. Dashed lines represent 90% uptake for each

element. Darker shading of data points again represents more acidic pH values. Aminated silica did not show an affinity for REE at $\text{pH} \leq 6.1$, although >90% adsorption of scandium (Sc), thorium (Th), and uranium (U) was observed. The raw silica support material showed negligible REE uptake under acidic conditions, but some uptake as pH was increased to 6.9. Generally, heavy REE proved more likely to adsorb to particle surfaces of the non-functionalized particles than light REE. This result was expected since HREE possess a higher charge density than LREE, due to the well-known phenomenon of 'lanthanide contraction' (United States Environmental Protection Agency 2012). PAA adsorbent uptake of REE was greatest under neutral pH conditions, with a preference for heavy REE and a maximum REE uptake of 95% for Yb at pH 7.2. PAA adsorbent uptake of REE was greatest under neutral pH conditions, with a preference for heavy REE and a maximum REE uptake of 95% for Yb at pH 7.2.

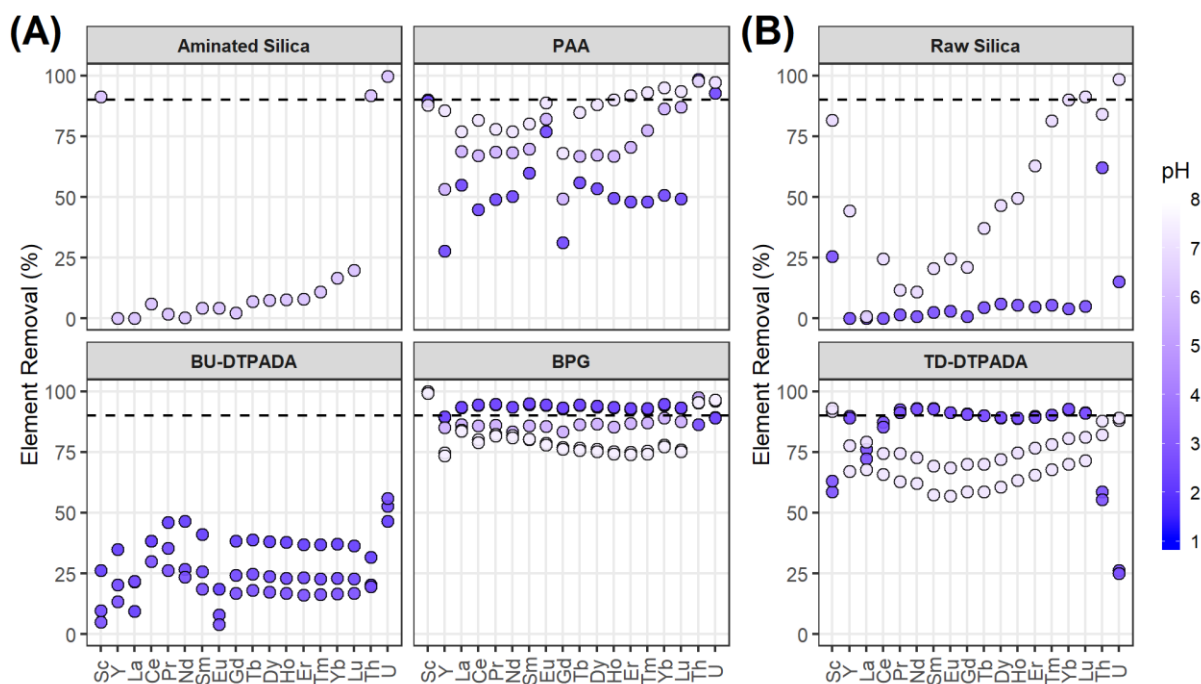


Figure 2.5. Adsorption of elements from Great Salt Lake brine onto silica particles as a function of pH. (A) Aminated silica and bottom-up functionalized adsorbents; (B) Raw silica and top-down functionalized DTPADA silica. Equilibrium pH for each sample is indicated by the data point shading; darker data points are more acidic ($\text{pH} 1-8$; $T \sim 20^\circ\text{C}$). Initial concentrations for each element shown in the mixture were approximately $60 \mu\text{g/L}$; full composition of the brine is shown in Table A.2 in Appendix A.

The BU-DTPADA adsorbent did not display strong adsorption capabilities for REE under the conditions tested. Even in acidic conditions, for which the BU-DTPADA adsorbent was shown

to be effective in synthetic brines, the material adsorbed <50% of the lanthanides from the brine. However, the TD-DTPADA was much more successful in adsorbing REE from the GSL brine, with a similar pH trend to that shown in Figure 2.3, i.e., peak uptake around pH 2, with somewhat diminished uptake in circumneutral to basic conditions. The BPG-functionalized silica was the strongest performer among the group of ligands tested, with relatively high REE uptake efficiencies for all measured samples.

Bisphosphonates are more likely to form stable complexes with cations than are monodentate phosphonate ligands, as evidenced by their high stability constants in the solution phase (Popov et al. 2001). As such, the enhanced REE uptake of BPG-functionalized adsorbent when compared to PAA adsorbent is unsurprising. Further, lanthanides are considered strong Lewis acids, so interactions with strong Lewis bases are highly favorable (Pearson 1963). The amine groups contained within DTPADA and BPG contribute to their high basicity and strengthen their attraction to REE.

Thermal stability of the functionalized adsorbents and their ability to bind REE at elevated temperatures are important performance parameters for application of the adsorbents in brine systems at elevated temperatures, e.g., brines in geothermal energy systems treated for resource recovery purposes. Geothermal brines harnessed for direct-use as an energy source are much hotter than typical groundwater sources, with temperatures routinely exceeding 150°C. Lower temperature brines are beginning to find secondary uses as well, such as direct heat sources for desalination processes (Turchi et al. 2015). Functionalized adsorbents with PAA and TD-DTPADA ligands exhibited higher REE uptake as the temperature of GSL brine increased from 20-100°C (Figure 2.6). These samples were prepared at pH values for which maximum REE uptake was observed in the preceding adsorption edge experiments.

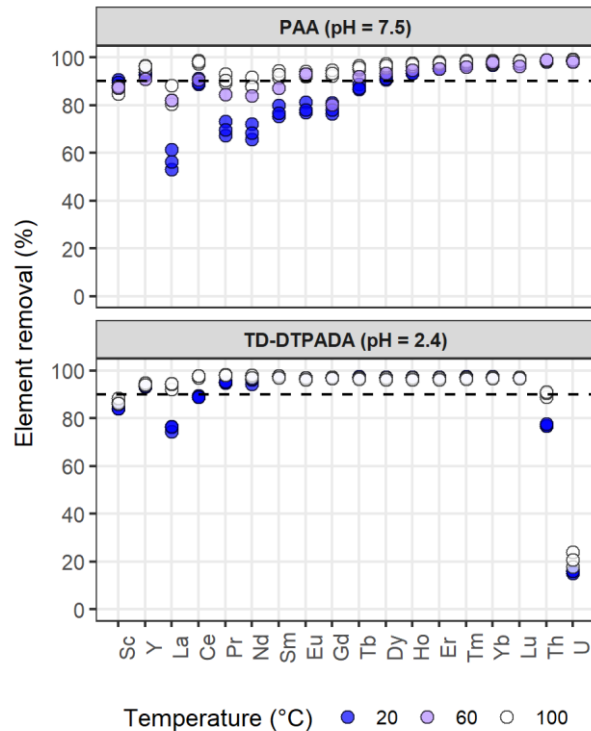


Figure 2.6. Impact of solution temperature on elemental adsorption from Great Salt Lake brine onto functionalized silica particles at fixed pH. Initial concentrations for each element shown in the mixture were approximately 60 $\mu\text{g/L}$.

While adsorption is typically viewed thermodynamically as an exothermic process (Thomas 1961), this type of ligand-binding proceeds endothermically, i.e., additional heat energy further enhances the interactions between surface-bound ligands and dissolved REE. Similar endothermic adsorption trends for REE onto various materials have been previously reported (Smith et al. 2016; Zhang et al. 2016) The addition of heat to the system is thought to facilitate the disruption of the hydration sphere surrounding lanthanides in solution, allowing improved binding with surface-tethered ligands (Anastopoulos et al. 2016). Adsorption of REE onto TD-DTPADA was highly efficient across the observed temperature range, with lanthanide uptake of >90% above 20°C.

Additionally, the TD-DTPADA material exhibited high selectivity in acidic brines towards REE over U, an element which is frequently found alongside the lanthanides in ores and presents

a challenge to traditional separation methods. This result is consistent with literature which has suggested that pH can influence the selectivity of DTPA ligands for lanthanides (Roosen and Binnemans 2014). Selectivity in acidic conditions for this experimental system may be the result of improved ligand availability to interact with REE in the aqueous solution. When protonated, lower attractive forces exist between unreacted primary amines on the particle surfaces and carboxyl groups in the attached ligand, allowing for greater flexibility of the bound ligand molecule to coordinate REE.

Separation factors for REE/U onto TD-DTPADA averaged 130 at pH 2.3-2.5, with α values for some REE reaching as high as 244 under the conditions tested. In comparison, $\alpha_{\text{REE/U}}$ for the raw and aminated silicas at their optimal pH values for REE uptake were typically less than 1 (i.e. no selectivity towards REE). Separation factors for each material are provided in Table A.3 in Appendix A.

2.3.3. Adsorbent Elution and Reuse

The ability to elute and recover adsorbed REE and reuse the adsorbent particles is important for determining the economic and technical viability of SPE technology for large-scale resource recovery. Elution is achieved by adding acid to the system to re-protonate the carboxyl and/or nitrogen groups on the ligands, resulting in the release of the bound REE. This concept is routinely employed to regenerate cation exchange resins using strong acids such as HCl or H₂SO₄.

An elution study was conducted to determine the acid concentration required to recover adsorbed REE efficiently. Different concentrations of HNO₃ (0.01-6.55 N) were used to determine the minimum possible acid concentration to elute the bound REE (Figure 2.7). Elution from TD-DTPADA particles was nearly 90% complete when using 6.55 N HNO₃. Some losses of REE were observed, resulting in minor differences between calculated masses of REE adsorbed vs. REE

eluted. These losses perhaps occurred during the DI rinse and decanting phases (designed to minimize cross-contamination) that took place in between adsorption and elution cycles, wherein a small mass of adsorbent particles may have been inadvertently poured out with the DI rinse solution. Sample dilution prior to analysis on ICP-MS may also have introduced a degree of error when assessing the mass balance for REE in the experimental system. Recovery efficiencies plateaued above 1N acid concentrations, suggesting diminishing returns beyond that point in this experimental design. Elution trends for BPG were similar to the TD-DTPADA, with a plateau in recovery observed above 1N (Figure A.3 in the SI).

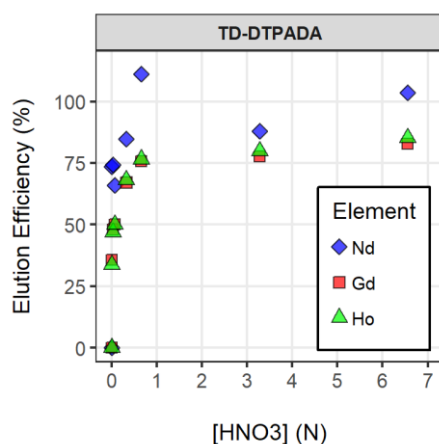


Figure 2.7. REE elution efficiency for DTPADA on silica as a function of nitric acid strength after one use cycle. Adsorption cycle was performed at pH ~ 1.8.

Data presented thus far have shown that REE can be adsorbed to ligand-functionalized silica particles and eluted with relatively low concentrations of strong acid. Implementation in a real resource recovery process will require the materials to be robust; particles will need to retain their performance through multiple adsorption/elution cycles. Figure 2.8.A shows the adsorption results (percent removal vs. pH) for each ligand through three usage cycles. The particles were eluted with HNO₃ (0.75 N), rinsed with DI water, and dried overnight at 100°C between adsorption cycles. Solids were allowed to cool and adsorption reactions were performed at room temperature (~20°C).

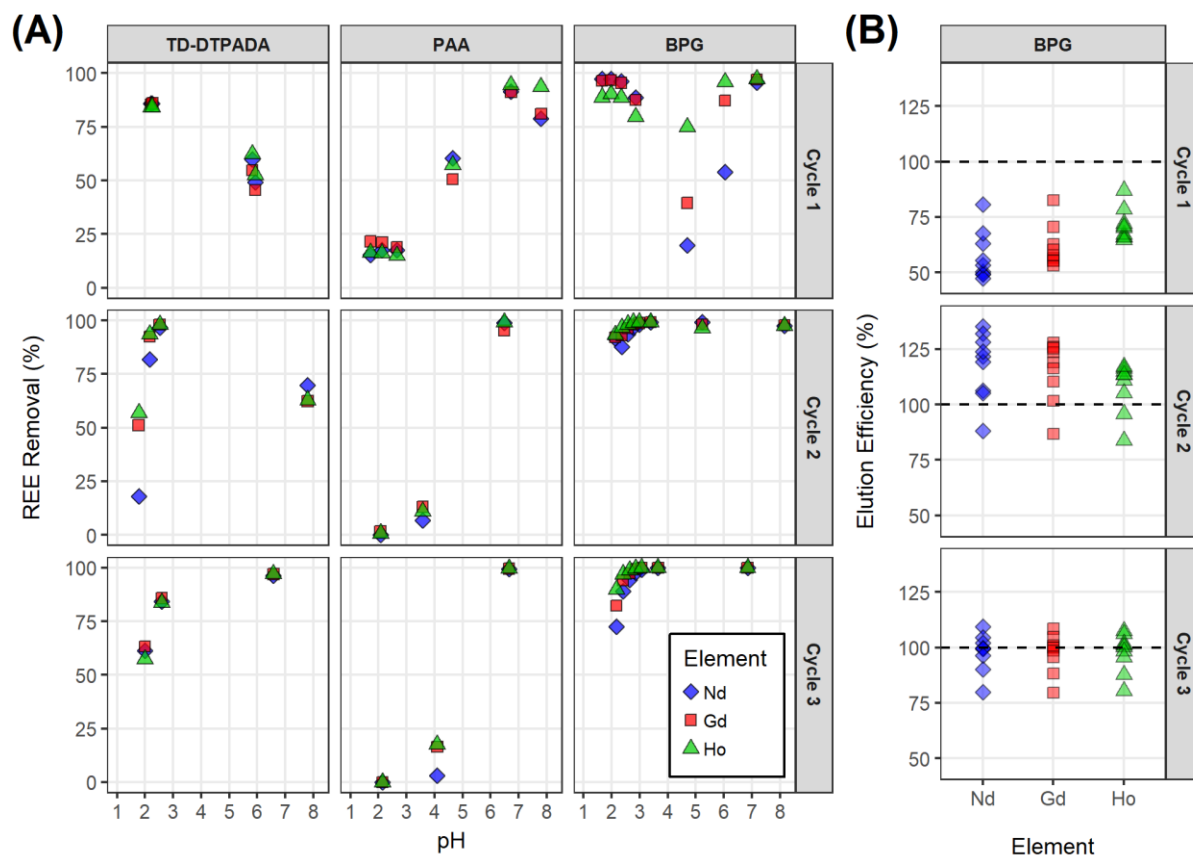


Figure 2.8. (A) Adsorption of 100 µg/L REE mixture from 0.5 M NaCl onto functionalized silica particles through three adsorption and elution cycles; (B) Elution data for BPG functionalized silica.

TD-DTPADA functionalized silica retained its performance with REE adsorption at pH 2.5 through all three cycles, and uptake at neutral pH seemed to improve slightly with more use. The reduced adsorption observed below pH 2.5 was attributed to diminished surface-REE interaction due to ligand protonation. Improved performance of TD-DTPADA and BPG at circumneutral pH, and the simultaneous diminished uptake in acidic conditions, may also be explained by the release of ligand from particle surfaces by acid-hydrolysis of the amide tether, leaving more basic primary amines on the surface. Similarly, PAA uptake trends were stable throughout the reuse study, suggesting strong and durable ligand attachments. The BPG ligand demonstrated high REE uptake in both acidic and basic pH ranges. In the first cycle, reduced REE uptake was observed at pH 4.5, but this minimum was not observed in subsequent cycles.

Elution data for BPG are presented in Figure 2.8.B. The first cycle yielded an average elution efficiency of 63% (comparable to the BPG elution results from Figure A.3 in the SI), while cycles two and three averaged 114% and 98%, respectively. It is hypothesized that the low elution efficiency in the first cycle may be attributable to residual reactants from the functionalization process, i.e., excess BPG molecules not covalently bound to the silica support surface remaining on the fresh BPG particle surfaces during the uptake step. These weakly attached compounds would be washed away prior to the elution, carrying with them some complexed REE and thus causing discrepancies between the calculated adsorbed mass and the measured concentrations in elution samples. Elution efficiencies of >100% in the second cycle also indicate recovery of additional REE mass not eluted during cycle 1. The evolution of BPG performance trends with additional use cycles may also be the result of sodium conditioning. Adsorbents were subjected to relatively high concentrations of NaCl in this study, which may play a role in their conversion by replacing hydrogen on the particles with sodium. The performance of each adsorbent was either preserved or improved after the first use.

2.4. Summary and Conclusions

Silica particles functionalized with BPG, DTPADA, and PAA were shown to be highly effective in adsorbing lanthanides from synthetic and real brine. Each material resulted in a unique REE adsorption profile with respect to pH, with some materials performing well in neutral-to-basic conditions (PAA, BPG), and others adsorbing REE most effectively in acidic solutions (DTPADA, BPG). In studies of competitive adsorption of REE with some major ions that commonly occur in brines such as acid mine drainage or geothermal fluids, REE uptake was found to be mostly unaffected by environmentally relevant concentrations of competing ions. Successful elution of adsorbed REE was achieved with HNO₃ concentrations as low as 0.7 N, with no degradation in adsorbent performance over multiple reuse cycles. The adsorbents were found to be selective for REE in experiments with both the synthetic and actual brine solutions, and at solution

temperatures as high as 100°C, as are encountered with brines in geothermal energy systems. The strong efficacy of these adsorbents highlights their potential for application in REE resource recovery and pre-concentration schemes.

CHAPTER 3

Adsorption Kinetics, Thermodynamics, and Isotherm Studies for Functionalized Lanthanide Chelating Resins

Contents of this chapter have been submitted for publication:

J. C. Callura, K. M. Perkins, J. Baltrus, N. R. Washburn, D. A. Dzombak, A. K. Karamalidis, 'Adsorption Kinetics, Thermodynamics, and Isotherm Studies for Functionalized Lanthanide Chelating Resins,' *Applied Materials & Interfaces* **SUBMITTED**

3.1. Introduction

This research expanded our previous work with ligand-functionalized adsorbent particles (Callura et al. 2018; Noack et al. 2016) by studying the performance of chemically modified resins (d ~0.6 mm) grafted with REE-selective ligands. Particles with large diameters, like those used in this study, facilitate continuous-flow processes, such as fixed-bed or fluidized-bed adsorption columns, though trade-offs are to be expected with regards to potentially slower uptake kinetics and lower adsorption capacity on an adsorbent mass basis. Before large-scale REE recovery systems can be developed, it is necessary to understand the performance trends and binding mechanisms of functionalized resins. Process design parameters are dependent on fundamental adsorption properties, such as kinetics, capacity, thermodynamics, and selectivity. In this work, we experimentally investigated the former three property types along with physical adsorbent properties, such as surface area and porosity.

The overall goal for this work was to characterize the REE adsorption performance of aminated resins grafted with three different REE-chelating ligands. Specific objectives were to determine the REE uptake kinetics, adsorption capacity, and thermodynamic parameters for lanthanide binding by large-scale functionalized resins. Experimental results were compared to modeling results based on speciation of the metals/ligands and solution phase ligand-lanthanide complexation.

3.2. Materials and Methods

3.2.1. Functionalization

A divinylbenzene-crosslinked polystyrene particle (d ~0.6 mm) containing primary amine surface groups was selected for this study due to its favorable performance in screening tests, as well as its high porosity and demonstrated chemical/thermal stability. Three ligands were employed for this study due to their well-documented affinity for REE: phosphonoacetic acid

(PAA), *N,N*-bis(phosphonomethyl)glycine (BPG), and diethylenetriaminepentaacetic dianhydride (DTPADA) (Grimes and Nash 2014; Krishnamurthy and Gupta 2004; Nash 1997).

The synthesis scheme used to produce these resins has been reported previously (Callura et al. 2018; Noack et al. 2016). Aminated resins were mixed with dimethylformamide (DMF), propylphosphonic anhydride (T3P), 4-(dimethylamino)pyridine (DMAP), and the target ligand in a one-pot reaction. After mixing for 24 hours at room temperature under inert atmosphere, the resins were transferred to centrifuge tubes and washed with DMF, followed by hot water ($T \sim 70^{\circ}\text{C}$), with excess fluid decanted between wash steps. Resins were then subjected to an additional cleaning phase by mixing with 0.75N trace metal grade nitric acid (HNO_3) overnight, followed by rinsing with deionized water. This cleaning step was previously shown to improve and stabilize performance by washing away excess unbound reactants (Callura et al. 2018).

Expected ligand configurations on the aminated resin surfaces are presented in Figure 3.1. The anhydride rings of DTPADA hydrolyze upon exposure to water (Bunton et al. 1963), resulting in the form shown here, though the 'DTPADA' label is used throughout this paper to maintain consistency with our previous work. Likely structures for REE-DTPADA complexes on particle surfaces are shown in Figure B.1 of the Appendix B. Other non-ideal ligand configurations may also be present along with those forms shown here. For example, surface-tethered ligands may interact electrostatically with residual surface amines or adjacent ligands.

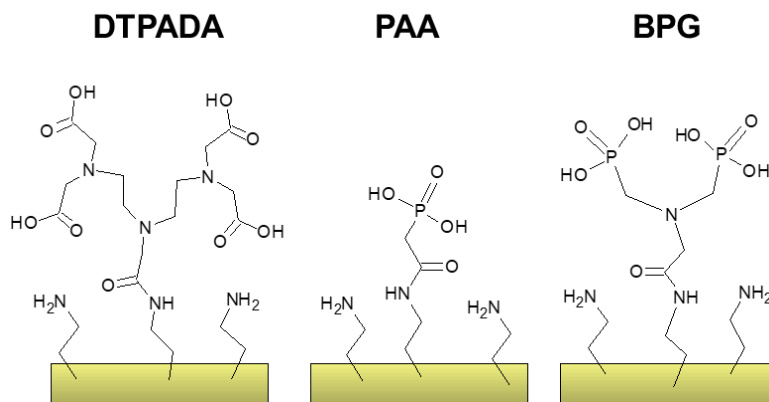


Figure 3.1. Expected configurations of surface-tethered REE-chelating ligands shown with residual unreacted primary amines.

3.2.2. Characterization

3.2.2.1. XPS for Quantification of Ligand Loadings

X-ray photoelectron spectroscopy (XPS) was used for quantification of ligand loading. The XPS measurements were carried out with a PHI 5600ci instrument using a monochromatic Al K α X-ray source. An electron flood gun was used to prevent sample charging during the analysis. The pass energy of the analyzer was 58.7 eV, the acquisition area had a diameter of ~800 μ m, and the scan step size was 0.125 eV. Binding energies were corrected for charging by referencing to the C 1s peak at 284.8 eV. Atomic concentrations were calculated from the areas under individual high-resolution XPS spectra using manufacturer-provided sensitivity factors. The C 1s and N 1s spectra were resolved into their individual components using CasaXPS software. Separate XPS analyses were carried out at two different spots on each of two sample adsorbent particles and the reported results are the averages of the values measured at those two spots. Details for data analysis on the XPS results are provided in the Appendix B.

3.2.2.2. BET for Determination of Specific Surface Area

The Brunauer–Emmett–Teller (BET) surface area and Barrett–Joyner–Halenda (BJH) pore size were determined for the adsorbent particles using nitrogen adsorption data collected via a

Micrometrics Gemini VII surface area analyzer. Prior to measurement, samples were degassed under vacuum for 24 hours at room temperature.

3.2.2.3. Adsorbent Titrations for Acid/Base Characteristics

Acid-base adsorbent titrations were performed to study particle surface chemistry using a Metrohm 798 MPT Titrino autotitrator. Solutions containing 50 mL 0.5M NaCl and 100 mg of resin particles were prepared and acidified with HCl prior to titration to ensure comparable pH starting points for each resin. Titrants were added to continuously-mixed solutions at variable rates (<100 $\mu\text{L}/\text{min}$) according to the slope of the pH vs. volume added curve, with the minimum flow rates administered in high slope regions. The base titration was performed with 0.1N NaOH in 0.5M NaCl to maintain a constant ionic strength. After pH 12 was reached, the autotitrator was flushed with 0.1N HCl in 0.5M NaCl and the titration was reversed by adding HCl until pH reached ~ 2 . Slopes of the pH-volume curves were analysed to determine equivalence points (identified by local slope maxima) and pK_A values (determined by finding the pH values at half equivalence points).

3.2.3. REE Adsorption Experiments

Adsorption kinetics studies were carried out by reacting mixtures containing 0.5M NaCl, 100 $\mu\text{g}/\text{L}$ each of Nd, Gd, and Ho (300 $\mu\text{g}/\text{L}$ total REE, prepared by dissolving $\text{Ln}(\text{NO}_3)_3$ salts), and 10 g/L functionalized resins at a fixed temperature (20°C) and pH value. High salt concentrations were selected to simulate the ionic strength of potential aqueous feedstocks to which these adsorbents could be applied (e.g., brines or various industrial wastes). Resins were pre-equilibrated for three hours with 0.5M NaCl prior to reaction with REE-containing solutions. Reaction times ranged from 5 minutes to 4 hours. Each data point represents an individual batch sample. Solution phase rare earth element concentrations were determined by inductively coupled plasma mass spectrometry (ICP-MS) before and after reaction, and removal efficiencies were calculated by differences between these values.

Thermodynamic properties of the resins were evaluated by conducting equilibrium adsorption experiments at varied temperatures. Batch samples were prepared with varied concentrations of Nd, Gd, and Ho at equal mass ratios (0.3-300 mg/L total REE) in 0.5M NaCl and 10 g/L resins at a fixed pH value. Samples were reacted for 24 hours by mixing at 300 revolutions per minute at three different temperatures (20°C, 60°C, 100°C).

Equilibrium adsorption isotherm studies were conducted by preparing batch samples with varied REE concentrations in 0.5M NaCl at fixed pH (6.5 for amine, PAA, BPG, or 2.5 for DTPADA) and fixed temperature (20°C, 60°C, or 100°C). Additionally, equilibrium adsorption pH edge studies were conducted at different REE loadings for BPG and DTPADA to determine the influence of adsorbate concentrations on pH trends. Individual batch samples containing a mixture of three REE in 0.5M NaCl and 10 g/L resins were prepared, and their pH values were modified by adding either HCl or NaOH.

3.2.4. Modeling of REE Complexation by Solution-Phase Ligands

Solution-phase complexation models were applied to evaluate differences in performance between free aqueous-phase ligands and surface-tethered ligands. Modeling of REE-DTPA and REE-PAA complexes in the solution-phase was performed using the U.S. Geological Survey's PHREEQC program (Charlton and Parkhurst 2011; Parkhurst and Appelo 2013) implemented in the R programming language (R Core Team 2017), as described in Appendix B. Surface ligand concentrations were determined by measuring surface concentrations from XPS analysis and equivalent solution-phase concentrations were calculated using the solids loading from adsorption experiments (i.e., surface ligand loading [mmol/g] * adsorbent loading [g/L]).

3.3. Results and Discussion

3.3.1. Characterization

3.3.1.1. Ligand Loading and Specific Surface Area

Our previous work (Noack et al. 2016) with functionalized silica ($d \sim 0.1$ mm) reported ligand loadings of 0.96 mmol/g (amine), 0.15 mmol/g (PAA), 0.09 mmol/g (BPG), and 0.27 mmol/g (DTPADA). Surface-bound ligand concentrations for the polymer resins (Table 3.1; additional XPS data are provided in Table B.1 of Appendix B) are higher than for the silica, despite the resins being ~ 6 times larger in diameter ($d \sim 0.6$ mm). This translates to ligand densities (mmol/m²) roughly two orders of magnitude higher for the polymer resins than for silica and is likely due to the higher degree of amination on the resin surface and greater porosity of the resins. Amine conversion efficiencies for functionalized resins (6-11%) were slightly lower than the functionalized silica (9-28%), so residual primary amines are expected to be present in addition to the surface-tethered ligands on both functionalized supports. Adsorption performance trends were similar for both functionalized supports (Figure B.10 of Appendix B).

Table 3.1. Summary of resin characterization results. Ligand loadings were calculated from XPS measurements, BET surface area and BJH pore volumes were determined from nitrogen adsorption tests.

Ligand	Ligand Loading (mmol/g)	Surface Area (m ² /g)	Avg Pore Width (nm)	Pore Volume (cm ³ /kg)			Ligand Density (mmol/m ²)
				Micro	Meso	Macro	
Amine	4.00	14.8	24.5	0.67	6.9	68	0.281
PAA	0.33	12.7	27.7	0.22	8.6	74	0.026
BPG	0.22	8.0	30.8	0.14	3.7	56	0.028
DTPADA	0.42	11.4	33.4	0.17	3.8	99	0.037

Attachment of chelating ligands to primary amines on the resin particle surfaces resulted in reduced surface area for the PAA, BPG, and DTPADA functionalized resins. Existing research has also shown that functionalization may decrease particle surface area (Hu et al. 2017). Table 3.1 shows higher average BJH pore sizes for PAA, DTPADA, and BPG functionalized materials

relative to the aminated support, which is likely a result of the ligands occupying the smallest micropores and shifting the pore width distributions. This is further evidenced by pore volume distributions for each material, which show that the aminated resins have the highest volume of micropores ($d < 2$ nm) among the tested materials.

Reaction parameters for resin functionalization were varied in an attempt to improve the ligand grafting efficiency. Standard synthesis conditions (reaction time = 24 hours, temperature = 20°C) which were used to produce the materials used in the following experiments (properties shown in Table 3.1) were altered by synthesizing the adsorbents for a longer time period (72 hours) or at a higher temperature (40°C), and their resulting ligand concentrations were measured using XPS (results shown in Table B.3 of Appendix B). PAA concentrations for the standard synthesis method (24 hours at 20°C) were higher than those from the previous batch (Table 3.1) which used the same conditions, indicating some degree of 'batch-to-batch' variability. Higher temperature and longer reaction time did not result in significantly different ligand loadings for PAA-functionalized resins, though the attachment of DTPADA and BPG ligands was improved in the altered conditions (18-48% improvement from standard method). These improvements may be related to factors such as thermal expansion of the adsorbent particles, which facilitates access of the ligands to the particle pore space. Calculations for maximum theoretical ligand concentrations, based on ligand molar volume and resin surface area, are shown in Appendix B and indicate that ligand loadings are not limited by steric effects. Further improvements may be possible by using different reagents and linkers for the resin synthesis.

The effect of molar ratio of ligand to surface amines on adsorbent performance was also evaluated. The ratio of BPG to surface amines was increased from the standard value of 2:1 to 5:1. Adsorption pH edge experiments were then performed with the resulting adsorbents (Figure B.2 of Appendix B). The 5:1 ligand ratio resulted in diminished performance when compared to the 2:1 ratio during the first use cycle. The adsorbents were then eluted with 0.75N HNO₃, rinsed

with DI, and dried, then used for another cycle. The adsorption trends of the 5:1 and 2:1 BPG-functionalized adsorbents converged in the second use cycle, suggesting that the high excess of ligand for the 5:1 synthesis may not result in improved covalent ligand attachment, but rather physical deposition of the excess ligand which are then washed away during the subsequent HNO₃ elution.

3.3.1.2. Acid/Base Titrations

Titration curves (Figure 3.2.A) were analyzed to find the equivalence points for each titration. Curve slopes were plotted against pH (Figure 3.2.B) to find peaks which indicate titration equivalence points. The corresponding titrant volumes were recorded to find the particle pK_A values (pH at ½ equivalence point). Data are truncated between pH 3 and 12 to emphasize the region of interest.

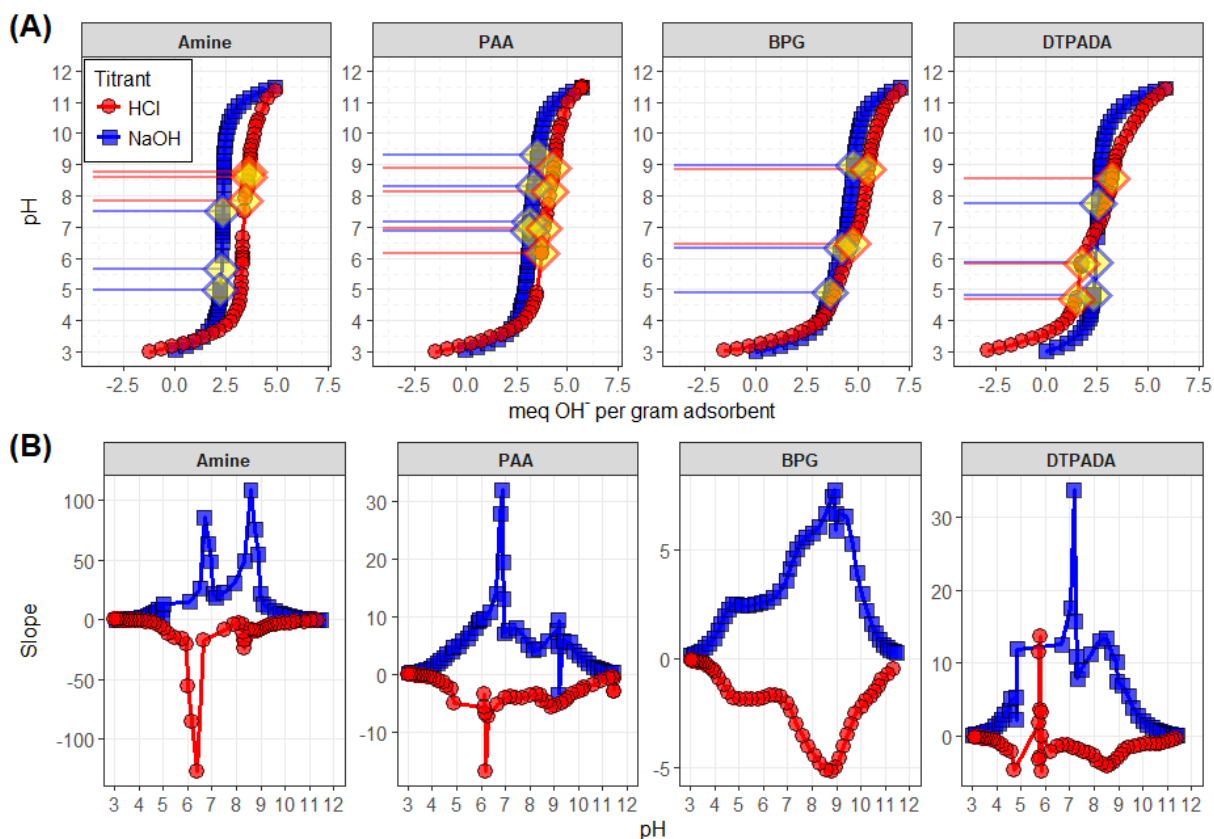


Figure 3.2. (A) Acid-base titration results for amine and functionalized resins. Yellow diamonds and solid horizontal lines indicate pK_A values. (B) Comparison of slope from panel A with sample pH.

Ligand acidity constants were expected to change upon attachment to particle surfaces due to the formation of an amide bond between the carboxyl groups present on each ligand and the primary amines on the resins. It has been reported that substitution of carboxyl groups from DTPA with an amide group results in greater ligand acidity (Paul-Roth and Raymond 1995; Sherry et al. 1988). In all cases, the acidity constants for the functionalized resins were different than reference values for the untethered solution-phase ligands (Table 3.2). Differences between acidity constants for acid vs. base titrations are attributed to hysteresis effects, which were most prevalent for the amine particles.

While primary amines should only have one pK_A value, additional equivalence points suggest the presence of other background functional groups. In contrast, the BPG and DTPADA

functionalized resins had fewer equivalence points than expected. This may be due to a shift of lower pK_A values below the studied range (i.e., below pH 2). Since the PAA, BPG, and DTPADA functionalized resins are expected to also have residual primary amines on their surfaces, these values should be taken as an approximation of overall surface functionality.

Table 3.2. Acidity constants for each functionalized resin derived from base (OH^-) or acid (H^+) titrations. Reference values are provided to show pK_A for each ligand in solution phase.

Ligand Titrant	Amine			PAA			BPG			DTPADA		
	OH^-	H^+	Ref. ^a	OH^-	H^+	Ref. ^b	OH^-	H^+	Ref. ^c	OH^-	H^+	Ref. ^d
pK_{A1}	7.5	8.8	9.25	9.3	8.9	7.69	9.0	8.8	10.89	7.8	8.5	9.86
pK_{A2}	5.7	8.6		8.3	8.1	4.66	6.3	6.5	6.77	5.9	5.8	8.32
pK_{A3}	5.0	7.8		7.2	6.9	1.12	4.9		5.20	4.8	4.7	4.12
pK_{A4}				6.9	6.2				2.0			2.85
pK_{A5}									-2			1.95

^a (Benjamin 2010);

^b (Nash 1997);

^c ("N,N-Bis(phosphonomethyl)glycine $\geq 98.0\%$ (T) | Sigma-Aldrich" n.d.);

^d (Gritmon et al. 1977)

3.3.2. REE Adsorption Results

3.3.2.1. Kinetics

Adsorption is measured as the mass of REE bound to the resins and increases with time until plateauing at the equilibrium value in well-mixed batch systems. Adsorbed phase concentrations (q) were calculated based on differences between initial (C_0) and equilibrium solution phase concentrations (C_e), sample volume (V), and resin mass (M), as shown in Equation 3.1.

$$q = \frac{(C_0 - C_e)V}{M} \quad (\text{Equation 3.1})$$

These experiments were conducted at relatively low adsorbate concentrations (300 $\mu g/L$ total REE) considering the expected REE uptake capacity for the functionalized resins. Uptake kinetics are expected to increase with increasing adsorbate concentrations due to sharper concentration gradients, so the rates shown here are conservative estimates.

Adsorption kinetics data are commonly described and interpreted using a variety of numerical models. First- and second-order kinetic models (Figure 3.4.A) are among the most routinely utilized in describing the time dependence of adsorption processes (Anastopoulos et al. 2016). First- and pseudo-second-order kinetics are defined in Equations 3.2 and 3.3, where k_1 is the first order rate constant, C is concentration at a time 't', and C_0 is the initial solution phase concentration.

$$\frac{-dC}{dt} = k_1 C \Rightarrow \ln C = -k_1 t + \ln C_0 \Rightarrow C = C_0 e^{-k_1 t} \quad \text{(Equation 3.2)}$$

$$\frac{-dC}{dt} = k_2 C^2 \Rightarrow \frac{1}{C} = \frac{1}{C_0} + k_2 t \Rightarrow C = \frac{1}{1/C_0 + k_2 t} \quad \text{(Equation 3.3)}$$

For an adsorbate molecule to interact and attach to the adsorbent surface, it must undergo 4 sequential transport processes: (1) advection with the bulk fluid, (2) diffusion into the liquid film at the interface of the adsorbent and fluid, (3) diffusion into the particle pore space, and (4) reaction with the adsorbent surface (illustrated in Figure 3.3). Intraparticle diffusion is shown here as one step, though it may be further differentiated into macropore, mesopore, and micropore diffusion. Binding kinetics can be rate-limited by any of these steps, though the limiting step is dependent on flow/mixing, adsorbate, and adsorbent properties.

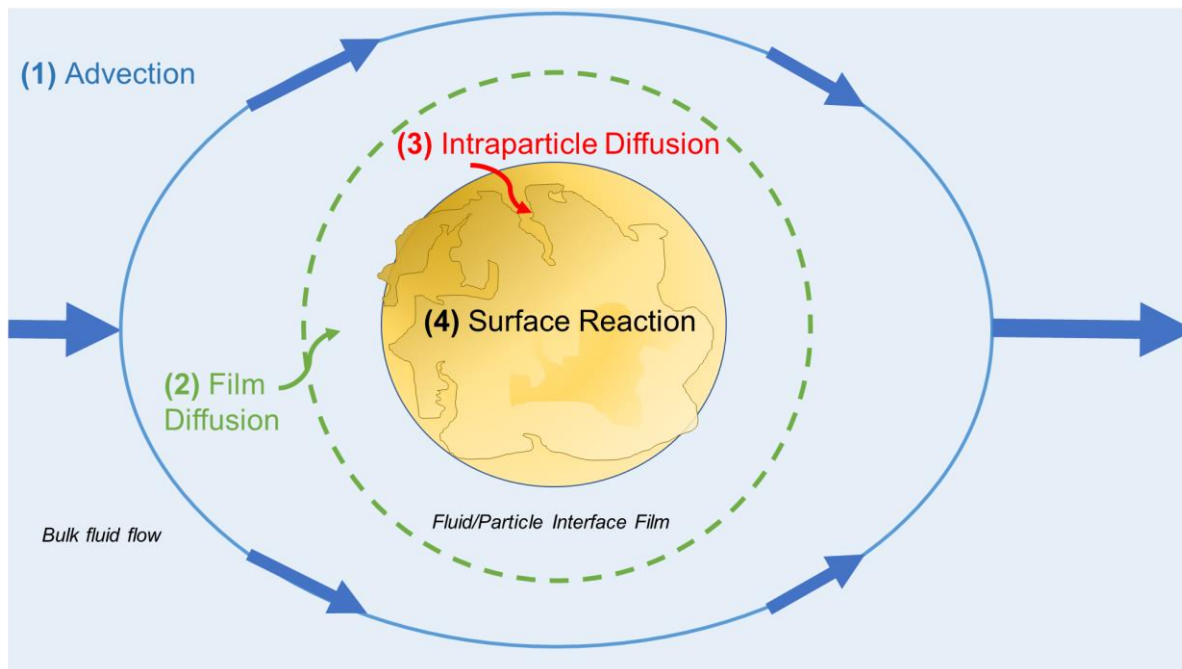


Figure 3.3. Summary of adsorbate transport processes.

While the first- and second-order models provide useful tools for assessing kinetic trends, they do not reveal information about the nature of rate-limiting steps. Mechanistic intraparticle diffusion models have been developed to describe processes of adsorption (Weber and Morris 1963). By plotting adsorption data as a function of the square root of time and conducting a piecewise linear regression (Figure 3.4.B), it becomes possible to observe linear regions associated with different stages of intraparticle diffusion of adsorbate (Galhoum et al. 2015, 2017; Smith et al. 2016; Yang et al. 2014). Equation 3.4 defines the rate ($k_{id,n}$) for each linear region, where the intercept (C_{id}) indicates boundary layer effects. The linear region with the lowest slope, and thus the highest intercept value, is the rate limiting step.

$$q_t = k_{id,n}t^{0.5} + C_{id} \quad \text{(Equation 3.4)}$$

Adsorption was most rapid for the BPG resins, followed by PAA, then DTPADA, as defined by their respective rate constants (Table 3.3). The aminated resins did not adsorb significant amounts of REE, due to the solution pH (5.3). Our previous work with silica supports (Callura et

al. 2018) revealed that uptake onto the aminated particles was negligible below pH 8. These experiments targeted pH values below 8 to minimize the potential for precipitation of REE as hydroxide species which occurs in basic conditions.

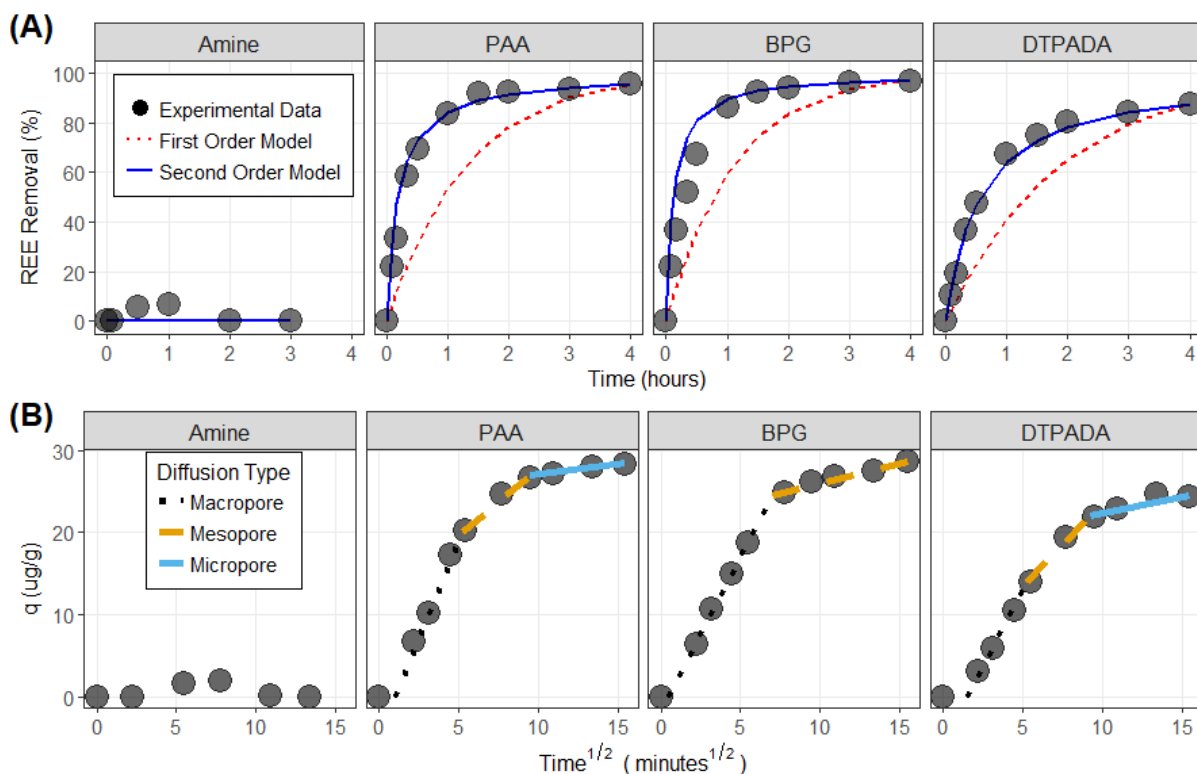


Figure 3.4. (A) Kinetics data for adsorption of total REE (Nd, Gd, Ho) on functionalized resins, fit with first- and second-order models. (B) Weber-Morris plots for intraparticle diffusion modeling of the kinetics data. ($C_0 = 100 \mu\text{g/L}$ each Nd, Gd, Ho, $300 \mu\text{g/L}$ total REE; $\text{NaCl} = 0.5\text{M}$; Resins = 10g/L ; Temperature = 20°C ; pH = 5.3 (Amine), 5.4 (PAA), 5.6 (BPG), 2.3 (DTPADA))

Table 3.3. Kinetic modeling parameters for adsorption on functionalized resins

Surface Ligand	First-Order (min^{-1})		Second-Order ($\text{g mg}^{-1} \text{min}^{-1}$)		Intraparticle Diffusion ($\mu\text{g g}^{-1} \text{min}^{-1/2}$)		
	k_1	R^2	k_2	R^2	$k_{id,1}$	$k_{id,2}$	$k_{id,3}$
PAA	0.0128	0.83	0.31	0.96	4.71	1.65	0.23
BPG	0.0151	0.88	0.49	0.99	3.77	0.49	-
DTPADA	0.0088	0.90	0.10	0.99	3.73	2.00	0.40

Nash et al. (Nash et al. 2012) previously reported that the formation of REE-DTPA complexes in solution proceeds as a pseudo-first-order process with an observed rate constant

of approximately 600-2,400 min^{-1} , depending on pH and ligand concentration. Comparing these estimates with observed rate constants shown in Table 3.3 suggests that the complexation reaction is not the rate-limiting step. First-order rate constants for REE complexation with solution phase DTPA are ~5 orders of magnitude higher than rates for the functionalized resins, though second-order rate models provided a better fit for the experimental data in this study.

Previous research on adsorption mechanisms has shown that y-intercepts of approximately zero for the first linear region of Weber-Morris plots indicate minimal influence from boundary effects at the fluid-particle film interface (Smith et al. 2016). The first y-intercept values from our experimental data (Figure 3.4.B) are ~0, so the mixing rate used in these experiments was sufficiently high to negate any significant influence from film diffusion at the particle interface as a rate limiting step. Thus, intraparticle diffusion was the dominant factor in controlling the speed of REE adsorption in the batch system. Micropore diffusion rates were not discernable for the BPG resins, since only two linear regions were observed in the BPG Weber-Morris plot (Figure 3.4.B). This finding is consistent with characterization results which showed that BPG had the lowest portion of micropores of the studied resins, with 80% less micropore volume than the aminated support.

3.3.2.2. *Thermodynamic Studies*

Data for thermodynamic properties such as Gibbs free energy, entropy, and enthalpy assist in the interpretation of adsorption mechanisms and binding strength. These parameters provide insight into the strength and type of bonds present in a chemical system and are derived from equilibrium adsorption isotherm data collected at fixed temperatures. Relationships between enthalpy (ΔH), entropy (ΔS) and Gibbs free energy (ΔG) at standard states are described in Equation 3.5. The equilibrium constant for adsorption (K_0) can be found by taking the intercept of the plot for the natural log of the ratio of adsorbed concentration (q , mg/g) to equilibrium solution phase concentration (C_e , mg/L) vs. adsorbed concentration (i.e., $\ln(K_0) = y\text{-intercept of } \ln(q/C_e)$)

vs. q) (Alam et al. 2005; Jin et al. 2017). The reaction quotient, Q, is used to calculate the change in Gibbs free energy (ΔG) from the standard state, where T is the reaction temperature (in Kelvin) and R is the gas constant (0.0083145 kJ/K-mol).

$$\ln K_0 = -\frac{\Delta H^0}{RT} + \frac{\Delta S^0}{R} \Rightarrow \Delta G^0 = -RT \ln(K_0) \Rightarrow \Delta G = \Delta G^0 + RT \ln Q \quad (\text{Equation 3.5})$$

Data from thermodynamic tests with the functionalized adsorbents (Figure B.14 and Figure B.15 of the Appendix B) were truncated below q values of 3 mg/g total REE to focus on the contribution from complexation of REE by surface-tethered ligands, rather than non-specific adsorption to other, weaker binding sites on the particle surfaces. This range of interest was determined from isotherm results presented later in Section 3.3.2.3. Thermodynamic parameters were calculated from the truncated datasets to evaluate the influence of temperature on REE adsorption (Table 3.4). Higher K_0 values indicate that adsorption onto the ligand-functionalized resins was more favorable than the unmodified aminated supports.

Table 3.4. Thermodynamic parameters for adsorption of REE mixtures (Nd, Gd, and Ho) from 0.5M NaCl solutions onto functionalized resins. (pH = 6.5 for Amine, PAA, and BPG or 2.5 for DTPADA)

Ligand	Element	T (°C)	ln(K ₀)	ΔG° (kJ/mol)	ΔH° (kJ/mol)	ΔS° (J/K-mol)
Amine	Nd	20	-4.90	11.95	15.90	10.52
		60	-5.28	14.63		
		100	-3.41	10.57		
	Gd	20	-4.60	11.21	13.84	6.30
		60	-4.97	13.76		
		100	-3.30	10.23		
	Ho	20	-4.52	11.01	10.18	-4.28
		60	-4.59	12.72		
		100	-3.57	11.08		
PAA	Nd	20	-0.35	0.85	12.58	37.06
		60	-0.89	2.46		
		100	0.85	-2.65		
	Gd	20	-0.72	1.76	13.41	37.36
		60	-0.99	2.75		
		100	0.53	-1.66		
	Ho	20	-0.63	1.55	14.49	41.32
		60	-1.04	2.87		
		100	0.73	-2.27		
BPG	Nd	20	3.17	-7.74	-24.28	-55.91
		60	2.18	-6.03		
		100	1.02	-3.17		
	Gd	20	3.46	-8.44	-15.86	-27.57
		60	1.79	-4.96		
		100	2.14	-6.65		
	Ho	20	2.48	-6.05	-7.57	-5.41
		60	2.02	-5.59		
		100	1.83	-5.67		
DTPADA	Nd	20	-0.37	0.91	-21.30	-77.65
		60	-2.17	6.00		
		100	-2.18	6.77		
	Gd	20	0.29	-0.70	-10.79	-33.37
		60	0.17	-0.47		
		100	-0.70	2.16		
	Ho	20	0.08	-0.21	-17.66	-57.15
		60	0.16	-0.43		
		100	-1.55	4.80		

While thermodynamic evaluations of solution-phase lanthanide complexation with the phosphonate ligands tested here are scarce in the literature, DTPA complexes have been extensively studied by other researchers (Choppin et al. 1977; Thakur et al. 2013; Tian et al. 2011). Gibbs free energy for solution-phase REE-DTPA complex formation is approximately -125 kJ/mol, while enthalpy is -30 to -50 kJ/mol, and entropy is 250-300 J/K-mol. Negative values for ΔG^0 in Table 3.4 indicate that adsorption is thermodynamically favorable and spontaneous for the BPG and DTPADA functionalized resins. Chelation of lanthanides onto the DTPADA and BPG adsorbents was slightly diminished with the addition of heat, and the enthalpy terms were negative, so adsorption was exothermic. In contrast, adsorption was endothermic for the aminated and PAA-functionalized resins.

3.3.2.3. Equilibrium Adsorption Isotherms

Equilibrium adsorption isotherms were conducted to provide insight into REE binding capacity of the functionalized resins and were fit with Freundlich and Langmuir models (Equations 3.6 and 3.7; linearized fitting for the Freundlich and Langmuir models is shown in Figure B.9 of Appendix B). Relevant parameters for these models include adsorbed REE concentration (q), equilibrium solution-phase REE concentration (C_e), Freundlich constant (K_F) which indicates the overall binding strength of an adsorbent, a linearity term (n) which describes the uniformity of binding energies for surface groups, Langmuir constant (K_L), and maximum adsorption capacity (q_{Max}).

$$\text{Freundlich: } q = K_F C_e^{1/n} \Rightarrow \log(q) = \log(K_F) + \frac{1}{n} \log(C_e) \quad (\text{Equation 3.6})$$

$$\text{Langmuir: } q = \frac{q_{Max} K_L C_e}{1 + K_L C_e} \Rightarrow \frac{1}{q} = \frac{1}{q_{Max} K_L C_e} + \frac{1}{q_{Max}} \quad (\text{Equation 3.7})$$

Adsorption isotherms (Figure 3.5), indicate the relative affinity of each functionalized resin towards REE. The upward trending curves at higher adsorbate loadings in Figure 3.5.A suggest

a mixture of strong and weak binding sites. In the upper concentration ranges, it is likely that the REE-selective ligand binding sites have been saturated, and additional uptake is the result of non-selective binding to residual amines or other surface groups. The absence of this plateau in the amine plot supports this hypothesis, as the aminated resins contain a more uniform distribution of relatively weak binding sites. Therefore, the reasonable operating capacity for these resins is estimated to be <30 mg total REE per gram of resin (300 mg/L in these batch conditions).

Freundlich and Langmuir parameters were initially calculated across the full range of concentrations for each functionalized resin, but the fit of each model to experimental adsorption data was unsatisfactory due to the curved shape of the isotherm profiles for PAA, BPG, and DTPADA resins. The Freundlich model provided an accurate description of adsorption onto the aminated supports, but the ligand-functionalized resins appear to contain two classes of binding sites: those with strong affinity for REE (i.e., PAA, BPG, and DTPA) and those with weak affinity for REE (i.e., primary amines, etc.). Therefore, a multi-site model approach was taken to account for both site types. Langmuir parameters (q_{Max} and K_L) were calculated from experimental data for the ligand-functionalized resins at lower REE loadings ($C_0 < 300$ mg/L total REE), while Freundlich parameters ($1/n$ and K_F) were calculated from the full set of isotherm data from the aminated supports (Table 3.5). These two models were then added together to calculate the total REE uptake from surface ligands and the other functional groups on the supports for each resin (Figure 3.5.A).

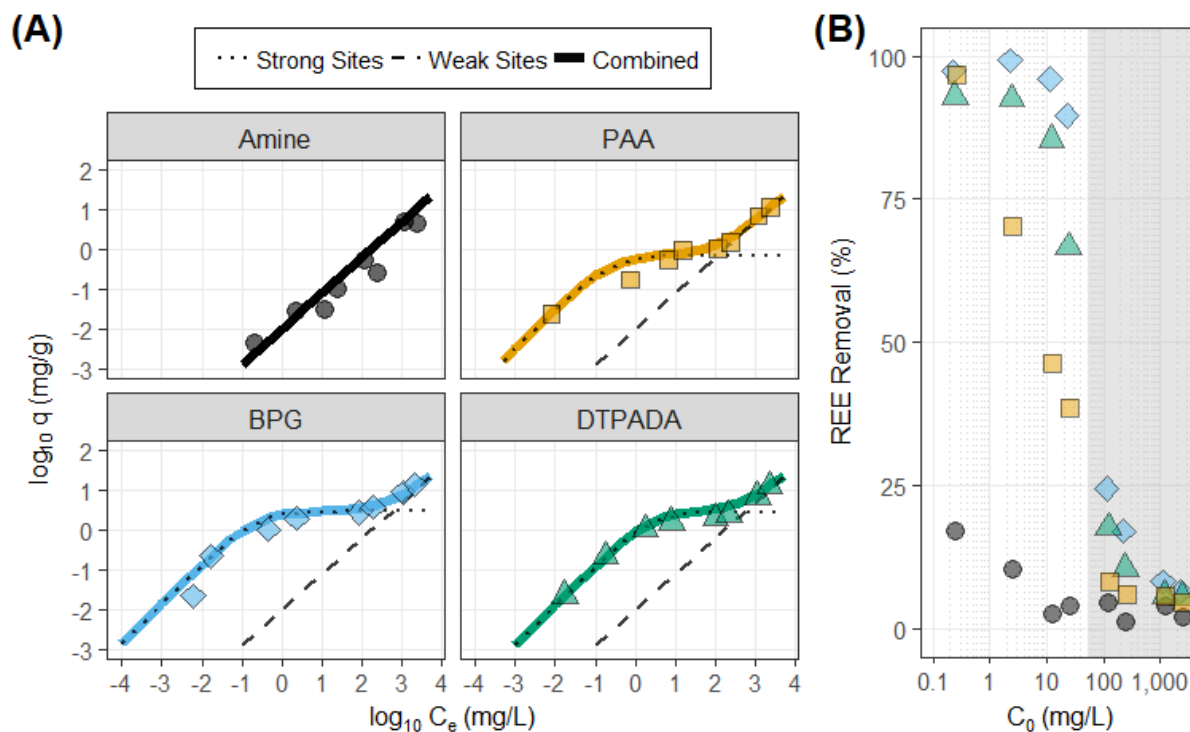


Figure 3.5. Isotherm plots for equilibrium adsorption of total REE (Nd, Gd, and Ho spiked at equal concentrations) on functionalized resins. (A) Log-log plot overlaid with isotherm models (Strong Sites = Langmuir model for ligand binding; Weak Sites = Freundlich model for uptake by aminated support; Combined = Strong Sites + Weak Sites). (B) Semi-log plot of total REE removal efficiency vs. spiked concentration. Gray shaded region shows approximate site saturation based on ligand loading for PAA, BPG, and DTPADA. (NaCl = 0.5M; Resins = 10 g/L; pH = 6.5 (Amine, PAA, BPG), 2.5 (DTPADA); Temperature = 20°C; Time = 24 hours)

Table 3.5. Isotherm model parameters for REE adsorption (mixture of Nd, Gd, and Ho in 0.5M NaCl) on functionalized resins.

Ligand	Freundlich (Weak Sites)		Langmuir (Strong Sites)	
	1/n	$K_F (L/g)^n$	$q_{Max} (mg/g)$	$K_L (L/g)$
Amine	0.9	0.01	-	-
PAA	0.9	0.01	0.72	4.397
BPG	0.9	0.01	3.01	4.658
DTPADA	0.9	0.01	2.92	0.44

3.3.2.4. Comparison of Surface-Tethered or Solution-Phase Ligands

Complexation models for solution-phase ligands were applied to evaluate differences between REE complexation by free aqueous-phase ligands and surface-tethered ligands. Modeling results suggest saturation of the ligands at loadings of ~70 mg total REE per gram of DTPADA resin or ~35 mg total REE per gram of PAA resin (Figure B.8 of Appendix B). Reasons for differences between these ligands are twofold: ligand loading was ~30% higher for DTPADA than PAA on a molar basis, and nearly one-third of PAA-lanthanide complexes take the form of 2:1 ligand:lanthanide chelates in solution at pH 6.5, while 1:1 complexes are the dominant form in DTPA-lanthanide systems (Nash 1997). Once tethered to the particle surfaces, PAA was expected to experience a larger drop in performance as a result of its reduced flexibility to form these two-ligand structures.

Chemical equilibrium modeling of REE complexation by free ligands in solution was compared to experimental results for REE adsorption on the functionalized resins (Figure B.12 of Appendix B). The chelation of REE by surface-bound DTPADA is approximated with reasonable accuracy by solution-phase models in lower concentration ranges ($R^2 = 0.99$ below 30 mg/L total REE). Experimental results diverge from the solution-phase model at higher concentrations, which indicates that REE affinity by the surface-bound ligand is diminished compared to free, untethered ligands in solution. Langmuir q_{Max} values for PAA and DTPADA (Table 3.5) are approximately one order of magnitude lower than the solution-phase models predict for REE-ligand complexation, though in all cases the functionalized resins performed favorably when compared to the aminated particle surfaces.

By translating the maximum adsorption capacity from the Langmuir models to ligand density and assuming 1:1 molar binding between REE and surface-tethered DTPADA, we estimate the surface concentration of DTPADA to be $\sim 1.9 \times 10^{-5}$ mol/g, rather than the 4.2×10^{-4} mol/g measured by XPS. Paul-Roth and Raymond (Paul-Roth and Raymond 1995)

previously found that amidation of two of DTPA's carboxyl branches diminished its complexation with Gd^{3+} ($K_{Gd-DTPA}$ dropped from $10^{22.46}$ to $10^{16.85}$), though much of the selectivity for Gd^{3+} over Ca^{2+} was retained. Similarly, Sherry et al. (Sherry et al. 1988) showed that amidation of one carboxyl group reduced the stability constants for Gd-DTPA from $10^{22.26}$ to $10^{19.68}$. A similar amide bond is formed between DTPADA and primary amines on the resin surfaces during functionalization, so it is reasonable to expect a similar decrease in capacity compared to non-substituted DTPA in the solution phase.

Solution models for PAA also provided a useful benchmark for evaluating observed surface PAA concentrations. Experimental adsorption results again indicated REE adsorption lower than for REE complexation in solution with an equivalent molar ligand concentration. Unlike DTPA, however, PAA does not exclusively form 1:1 complexes with REE in solution. The reduced mobility of the surface-tethered PAA ligands likely plays a role in their diminished binding capacity compared to solution-phase ligands, as formation of 2:1 complexes (i.e., 2 PAA molecules bound to one REE molecule) may be hindered by ligand spacing on the resin surfaces. Using the same approach as for DTPADA, the Langmuir q_{Max} value for PAA can be converted to an effective ligand concentration of 4.6×10^{-6} mol/g, rather than the 3.3×10^{-4} mol/g from XPS measurements.

3.3.2.5. *Effect of pH on REE Binding Capacity*

Solution pH is a master variable for the adsorption and recovery of REE by the functionalized resins, affecting both the adsorption capacity and complexation efficiency. Silica adsorbents functionalized with BPG and DTPADA and treated with HNO_3 were previously shown to have optimal uptake at $pH > 3$ and $pH 2-3$, respectively (Callura et al. 2018). However, these tests were conducted at low adsorbate concentrations (300 $\mu g/L$ total REE). Repo et al. (Repo et al. 2010) found that adsorption pH trends may change as a function of adsorbate concentrations in their study of chitosan functionalized with ethylenediaminetetraacetic acid (EDTA) and DTPA. This was attributed to electrostatic interference between negatively charged ligands and positively

charged amines on the supports at pH 3-5, which was prevented or disrupted at higher metal concentrations. A similar result (adsorption only in low pH at low adsorbate loadings) was also observed for DTPA-functionalized silica in our previous work (Noack et al. 2016).

Figure 3.6.A shows that adsorption pH trends for DTPADA reverse at total REE concentrations of 30 mg/L. While acidic conditions favor uptake on DTPADA-functionalized resins at low REE concentrations, adsorption was observed in the circumneutral range at 30 mg/L REE. This concentration corresponds approximately to the maximum potential loading for these resins (q_{Max} from the Langmuir isotherm model).

The BPG resin did not exhibit any notable trend reversal with increasing concentrations (Figure 3.6.A). This result is consistent with the findings of Repo et al. (Repo et al. 2010) who showed that DTPA, which is a relatively large molecule (compared to both EDTA in their study and BPG in ours), is more likely to undergo crosslinking due to its long, flexible branches. Possible structures for crosslinked DTPA resins are shown in Figure B.16 of Appendix B.

The isotherm data presented in Figure 3.6.B confirm that binding of lanthanides onto the DTPADA resins in circumneutral conditions is minimal at low adsorbate loadings but increases at higher concentrations to converge with the low pH data series above 30 mg/L total spiked REE. While the data presented here show total REE concentrations, it is also interesting to note that the individual element trends change as a function of pH. At pH 2.6, total REE uptake at the highest spiked concentration was 4.4 mg/g with selectivity towards heavy REE ($q_{\text{Nd}} = 0.7$ mg/g, $q_{\text{Gd}} = 1.4$ mg/g, $q_{\text{Ho}} = 2.2$ mg/g), while pH 6.8 resulted in a maximum total uptake of 5.5 mg/g with selectivity towards lighter REE ($q_{\text{Nd}} = 2.5$ mg/g, $q_{\text{Gd}} = 1.6$ mg/g, $q_{\text{Ho}} = 1.3$ mg/g). This translates to separation factors (defined by Equation 3.8) of $\alpha_{\text{Ho/Nd}} = 3.64$ at pH 2.6 and $\alpha_{\text{Nd/Ho}} = 2.26$ at pH 6.8. Solution phase DTPA is more selective towards heavy REE, with $\alpha_{\text{Ho/Nd}} \sim 15$, and this selectivity is not dependent on pH (determined by comparing stability constants for each REE-DTPA

complex (Grimes and Nash 2014)). Individual element data are shown in Figure B.13 of Appendix B.

$$\alpha_{A/B} = \frac{[(C_0 - C_e)/C_e]_A}{[(C_0 - C_e)/C_e]_B} \quad (\text{Equation 3.8})$$

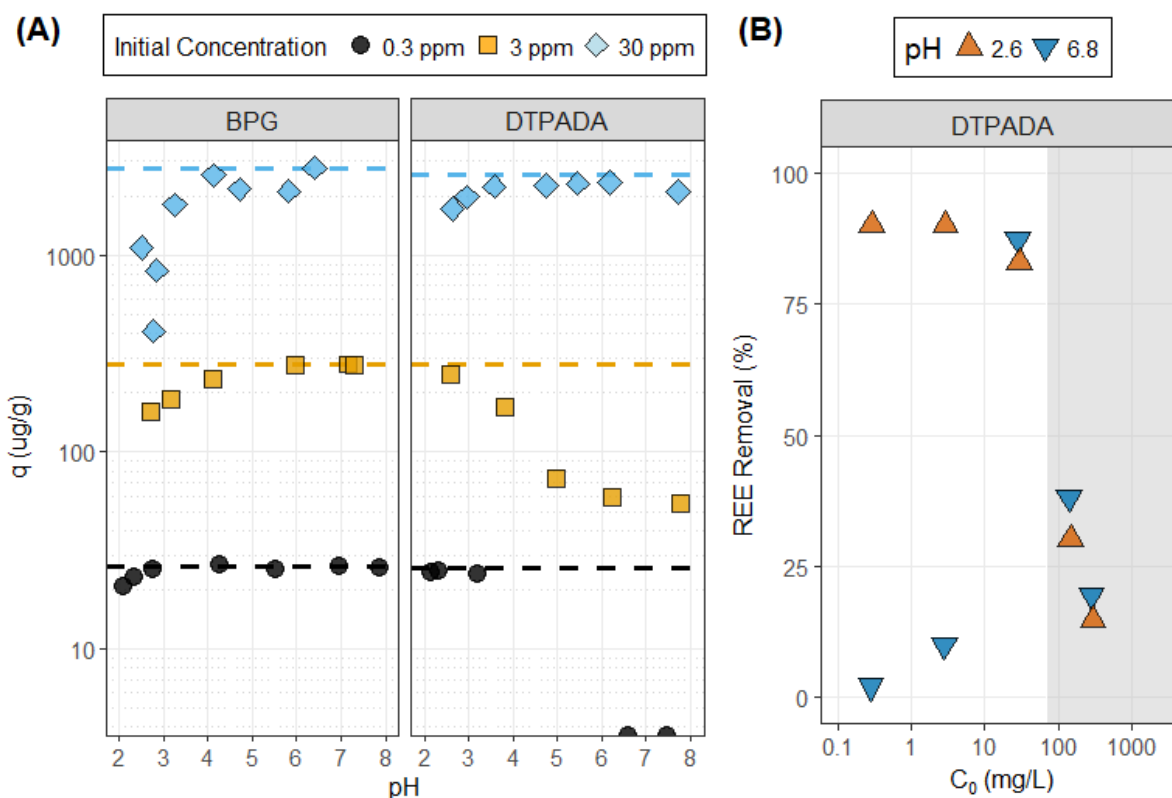


Figure 3.6. (A) Adsorption pH edges with varied adsorbate concentrations. Initial concentrations represent total REE (Nd, Gd, Ho spiked at equal concentrations on mass basis). Dashed lines indicate 100% removal of spiked REE. (B) Isotherm results for DTPADA resins at different fixed pH values. Results are shown as removal efficiency vs. total spiked concentration; gray shaded region indicated expected saturation of surface DTPADA. (NaCl = 0.5M; Resins = 10 g/L; Temperature = 20°C; Time = 24 hrs)

3.4. Summary and Conclusions

The goal of this research was to evaluate the physical/chemical properties and REE adsorption performance for ligand-modified resins. Batch adsorption experiments were conducted to determine kinetic, thermodynamic, and isotherm parameters for REE adsorption on functionalized resins. Rate constants were developed for first-order, pseudo-second-order, and

intraparticle diffusion models. Results from these tests and analyses indicate that uptake of lanthanides by the functionalized resins is kinetically limited by intraparticle diffusion. Adsorption capacities were determined through isotherm tests, and uptake/selectivity trends with respect to pH were found to be dependent on adsorbate concentrations. Isotherm results provided evidence for the presence of a mixture of different binding sites on each functionalized resin, with attachment of REE-selective ligands to resin surfaces resulting in improved REE extraction. Characterization tests provided estimates for ligand loading and particle surface area for each resin.

These resins show promise for separations processes due to their affinity for binding REE, though additional work is required to improve ligand grafting efficiency and better understand their REE selectivity. While some degree of intra-lanthanide selectivity was observed, the primary utility of the functionalized resins may be in group-wise separation of REE from bulk ions in solutions. These results provide new insight into the binding properties for lanthanides onto surface-tethered chelating ligands.

CHAPTER 4

Recovery of Rare Earth Elements with Ligand-Functionalized Polymers in Fixed-Bed Adsorption Columns

Contents of this chapter are in preparation to be submitted for publication.

4.1. Introduction

Adsorption columns are widely used for the removal of compounds from fluids and gases. With the development of selective adsorption media, it is possible to extract and recover target elements from complex mixtures. Performance of fixed-bed columns depends on the composition of influent fluids, which may contain numerous elements at different concentrations, and system operating conditions, which can be tailored to maximize the recovery of desirable elements. Ideal behavior for an adsorption column system would allow for continuous and repetitive cycles of adsorption and desorption/recovery with minimal degradation of uptake capacity.

The primary objective of this work was to study the REE selectivity and extraction performance of small-scale fixed-bed adsorption columns packed with functionalized adsorbent resin beads. A bisphosphonate ligand, which showed promise for REE extraction in our previous work (Callura et al. 2018; Noack et al. 2016) and has been used by others in studies investigating its metal chelating properties in solution (Bretti et al. 2018; Mateescu et al. 2007; Menelaou et al. 2009, 2011; De Stefano et al. 2016), was chemically attached to a resin support containing primary amine surface groups. The REE extraction capacity and selectivity of the functionalized resin beads were evaluated alongside the non-functionalized aminated resin beads in batch and flow-through column experiments. Experiments were performed to identify the influence of flow rate, feedstock composition, and column geometry on REE adsorption. Operating conditions were systematically varied to determine the impact of each parameter on REE transport and adsorption in the columns. Outcomes of this research will facilitate the design of full-scale adsorption columns and prediction of system performance.

4.2. Materials and Methods

4.2.1. Adsorbent Synthesis and Characterization

A divinylbenzene-crosslinked polystyrene resin (individual bead diameter approximately 0.6 mm) containing primary amines was used as the support for attachment of the bisphosphonate ligand *N,N*-bis(phosphonomethyl)glycine (BPG). Synthesis methods for the functionalized adsorbent resins are presented in Chapter 3. All resin materials (except for those used in Section 4.3.3: Adsorbent Regeneration and Reuse) were washed with 0.75N HNO₃, rinsed with deionized water, and dried before use. The resin adsorbents were previously characterized to determine surface area and ligand concentrations (Chapter 3). Images of the BPG-functionalized and aminated resin surfaces were collected using a scanning electron microscope (SEM) at 1000x, 2500x, 10000x, and 25000x magnification levels.

Ligand concentrations on the resin surfaces were estimated by X-ray photoelectron spectroscopy (XPS) for BPG-functionalized resins after 0, 1, and 6 use cycles to evaluate their durability. Details regarding data analysis and XPS measurements are provided in Chapter 3 and Appendix B. To summarize, elemental composition of the resins was measured using XPS and P concentrations were determined by the change in surface phosphorus relative to the non-functionalized support. The BPG ligand has two phosphorous molecules per mole, so P concentrations were converted to bulk values and divided by two to calculate moles of BPG per gram of functionalized resin.

4.2.2. Column Experiments

Fixed-bed columns were chosen for this study to maximize the reactive surface area within the bed. An illustration of the experimental setup for column tests is shown in Figure 4.1.

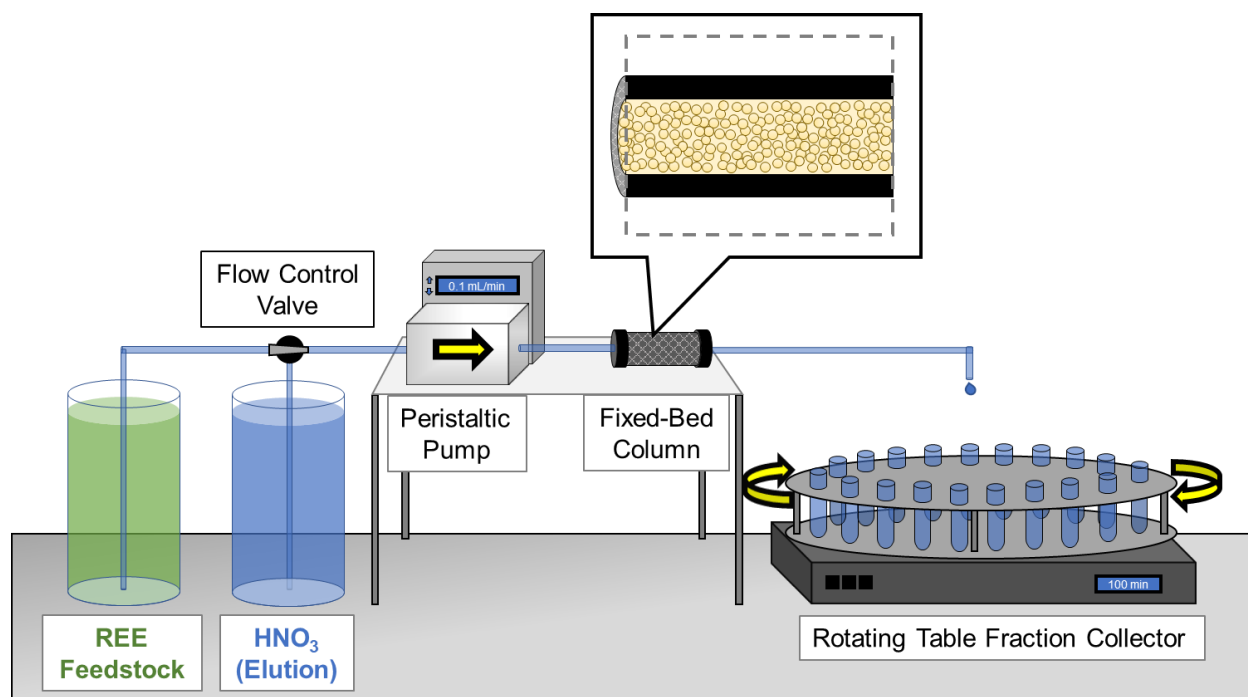


Figure 4.1. Illustration of experimental setup for fixed-bed column tests.

All column experiments, except for the wide-aspect-ratio tests, were performed with a polyether ether ketone (PEEK) column (column diameter = 0.46 cm; packing depth = 4.98 cm), Masterflex L/S digital standard drive peristaltic pump, and polyvinylchloride (PVC) based tubing. Polypropylene columns were used for the wide-aspect-ratio tests (column diameter = 1.27 cm; packing depth = 0.65 cm). The ratio of column diameter to bead diameter was 7.7 in the PEEK columns and 21 in the polypropylene columns. While some degree of wall effects may occur at lower column diameter to bead diameter ratios (i.e., less than 50), these effects are small at low flow rates, such as those employed in this study (Mehta and Hawley 1969). Columns were dry-packed by pouring resin beads into the opening and tapping the column to facilitate particle settling. Adsorbent mass was determined by taking the difference of column weight before and after packing.

Components were flushed with 0.75N HNO₃ and deionized water before and after each use to prevent cross-contamination between runs. All column materials were inert to inorganic

compounds. Columns were conditioned prior to each run by pumping 0.5M NaCl at the same flow rate and desired effluent pH used for each test (Q = 37 BVH or 7 BVH) until the effluent pH was stable at the target value for at least 20 bed volumes. Conditioning was accelerated where necessary by pumping either 0.5N HCl or 0.5N NaOH through the column until the target pH was approached, then the influent solution was switched back to 0.5M NaCl. Suggested service flow velocities for conventional ion exchange resins are on the order of 5 m/hour (*Dow Water Solutions DOWEX™ Ion Exchange Resins Product Information Catalog 2018*), which translates to a flow rate of approximately 100 BVH in this column system. Lower flow rates were chosen here to minimize the potential effects of kinetic limitations.

Samples were collected at discrete time intervals using an Eldex Universal Fraction Collector. Flow rate and effluent pH were monitored throughout each run to ensure stability and pH values are reported in the figure caption for each experiment. All tests were conducted at influent pH values of 6-7 with 0.5M NaCl background.

Concentrations of dissolved REE were determined by inductively coupled plasma-mass spectrometry (ICP-MS) measurements and adsorption was calculated based on differences between spiked and equilibrium solution-phase concentrations. Operating conditions for ICP-MS analysis were consistent with those reported previously (Chapters 2, 3, and Appendix A).

4.2.3. REE Selectivity Experiments

Adsorbent selectivity was evaluated through multi-element competitive batch adsorption isotherm experiments. Adsorbents (solids loading = 10 g/L) were added to 0.5M NaCl solutions containing different groups of metals spiked at equal concentrations (0.1-100 mg/L each) on a mass basis: (A) Nd+Gd+Ho; (B) Nd+Gd+Ho+Fe+Ni+Cu; (C) Nd+Gd+Ho+Mg+Ca+Ba or (D) Nd+Gd+Ho+Al+Fe+Co+Ni+Ba+Pb+Th+U. Groups B and C were selected to isolate s-block and d-block metals, respectively, while Group D was used to study a wide variety of metals which

were expected to have a range of competitive effects. Samples were mixed on an end-over-end agitator (30 RPM) at room temperature ($T = 20^{\circ}\text{C}$) until equilibrium was reached ($t = 24$ hours), and the supernatant fluid was sampled, acidified with 5% HNO_3 , and analyzed using ICP-MS to determine metal concentrations. The resins were then rinsed with deionized water (10 mL x 3), dried ($T = 100^{\circ}\text{C}$), and mixed with 0.75N HNO_3 (solids loading = 10 g/L; $t = 12$ hours) to elute and recover adsorbed metals. The eluate solutions were sampled and analyzed to determine recovered concentrations of each metal.

Group D was also used to evaluate selectivity of the adsorbents in the column system. A mixture containing 1 mg/L of each element from Group D (total metal concentration = 11 mg/L) was prepared in 0.5M NaCl at pH 6.5 and pumped through columns containing either BPG-functionalized resins or the aminated support at a flow rate of 7 BVH for approximately 600 bed volumes. Effluent samples were collected for 50 minutes each (5 mL per sample), acidified with 5% HNO_3 , and their REE concentrations were analyzed using ICP-MS. Samples which were not acidified for ICP-MS analysis were used to determine effluent pH from the columns. The columns were then rinsed with deionized water for at least 10 bed volumes and adsorbed metals were eluted by pumping 0.75N HNO_3 through the columns at a flow rate of 7 BVH.

4.2.4. Adsorbent Regeneration and Reuse Experiments

Reusability of the functionalized resins was evaluated using batch and fixed-bed column experiments. Batch pH adsorption edge tests were performed by adding adsorbents to 0.5M NaCl solutions (solids loading = 10 g/L) containing a mixture of REE (Nd, Gd, and Ho) spiked at 100 ug/L each. The pH value of each sample was controlled by adding different volumes of either 0.5N NaOH or 0.5N HCl to the solution, and the samples were mixed on an end-over-end agitator at 30 RPM for 24 hours at room temperature. Supernatant fluids were sampled, acidified with 5% HNO_3 , and analyzed by ICP-MS. After the initial adsorption phase, the remaining fluids were decanted, the resins were rinsed with deionized water (10 mL x 2), dried ($T = 100^{\circ}\text{C}$), and eluted

with 0.75N HNO₃ (solids loading = 10 g/L; t = 12 hours). REE concentrations were measured from the resulting eluate, and the solids were rinsed with deionized water and dried again before being used for another adsorption/elution cycle.

Reusability in the flow-through system was determined by dry packing a fixed-bed column with BPG-functionalized resins. The packed column was then conditioned with 0.5M NaCl as described previously and the influent solution was switched to a mixture containing 1 mg/L of each REE (Nd, Gd, and Ho) in 0.5M NaCl. Adsorption cycles were carried out at 37 BVH for approximately 1,500 bed volumes, and the columns were rinsed with deionized water and eluted with 0.75N HNO₃, using the same protocol described previously and a flow rate of 37 BVH to match the adsorption phase flow rate. The column was flushed with deionized water for approximately 10 bed volumes then subjected to four more conditioning/adsorption/elution cycles using the same conditions for each cycle.

4.3. Results and Discussion

The functionalization procedure did not visibly alter the resin bead surfaces, though attachment of the BPG ligand to the aminated supports did change their chemical properties and improve their REE affinity as reported previously (Chapter 3). Both the aminated resins and the BPG-functionalized resins appear as small hard spheres to the naked eye but possess roughness which increases their surface area and is visible at greater magnification levels (Figure 4.2).

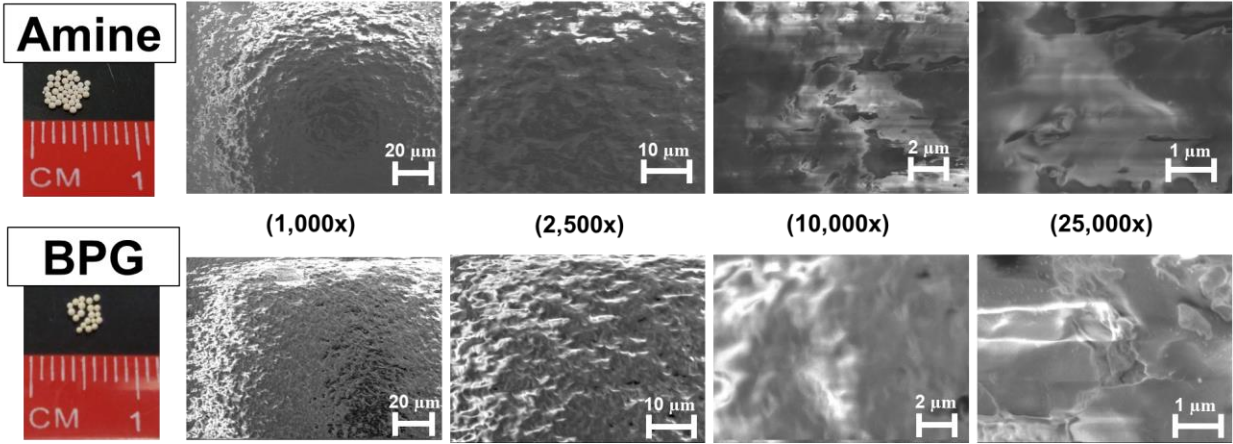


Figure 4.2. SEM images of aminated and BPG-functionalized polymeric resin adsorbents.

4.3.1. Fixed-Bed Column Experiments

Bed depth, diameter, and flow rate are among the critical design parameters for fixed-bed adsorbent column systems. From these three variables, it is possible to calculate other system properties that are relevant to column performance. Bed volume (Equation 4.1), Empty Bed Contact Time (Equation 4.2), and superficial velocity (Equation 4.3) are all useful parameters in determining adsorbate breakthrough. These parameter values and other characteristics for the columns used in these experiments are shown in Table 4.1. Column breakthrough is determined by measuring the ratio of effluent concentration (C) to influent concentration (C_i), and adsorbed concentrations (q) can be calculated from the difference between C_i and C for a fixed time period (Equation 4.4).

$$\text{Bed Volume (BV)} = \text{Bed Depth} \times \pi \times \left(\frac{\text{Bed Diameter}}{2}\right)^2 \quad (\text{Equation 4.1})$$

$$\text{Empty Bed Contact Time (EBCT)} = \frac{\text{Bed Volume}}{\text{Volumetric Flow Rate}} \quad (\text{Equation 4.2})$$

$$\text{Superficial Velocity (u)} = \frac{\text{Volumetric Flow Rate}}{\pi \times \left(\frac{\text{Bed Diameter}}{2}\right)^2} \quad (\text{Equation 4.3})$$

$$\text{Adsorbed Concentration (q)} = \frac{(C_i - C) \times \text{Volumetric Flow Rate} \times \text{Time}}{\text{Adsorbent Mass}} \quad (\text{Equation 4.4})$$

Table 4.1. Geometry and flow characteristics for adsorption columns used in this study.

Bed Depth (cm)	4.98	4.98	0.65
Bed Diameter (cm)	0.46	0.46	1.27
Aspect Ratio (Packing Depth:Column Diameter)	11:1	11:1	1:2
Bed Volume (mL)	0.82	0.82	0.82
Approx. Adsorbent Mass (mg)	300	300	300
Flow Rate (mL/min)	0.5	0.1	0.1
Flow Rate (bed volumes/hour (BVH))	37	7	7
Superficial Velocity (mm/min)	30	6	1
Empty Bed Contact Time (min)	2	8	8

Flow-through column experiments were conducted to study the resin performance in a fixed-bed column configuration under continuous flow, and to establish baseline operating conditions for subsequent experiments. Results of column experiments for a mixture of three REE (Nd, Gd, and Ho) in 0.5M NaCl at pH 6.5 passed through aminated resin beads or BPG-functionalized resin beads are shown in Figure 4.3. As expected, the BPG-functionalized resin column outperformed the aminated support ('amine'). The amine column reached complete breakthrough after 100 bed volumes, whereas the BPG column only hit ~20% breakthrough after 500 bed volumes. Both columns demonstrated a preference for heavier REE ($q_{Ho} > q_{Nd}$), though total REE adsorption onto the amine column was negligible.

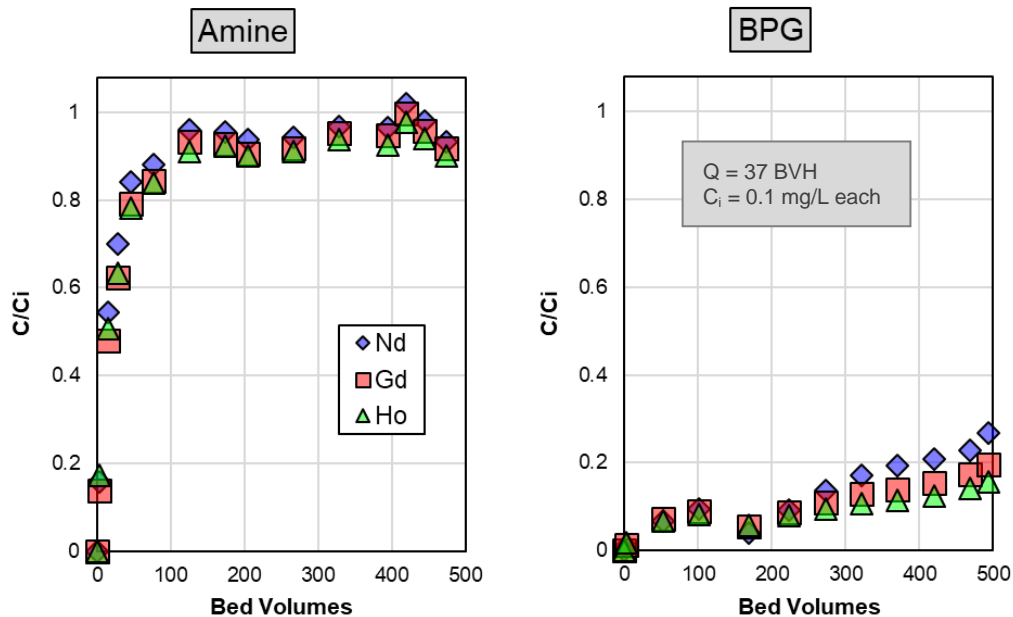


Figure 4.3. Breakthrough curves for REE mixtures in columns packed with aminated support or BPG-functionalized resins. ($C_i = 0.1$ mg/L each for Nd, Gd, and Ho; $I = 0.5M$ NaCl; pH = 7.0 ± 0.3 for amine, 6.7 ± 0.1 for BPG; $Q = 37$ BVH; Aspect Ratio = 11:1)

Adsorption kinetics such as film and intraparticle diffusion influence adsorption dynamics within fixed-bed columns (Benjamin and Lawler 2013), so further tests were conducted to determine the appropriate operating conditions to limit these effects. In continuous flow systems, adsorption is typically limited by intraparticle diffusion, rather than film diffusion (Benjamin and Lawler 2013). Adsorbents in column systems are continually exposed to fresh fluids, so the driving force (i.e., concentration gradients) from fluid to particle surfaces are greater.

To evaluate the influence of contact time, another column test was performed with the BPG-functionalized resin using the same operating conditions as before ($Q = 37$ BVH, $[REE]_i = 0.1$ mg/L each). The column was run for a period of ~ 100 bed volumes, then the pump was turned off for 12 hours. The pump was then started again and run for another ~ 400 bed volumes, then turned off once more. Finally, the pump was turned on again and run for another 750 bed volumes.

The intermittent operation test was conducted to determine whether adsorption was kinetically limited under the set operating conditions. Results of the intermittent operation column tests are presented in Figure 4.4. Adsorption efficiency improved after each stop period, suggesting that the adsorbate molecules migrated further into the adsorbent particles, allowing additional adsorbate to diffuse toward the resin surfaces. This indicated that a flow rate of 0.5 mL/min (~ 37 bed volumes per hour) was excessively high for the experimental column configuration.

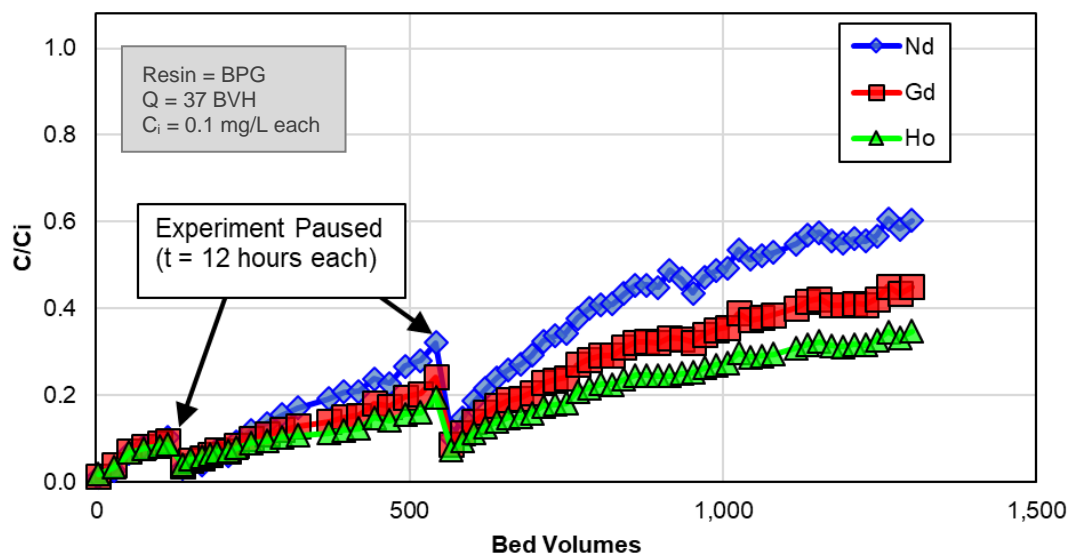


Figure 4.4. Column results for BPG-functionalized resins with intermittent operation. The system was shut off for 12 hours each after ~150 and ~550 bed volumes, before resuming the experiment. ($C_i = 0.1$ mg/L each for Nd, Gd, and Ho; $I = 0.5M$ NaCl; $pH = 6.4 \pm 0.5$; $Q = 37$ BVH; Aspect Ratio = 11:1)

Next, the influence of flow rate was addressed directly by operating two identical columns at different volumetric flow rates, either 0.1 or 0.5 mL/min (7 BVH or 37 BVH). Results are presented in Figure 4.5. The influent concentration for both columns was increased from the previous tests (Figure 4.3 and Figure 4.4) from 0.1 mg/L to 1 mg/L for each REE (total REE = 3 mg/L) to shorten the time required to reach breakthrough and complete each experiment. Adsorption efficiency improved at a flow rate of 7 BVH compared to 37 BVH, as shown by the lower C/C_i values on the left panel of Figure 4.5. An initial dip of decreasing C/C_i was observed

for both flow rates (0-285 BV for 7 BVH; 0-500 BV for 37 BVH). This dip may be the result of sodium displacement from the resin surfaces. The columns were conditioned with 0.5M NaCl to match the matrix of the influent fluids and stabilize pH, so the ligands and surfaces can loosely bind Na from solution. Attraction of the REE to BPG-functionalized resins is much stronger than Na, so the Na attached to ligands and other surface groups can be pushed off to allow for more energetically favorable interactions. The dip was not observed in the previous results, perhaps since the previous tests were conducted at lower adsorbate concentrations and less Na needed to be displaced per unit time on a molar basis.

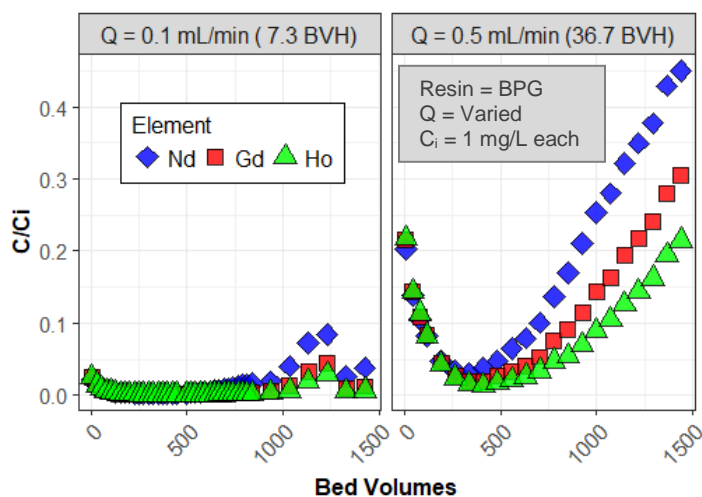


Figure 4.5. Effect of volumetric flow rate on REE breakthrough for BPG-functionalized resins. ($C_i = 1$ mg/L each for Nd, Gd, and Ho; $I = 0.5$ M NaCl; $pH = 5.8 \pm 0.2$ for both series; $Q = 7$ or 37 BVH; Aspect Ratio = 11:1)

The region of the column in which adsorption actively occurs is called the mass transfer zone (MTZ), and it moves through the column at a fixed rate after an initial establishment period (Benjamin and Lawler 2013). Its properties can be determined by measuring concentrations of the adsorbate in the column effluent and is defined as the range where C/C_i falls between 0.1-0.9. The region behind the MTZ in a column consists of adsorbent particles which have already been saturated with adsorbate and whose capacity is exhausted, while the region ahead of the MTZ consists of fresh, unspent particles. The length and velocity of the MTZ through the column

is influenced by system operating conditions and may be tuned by altering the column design. Generally, a shorter MTZ indicates more efficient column operation, although the optimal length depends on the application. A longer MTZ may be preferable where certain effluent concentration limits must be met, as operators will have earlier indication of breakthrough status, whereas a short MTZ is desirable in resource recovery schemes since the higher adsorption loadings can be achieved more quickly.

The velocity of the MTZ (v_{MTZ}) is directly affected by the fluid velocity. Reducing the volumetric flow rate slows the fluid down and generally allows for improved adsorbate mass transfer. Another way to alter the velocity of influent fluid is by modifying the column geometry. By increasing the cross-sectional area, the superficial velocity drops proportionally (e.g., doubling the diameter decreases the superficial velocity by a factor of 4 for a fixed volumetric flow rate).

To address the influence of superficial velocity on REE adsorption, two columns with different geometries, but identical bed volumes and adsorbent mass, were prepared. The standard column configuration used for other experiments in this chapter had an aspect ratio (column depth:diameter) of 11:1 and a superficial velocity of 6 mm/min at $Q = 0.1$ mL/min (7 BVH), while the wide column used for comparison had an aspect ratio of 1:2 and a superficial velocity of 1 mm/min. Both columns were subjected to the same volumetric flow rate (~7 bed volumes per hour) and influent solution ($C_i = 1$ mg/L each Nd, Gd, and Ho in 0.5M NaCl at pH 6.5), and their breakthrough profiles were recorded. Data were truncated to C/C_i values between 0.1 and 0.9 and the amount of bed volumes treated was set to 0 at $C/C_i = 0.1$ to focus on MTZ profiles. Results for the tests conducted at the two aspect ratios are presented in Figure 4.6.

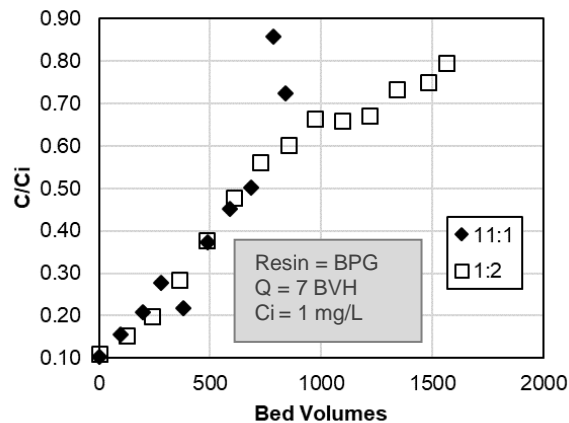


Figure 4.6. Effect of column aspect ratio (column depth:diameter) on total REE (sum of Nd, Gd, and Ho) C/C_i slope within mass transfer zone. Values on the x-axis indicate the number of bed volumes treated after 10% breakthrough. ($C_i = 1$ mg/L each for Nd, Gd, and Ho; $I = 0.5$ M NaCl; $\text{pH} = 5.8 \pm 0.2$ for 11:1 aspect ratio, 6.1 ± 0.1 for 1:2 aspect ratio; $Q = 7$ BVH; Aspect Ratio = 11:1 or 1:2)

As shown in Figure 4.6, columns with the two aspect ratios displayed nearly identical trends for C/C_i vs. bed volumes treated throughout most of the mass transfer zone, though some divergence was observed at higher concentrations. This suggests that the adsorption kinetics were not limited by superficial velocity for the flow regime studied. A superficial velocity of 1 mm/min (0.06 m/hour) did not yield improved adsorption onto the BPG-functionalized resins compared to 6 mm/min (0.36 m/hour). Therefore, operating superficial velocities of ~ 0.4 m/hour are sufficient for operation with the BPG-functionalized resins, though faster speeds may be used if peak efficiency is not required. For comparison, Dow Chemical suggests operating velocities of 5 m/hour for their DOWEXTM resins which are widely used for water softening (*Dow Water Solutions DOWEXTM Ion Exchange Resins Product Information Catalog 2018*). Based on the data obtained, it is possible to estimate appropriate design parameters for adsorption columns of various scales (as shown in Table C.3 of Appendix C).

Adsorbate concentration is another primary factor in determining the length and velocity of the MTZ. To determine the influence of influent concentration on REE breakthrough, three columns were prepared and operated with different adsorbate loadings ($C_i = 0.1, 1, \text{ or } 10$ mg/L

each Nd, Gd, and Ho). Each column had the same geometry (11:1 aspect ratio) and was operated at the same flow rate ($Q = 7$ BVH). Results are presented in Figure 4.7. Target pH values were the same for each column, though some variation in effluent pH was observed for each series; effluent pH values were 6.1 ± 0.4 for 0.1 mg/L, 5.8 ± 0.2 for 1 mg/L, 5.5 ± 0.4 for 10 mg/L. Adsorption capacity for the BPG-functionalized resins does not change significantly as a function of pH in this range, so the difference in effluent pH between is not expected to effect the results (see data from Figure 3.6.A in Chapter 3). As indicated in Figure 4.7, breakthrough time decreased with increasing C_i .

The MTZ slope for each series also increased at higher influent concentrations (C/C_i slopes after 10% breakthrough of total REE shown in Figure 4.8). Values for v_{MTZ} at 0.1, 1, and 10 mg/L were 1.08, 1.09, and 1.22 mm/min, respectively (calculations shown in Appendix C). By using these velocities in conjunction with the time between MTZ entry and exit of the column (time at 90% breakthrough – time at 10% breakthrough) the MTZ length is calculated to be 2160 cm for 0.1 mg/L, 749 cm for 1 mg/L, and 116 cm for 10 mg/L. In all cases, the calculated MTZ length was longer than the actual column depth, which indicates that the column is too short to contain the entire MTZ. The MTZ was approximately 95% shorter and moved 13% faster at 10 mg/L than 0.1 mg/L C_i . The observation of shorter MTZ lengths at higher concentrations was attributed to improved diffusion resulting from larger concentration gradients between the bulk fluid and resin surfaces.

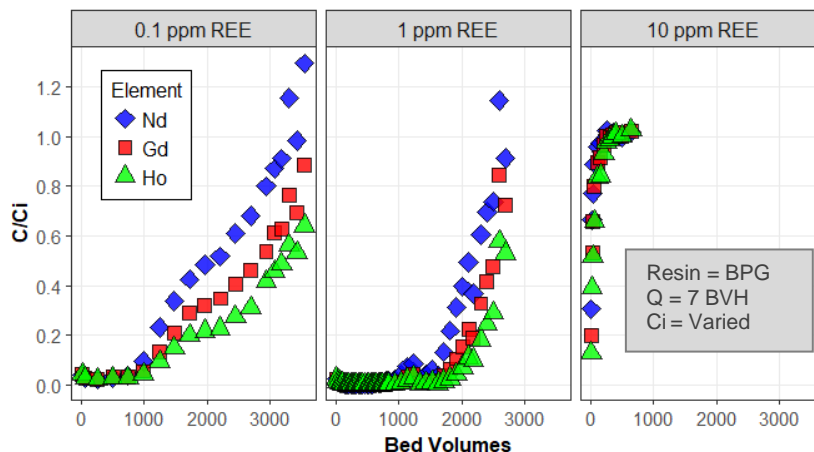


Figure 4.7. Effect of influent concentration of REE breakthrough for BPG-functionalized resins. ($I = 0.5M$ NaCl; $pH = 6.1 \pm 0.4$ for 0.1 mg/L, 5.8 ± 0.2 for 1 mg/L, 5.5 ± 0.4 for 10 mg/L; $Q = 7$ BVH; Aspect Ratio = 11:1)

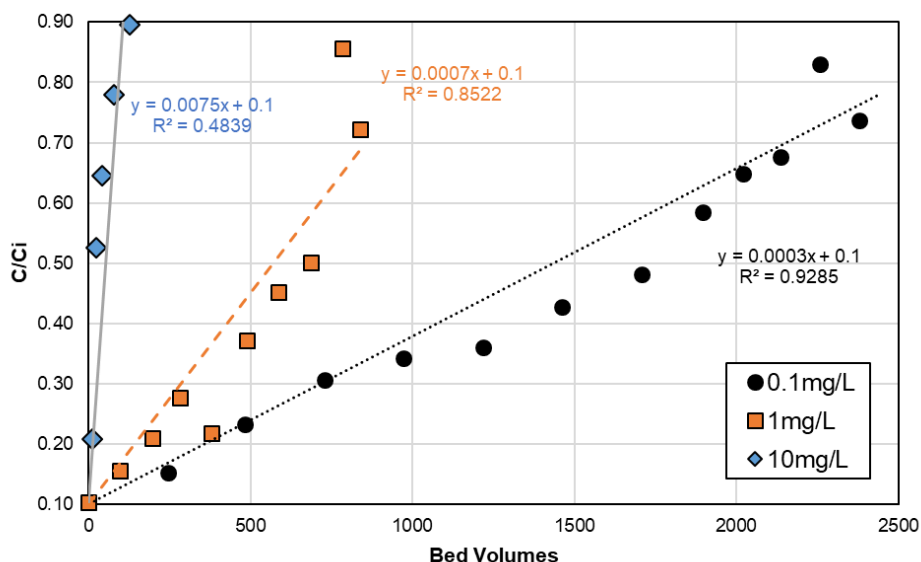


Figure 4.8. Analysis of C/C_i slope within column mass transfer zone. Data from Figure 4.7 were converted to total REE values (sum of Nd, Gd, and Ho) and truncated to show C/C_i trends from 10-90% breakthrough for each influent concentration. Values on the x-axis indicate the number of bed volumes treated after 10% breakthrough.

4.3.2. REE Selectivity Experiments

4.3.2.1. Batch Competitive Isotherms

Real matrices that could be used as REE feedstocks contain mixtures of metals with different properties. It is important to quantify the ability of the functionalized resins to adsorb REE

from competitive systems with such mixtures as the presence of other ions may affect REE uptake.

Competitive isotherms were developed to evaluate the capacity and selectivity of the aminated supports and the BPG-functionalized resins. Results of the batch competition experiments are presented in Figure 4.9. Different groups of metals were used for each series, based on their electronic properties and groupings on the periodic table (Table 4.2).

Table 4.2. Element groupings for selectivity experiments.

Group	Elements in mixture
A REE only (control group)	Nd, Gd, Ho
B d-block	Nd, Gd, Ho, Fe, Ni, Cu
C s-block	Nd, Gd, Ho, Mg, Ca, Ba
D s-block, d-block, f-block	Nd, Gd, Ho, Al, Fe, Co, Ni, Ba, Pb, Th, U

The BPG-functionalized resins demonstrated more favorable adsorption of REE than the aminated supports in each series. Further, REE uptake was less affected by the presence of competing ions, showing greater selectivity of the functionalized resins. BPG-functionalized resins did not experience any significant decrease in REE adsorption capacity with the addition of other metals, whereas performance of the aminated support suffered at high concentrations (Figure 4.9.B). Recovery efficiencies for each individual element in Group D are shown in Figure C.2 of Appendix C. Separation factors (α) for REE over competing metals in Group D are summarized in Table C.1 of Appendix C. The BPG-functionalized resins showed favorable separation ($\alpha_{\text{REE/Competing_Metal}} > 1$) for REE over every other metal in Group D except for Pb. BPG-functionalized resins were far more selective than the aminated resins, as α values were at least one order of magnitude higher for BPG-functionalized resins than the aminated resins in most cases, and as much as ~700 times higher for REE/Th. Separation factors for REE over Th on the BPG-functionalized resins were as high as ~2,400.

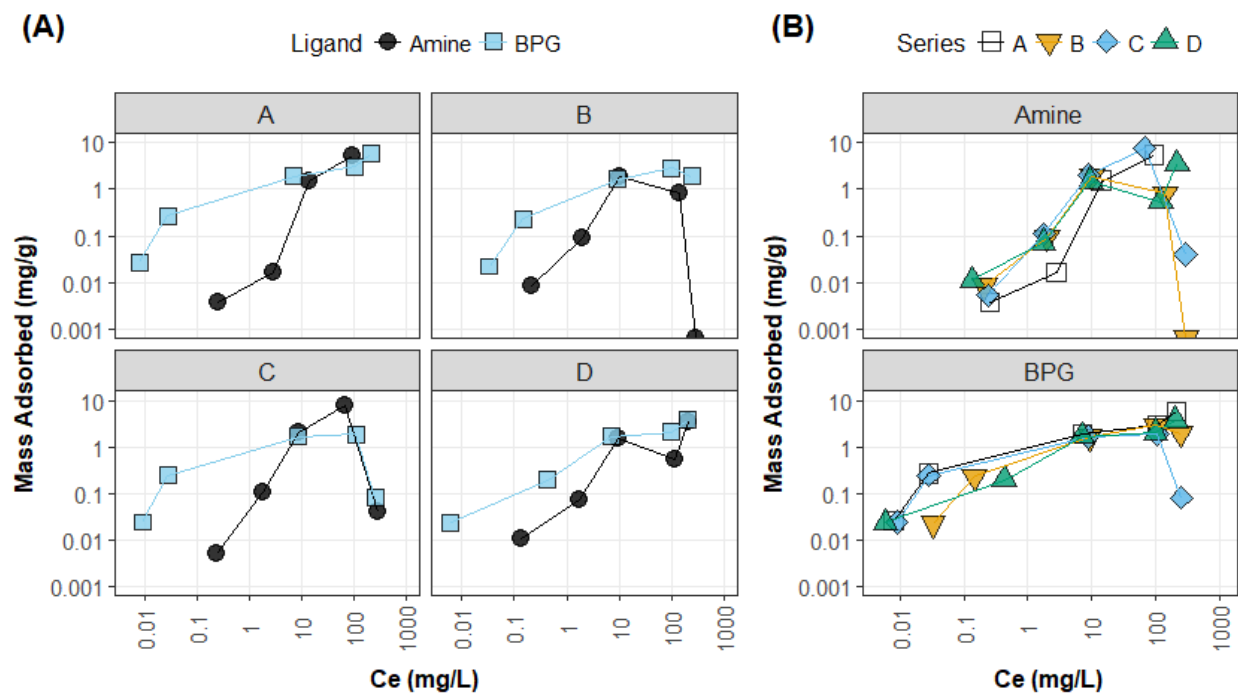


Figure 4.9. Adsorption isotherm results for total REE (sum of Nd, Gd, and Ho) from solutions containing different mixtures of metals spiked at equal concentrations on a mass basis ($C_i = 0.1-100$ mg/L each). (A) Isotherm data organized by element groupings (listed in Table 4.2) to show comparison between ligands. (B) Organized by ligand to show competition effects of different mixtures. ([NaCl] = 0.5M; pH = 7.3 ± 0.3 for amine, 6.5 ± 0.1 for BPG; Adsorbent Loading = 10 g/L; Time = 24 hours)

4.3.2.2. Fixed-Bed Adsorption of REE from Multi-element Feedstock

Selectivity within the column system was evaluated using an influent solution containing all metals from Group D at concentrations of 1 mg/L each in 0.5M NaCl (Figure 4.10). While the metals were spiked at the same concentration, some elements precipitated out of solution. The influent stock solution was sampled immediately after preparation and again one day later before the column runs began. A visible orange layer of solids, indicating ferric hydroxide, had appeared at the bottom of the influent bottle overnight. Dissolved concentrations in each sample were approximately the same for most metals, though aluminum, iron, thorium, and uranium were much lower in the later sample ($C(t_2)/C(t_1) = 0.04$ for Al, 0.03 for Fe, 0.03 for Th, and 0.20 for U). Equilibrium modeling was performed using the U.S. Geological Survey's PHREEQC program (Charlton and Parkhurst 2011; Parkhurst and Appelo 2013) implemented in the R programming

language (R Core Team 2017) (Figure C.1 of Appendix C) to evaluate the expected metal speciation in the influent solution under the experimental conditions (pH 6.5, [NaCl] = 0.5M, C_i = 1 mg/L each). According to the model, precipitation is expected for Al, Fe, and Th at the experimental pH, and U is mostly in the neutrally charged form ($UO_2(OH)_2$), which is its least soluble. Al and Fe curves are not shown on the following plots, as their concentrations in the influent solution were below the limit of accurate detection by ICP-MS.

Breakthrough curves for the REE and other metals on the aminated support showed rapid column exhaustion, with breakthrough occurring at <100 bed volumes (Figure 4.10). The column packed with BPG-functionalized resins again outperformed the aminated support, with 80% breakthrough of total REE after 600 bed volumes. The BPG column showed selectivity towards REE over Ba, Co, and Ni, though Pb proved to be a problematic competing species. Values for C/C_i of Th and U were low throughout the experiment, but their C_i values were also much lower than that of the REE due to precipitation as discussed above. Total adsorption results for each metal in the multi-element column test, summarized in Table C.2 of Appendix C, show that REE adsorption onto the BPG-functionalized resins was more than an order of magnitude higher than onto the non-functionalized aminated resins, despite the BPG-functionalized column only reaching 80% REE breakthrough.

Each column was then rinsed with deionized water and eluted with 0.75N HNO_3 after the adsorption phase. Effluent concentrations for Th and U were the highest of all elements for the eluted amine column, despite being present at lower influent concentrations. The aminated support mainly adsorbed the actinides, with negligible uptake of other metals. The BPG column elution yielded recovery in the following order: Ni>Ho>U/Co>Gd>Ho>Pb>>Ba/Th. Recovered concentrations were low for Pb, despite the high measured uptake from breakthrough curves of the adsorption phase. This may be an indication that the HNO_3 concentration used for elution (0.75N) was too low to liberate bound Pb. For both resins, nearly complete elution was achieved

within the first five bed volumes, though uranium was more slowly released from the BPG-functionalized resins.

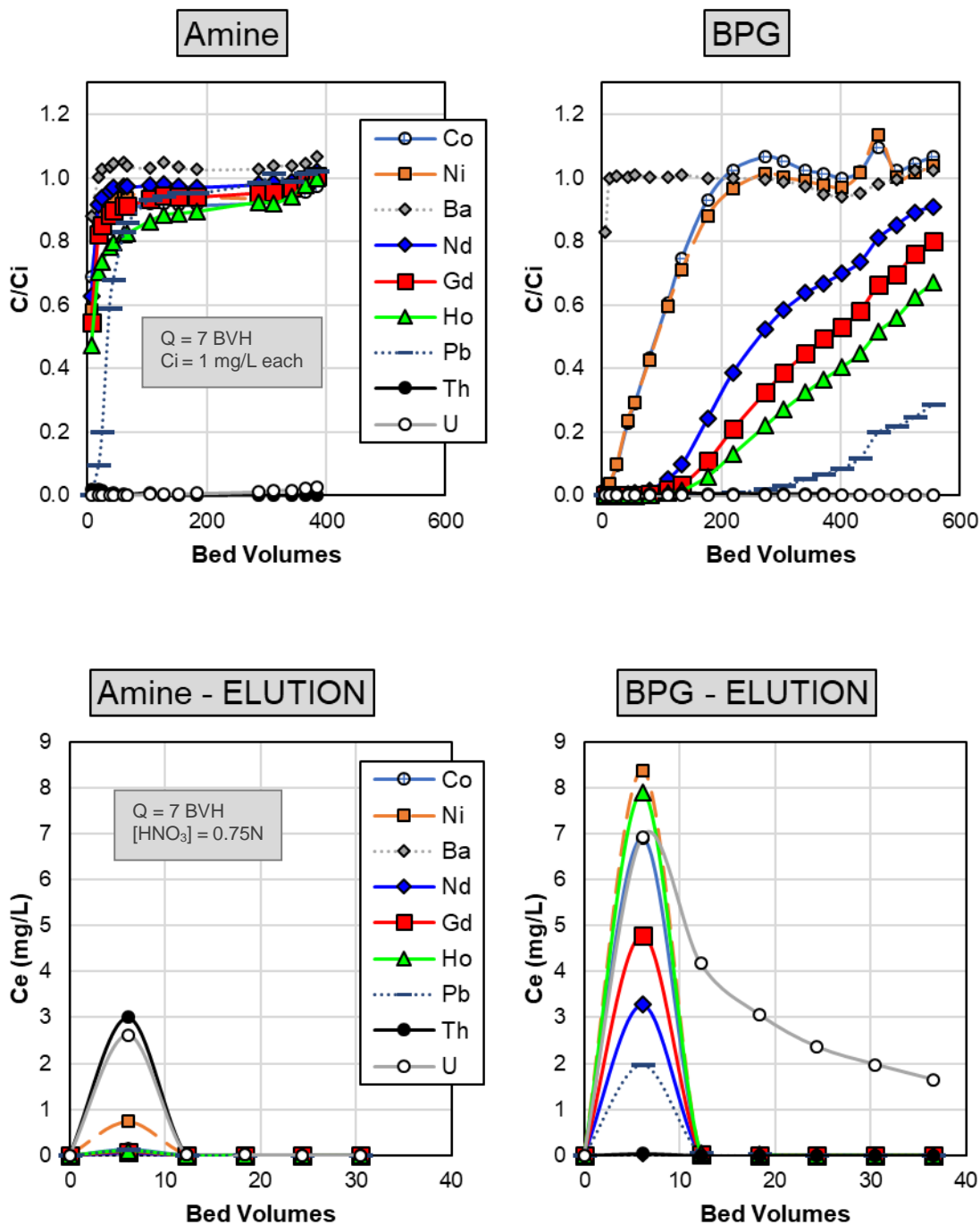


Figure 4.10. Adsorption (top) and elution (bottom) results for column tests with mixture of metals (Group D shown in Table 4.2) in 0.5M NaCl solution. ($C_i = 1$ mg/L of each metal; $I = 0.5M$ NaCl; $pH = 5.9 \pm 0.2$ for amine, 5.4 ± 0.3 for BPG; $Q = 7$ BVH; Aspect Ratio = 11:1)

4.3.3. Adsorbent Regeneration and Reuse

4.3.3.1. Batch Reuse Experiments

Adsorption pH edge tests from batch experiments showed that BPG-functionalized resins were highly efficient at adsorbing REE in most pH ranges, while the aminated supports had negligible uptake below pH 7 (Figure 4.11). These trends are consistent with pH edge results on BPG-functionalized silica adsorbents (Chapter 2). The resins were then eluted with 0.75N HNO₃, rinsed with deionized water, and dried before being reused for another adsorption cycle. Adsorption trends were stable for the aminated supports in the second cycle and improved for the BPG-functionalized resins. The improved adsorption above pH 3 for the BPG-functionalized resins was also observed with BPG-functionalized silica (Chapter 2).

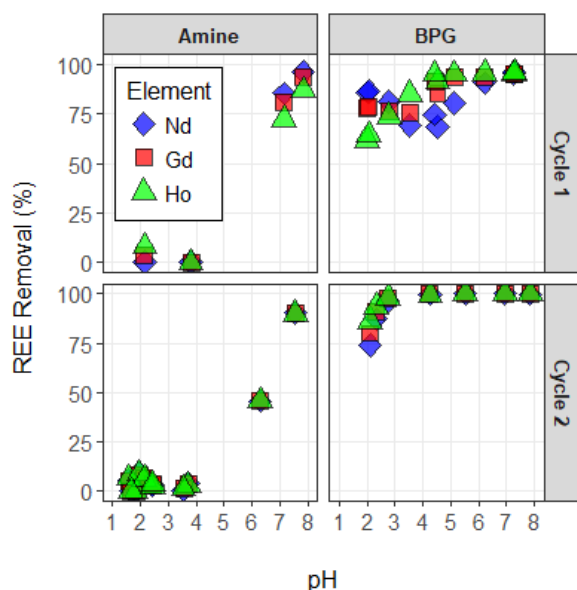


Figure 4.11. Mixed-element adsorption pH edges for aminated or BPG-functionalized resins through 2 use cycles. Resins were rinsed with deionized water, dried, and eluted with 0.75N HNO₃ between adsorption cycles. (C_i = 100 ug/L each for Nd, Gd, Ho, 300 ug/L total REE; NaCl = 0.5M; Adsorbents = 10 g/L; Temperature = 20°C; Time = 24 hours)

4.3.3.2. Column Regeneration and Reuse

Adsorbent reusability was studied in the column system by operating columns packed with BPG-functionalized resins for five adsorption/elution cycles (Figure 4.12). Volumetric flow rates

of 0.5 mL/min (37 BVH) were used for this test to allow for more rapid determination of resin reusability. Breakthrough trends showed that REE adsorption improved after the second cycle and the resins performed consistently in cycles 3-5. This finding is in agreement with the batch results (Figure 4.11), which showed improvement after resin use. Elution was more rigorous in the batch system – adsorbents were shaken with nitric acid, rather than flowing acid through the column – so the requirement of an additional cycle before the observation of consistent results in the column system is not surprising.

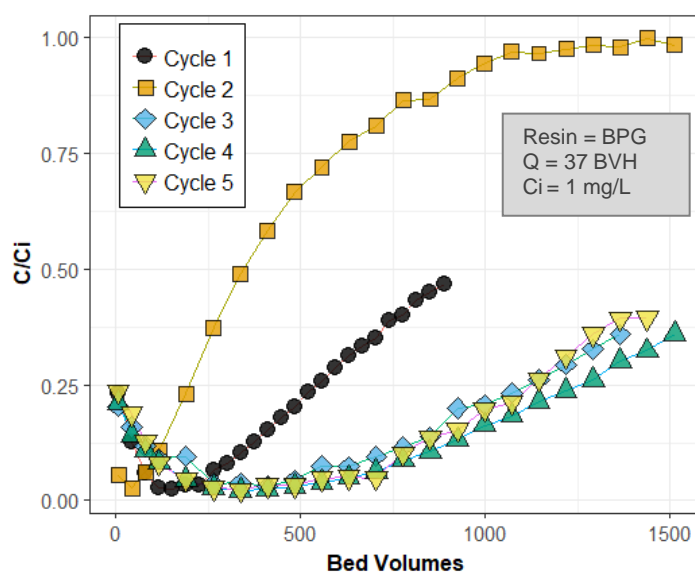


Figure 4.12. Breakthrough curves for total REE (sum of Nd, Gd, and Ho) on column reused for 5 cycles. Column was eluted with 0.75N HNO₃, rinsed with deionized water, and reconditioned with 0.5M NaCl between each adsorption cycle. ($C_i = 1$ mg/L each for Nd, Gd, Ho; $I = 0.5M$ NaCl; pH = 6.1 ± 0.1 for cycle 1, 5.9 ± 0.2 for cycle 2, 6.0 ± 0.2 for cycle 3, 5.8 ± 0.2 for cycle 4, and 6.0 ± 0.1 for cycle 5; $Q = 37$ BVH; Aspect Ratio = 11:1)

Data from the breakthrough curves for each cycle were transformed to show the mass of REE adsorbed onto the particles throughout the process (Figure 4.13.A). Complete recovery of adsorbed REE would appear as a return to zero on the y-axis on this plot, but elution efficiencies of <100% resulted in q values greater than zero at the start of cycles 2-5. This is likely attributable to losses of weakly adsorbed REE (i.e., not bound to ligand sites) during rinsing cycles. Elution data again showed that the highest REE concentrations in the eluate were measured within the

first 5 bed volumes of each elution cycle (Figure 4.13.B). Elution also showed the potential for concentration of the REE. Concentration factors (C_{eluted} / C_i) of >200x were observed for the eluent solutions, though higher values are likely possible by either decreasing the elution volume or slowing flow through the column during the recovery phase.

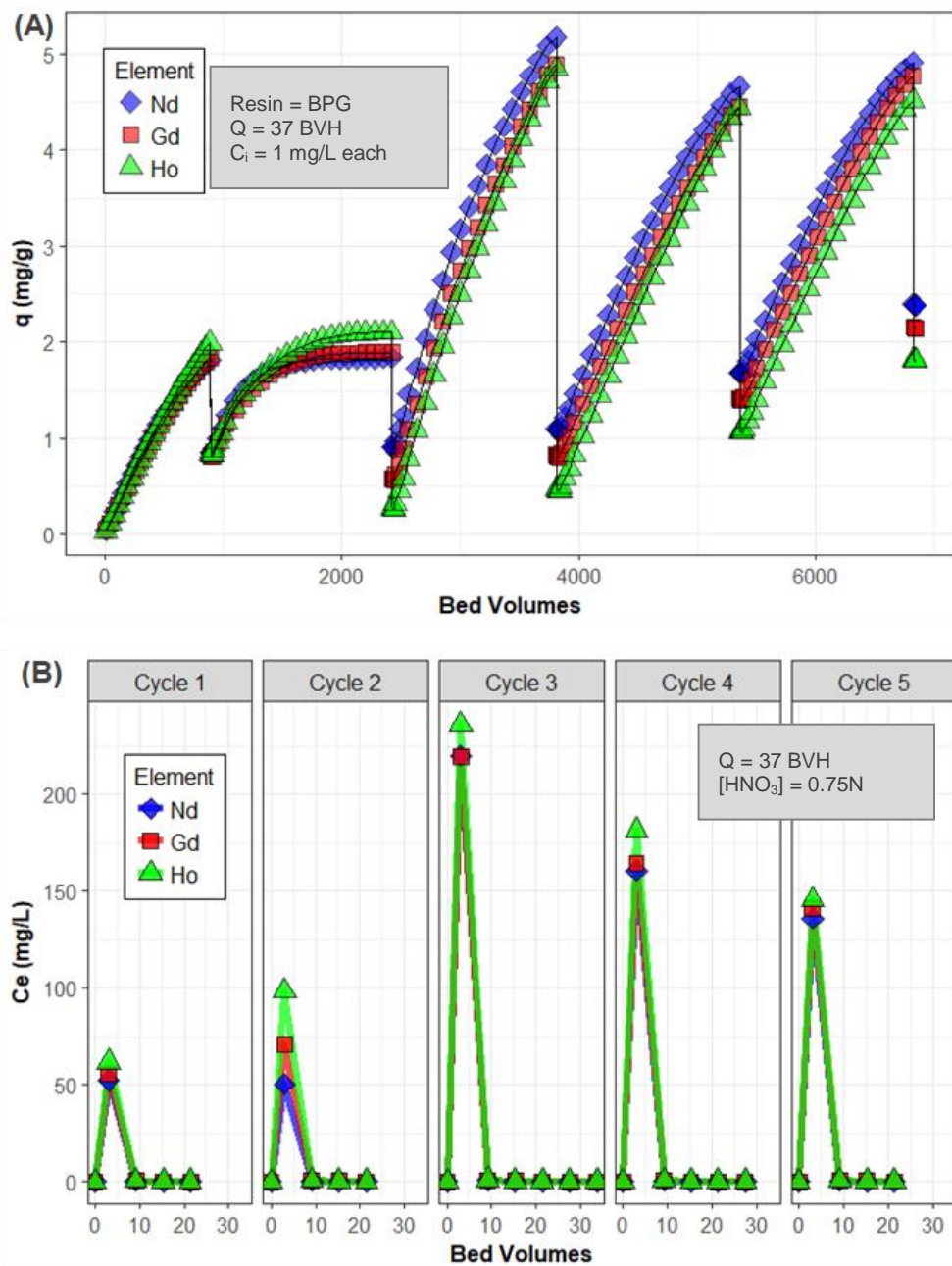


Figure 4.13. Adsorption and elution plots for Figure 4.12 data showing material reuse through 5 cycles. (A) Mass of REE adsorbed onto BPG-functionalized resins shown as a function of bed volumes treated. Sharp decreases in ‘ q ’ values indicate recovery of adsorbed REE from the resins via elution with 0.75N HNO_3 . (B) Elution data for each cycle showing effluent REE concentrations in the eluate.

4.3.4. Surface Ligand Concentrations and Their Durability

Ligand concentrations were estimated by XPS measurement for freshly synthesized BPG-functionalized resins, HNO₃-treated BPG resins, and BPG resins which were washed with 0.75N HNO₃ then used in a column for six cycles (representing 0, 1, and 7 use cycles). BPG concentrations on the surface of the resin beads before use were 0.57 mmol/g and dropped by 60% after the first HNO₃ wash cycle but were stable thereafter. The performance of the functionalized resins improved after the first use, so the ligand loss in cycle 1 was apparently due to weakly-bound or surface-precipitated ligands which were not covalently attached. These results, coupled with the performance trends from Figure 4.11 and Figure 4.12, show that the fraction of BPG ligands firmly attached to the particle surfaces was sufficient to maintain REE removal performance including adsorption capacity.

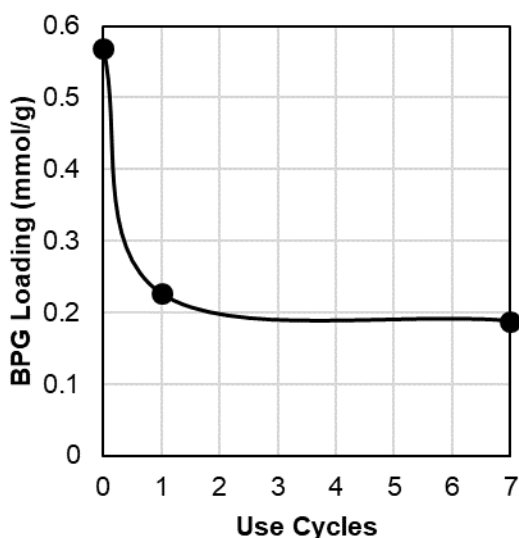


Figure 4.14. Ligand concentration on BPG-functionalized resins after multiple use-cycles.

4.4. Summary and Conclusions

The performance and durability of polymeric resin beads containing primary amine surface groups functionalized with *N,N*-bis(phosphonomethyl)glycine (BPG) were evaluated through

continuous-flow, fixed-bed adsorption experiments. BPG-functionalized resins showed improved performance after 1-2 use cycles and consistent REE adsorption was observed through five cycles. Column experiments with multi-element mixtures containing REE and competing ions revealed that REE uptake was over an order of magnitude higher for the BPG-functionalized resins than the non-functionalized aminated resins. Batch adsorption experiments with competing ions were also performed to help interpret results. Attachment of ligands to the resin surfaces greatly improved their REE binding capacity and selectivity. Separation factors were determined for REE over competing metals from multi-element competitive adsorption isotherms and values for BPG-functionalized resins were up to 700 times higher than the non-functionalized aminated resins. It is clear from these results that the functionalized adsorbents are much more effective than conventional aminated ion exchange materials at binding REE.

Systematic evaluation of breakthrough curves for the BPG-functionalized column system provided information required to design larger-scale column systems. The influence of volumetric flow rate, influent concentration, and column geometry on REE adsorption were investigated. Flow rates of 7 bed volumes per hour were found to be preferable to 37 bed volumes per hour due to adsorption kinetics limitations of the resins which resulted in premature breakthrough of REE at the higher flow rates. Influent REE concentration was found to have a significant impact on the length and velocity of the mass transfer zone. REE concentrations of 10 mg/L resulted in mass transfer zones that were 95% shorter and moved 13% faster than 0.1 mg/L. Experiments conducted with different column geometries revealed that superficial velocities lower than 0.4 m/hour did not improve adsorption, providing a lower bound for acceptable fluid velocity. These values may be altered by tailoring resin properties (e.g., porosity, hydrophilicity) to improve performance.

CHAPTER 5

Conclusions

5.1. Research Goals

The goal of this research was to evaluate the potential of ligand-functionalized adsorbents as a method for REE extraction from saline waters. This study was designed to advance the understanding of interactions between REE and functionalized adsorbents using batch and continuous-flow adsorption experiments. Specific research objectives were as follows: **(1)** Investigate adsorption of REE onto functionalized model supports; **(2)** Characterize large-scale functionalized polymer resins and evaluate their REE binding mechanisms; and **(3)** Determine selectivity and study fixed-bed column performance of functionalized adsorbents.

5.2. Summary of Major Findings

5.2.1. Major Findings from Objective 1

Silica adsorbents were functionalized with three different ligands – diethylenetriaminepentaacetic dianhydride (DTPADA), phosphonoacetic acid (PAA), and *N,N*-bis(phosphonomethyl)glycine (BPG) – using two different synthesis approaches – ‘Bottom-Up’ or ‘Top-Down’. Surface ligand concentrations and amine conversion efficiencies were found for DTPADA- (0.268 mmol/g; 28% efficiency), PAA- (0.15 mmol/g; 16% efficiency), and BPG-functionalized silica (0.086 mmol/g; 9% efficiency). The ‘Top-Down’ synthesis method yielded higher ligand attachment (0.463 mmol/g; 48% efficiency) and improved performance for the DTPADA ligand. Each adsorbent was found to have a different optimal pH for adsorption, with DTPADA performing favorably in acidic conditions, PAA in circumneutral conditions, and BPG in both acidic and basic solutions. REE affinity of the ligand-functionalized silica particles was retained in the presence of competing ions (up to 1 g/L of Ca, Mg, Zn, Al, Fe).

Data generated in support of this objective demonstrated the ability of ligand-functionalized adsorbents to adsorb and recover REE from real brine matrices and solutions containing high concentrations of competing ions. These results give context for the reasonable

operating conditions for the functionalized adsorbents, as well as potential limitations based on competitive effects of other ions. Attachment of the ligands resulted in greatly improved REE adsorption compared to the non-functionalized supports. Elution and regeneration experiments also showed that REE can be recovered and demonstrated adsorbent reusability.

5.2.2. Major Findings from Objective 2

This study showed the reproducibility of the functionalization methods using a larger, practically-relevant aminated polymer resin support and probed the fundamental physical and chemical properties of ligand-functionalized resin adsorbents. DTPADA, PAA, and BPG ligands were grafted to the aminated resin surfaces (ligand concentration, amine conversion efficiency = 0.42 mmol/g, 11% for DTPADA; 0.33 mmol/g, 8% for PAA; 0.22 mmol/g, 6% for BPG) and their performance was tested in batch experiments employing a range of conditions. Surface areas for each resin were found to be 14.8 m²/g (amine), 11.4 m²/g (DTPADA), 12.7 m²/g (PAA), and 8.0 m²/g (BPG), and total pore volumes were 76 cm³/g (amine), 103 cm³/g (DTPADA), 83 cm³/g (PAA), and 60 cm³/g (BPG).

Adsorption was found to follow pseudo-second-order kinetics and was limited by diffusion of REE into the pore space. REE adsorption capacity was measured for each resin (Langmuir q_{Max} = 0.12mg/g for amine, 2.9 mg/g for DTPADA, 0.72 mg/g for PAA, and 3.0 mg/g for BPG), and a multisite model was presented which combined Langmuir behavior for the strongly binding ligand sites and Freundlich parameters for weaker sites. Comparison of the surface-tethered ligands on the functionalized resins to solution-phase ligands using equilibrium complexation models showed that attaching the ligands to the resins reduced their REE binding capacity, though resin functionalization improved REE adsorption relative to the non-functionalized aminated resin.

5.2.3. Major Findings from Objective 3

Research for Objective 3 addressed factors essential to fixed-bed adsorption column design and operation using polymer resins functionalized with *N,N*-bis(phosphonomethyl)glycine (BPG). The performance and durability of the BPG-functionalized resin beads were evaluated through batch and continuous-flow, fixed-bed adsorption experiments. BPG-functionalized resins showed improved performance after 1-2 use cycles and consistent REE adsorption was observed through five cycles. Column experiments with multi-element mixtures containing REE and competing ions revealed that REE uptake was over an order of magnitude higher for the BPG-functionalized resins than the non-functionalized aminated resins. Separation factors for REE over competing metals were determined from multi-element competitive adsorption isotherms and values for BPG-functionalized resins were up to 700 times higher than the non-functionalized aminated resins. Attachment of ligands to the resin surfaces greatly improved their REE binding capacity and selectivity.

Experimental results showed the influence of engineering parameters (flow rate, column geometry) and solution chemistry on REE transport in a model fixed-bed column system. Superficial fluid velocities of 0.4 m/hour were determined to be acceptable for column operation. Movement of the mass transfer zone through columns was measured using a range of conditions, facilitating the prediction of dynamic column performance. Adsorbate transport in the column system was significantly impacted by influent concentration; the mass transfer zone was 95% shorter and had a 13% higher velocity at influent REE concentrations of 10 mg/L compared to 0.1 mg/L. Parameters were developed relevant to the design of full-scale column systems.

5.3. Summary of Novel Contributions

This research demonstrated the viability of ligand-functionalized silica and polymeric resin adsorbents for resource recovery schemes targeting REE in saline waters. Critical adsorbent

properties were measured and insight into their adsorption mechanisms was gained. Specific novel contributions are summarized as follows:

- (1) Determined optimal pH conditions for REE adsorption using small-scale ligand-functionalized silica adsorbents and identified the influence of competing ions on their performance.
- (2) Showed scalability of synthesis reactions by functionalizing practically-relevant large-scale adsorbent resins and characterized their physical/chemical properties.
- (3) Measured kinetic rates and adsorption capacities for REE adsorption onto the large-scale functionalized resins and gained insights into the physical-chemical adsorption mechanisms.
- (4) Quantified REE selectivity and the reusability of the ligand-functionalized resins in batch and fixed-bed column configurations.

5.4. Recommendations for Future Work

This work focused on the performance-relevant characteristics of ligand-functionalized silica and polymer resin adsorbents. The viability of the materials for full-scale implementation depends partially on technical performance data, like the information presented herein, though economics will play a large role in determining the adoption of new technologies. To that end, a thorough technoeconomic analysis should be conducted to evaluate the cost of this approach relative to other methods. Reagent and material prices do not scale linearly from the small volumes used in this study to those that would be required to produce industrial quantities of the functionalized adsorbents. These factors, along with potential market volatility for REE, should be considered.

Attachment efficiencies were very low for ligands onto these adsorbents – only ~10% of surface amines were reacted to form bonds with the grafted ligands. This value was consistent

for both types of supports used (silica and polymeric resins) and did not change significantly when reaction parameters were altered during synthesis. This is an indication of the limitations of the synthesis approach employed. Other methods should be investigated to increase concentrations of surface-bound ligands. Improvements of the ligand grafting could have a dramatic effect on adsorbent capacity and would change the design parameters for full-scale column systems. It may be a worthwhile endeavor to explore the possibility of functionalizing nanoparticles, which have high surface area to volume ratios, and then attaching them to immobile supports such as large-scale adsorbents or membranes. The functionalization scheme may also be tailored for use with other supports. While many potential supports were screened in this work (e.g., activated carbon, metal oxides, polymeric resins, silica particles), particles with higher surface area and higher surface amine concentrations than those presented here may yield more efficient ligand attachment on a particle mass basis.

Regeneration and reuse of the functionalized adsorbents was investigated in this project, but other conditions might influence their durability. Long-term durability and stress tests should be conducted to determine the acceptable life-span of the adsorbents. Ligand concentrations and REE adsorption capacity should be measured through many use cycles (100+) to identify particle degradation rates. Also, recovery of REE and individual element separations may be improved by using multiple columns with different selectivity profiles. Higher purity concentrates may be produced by developing chromatographic elution schemes for the REE-loaded columns.

REFERENCES

- Alam, J. B., Dikshit, A. K., and Bandyopadhyay, M. (2005). "Evaluation of thermodynamic properties of sorption of 2,4-D and atrazine by tire rubber granules." *Separation and Purification Technology*, 42, 85–90.
- Almeida, S. da N., and Toma, H. E. (2016). "Neodymium(III) and lanthanum(III) separation by magnetic nanohydrometallurgy using DTPA functionalized magnetite nanoparticles." *Hydrometallurgy*, Elsevier, 161, 22–28.
- An, X., and Li, C. (2013). "Experiments on densifying packing of equal spheres by two-dimensional vibration." *Particuology*, Elsevier, 11(6), 689–694.
- Anastopoulos, I., Bhatnagar, A., and Lima, E. C. (2016). "Adsorption of rare earth metals: A review of recent literature." *Journal of Molecular Liquids*, 221, 954–962.
- Ashour, R., Samouhos, M., Legaria, E. P., Svärd, M., Hogblom, J., Forsberg, K., Palmlof, M., Kessler, V. G., Seisenbaeva, G. A., and Rasmuson, Å. C. (2018). "DTPA-functionalized silica nano- and microparticles for adsorption and chromatographic separation of rare earth elements." *ACS Sustainable Chemistry & Engineering*.
- Babu, C. M., Binnemans, K., and Roosen, J. (2018). "EDTA-Functionalized Activated Carbon for the Adsorption of Rare Earths from Aqueous Solutions." *Industrial & Engineering Chemistry Research*, American Chemical Society, 57, 1487–1497.
- Benjamin, M. M. (2010). *Water Chemistry*. Waveland Press.
- Benjamin, M. M., and Lawler, D. F. (2013). *Water quality engineering: Physical/chemical treatment processes*. John Wiley & Sons.
- Bretti, C., De Stefano, C., Lando, G., and Sammartano, S. (2018). "Solubility, acid-base properties and thermodynamics of interaction between three NTA-phosphonate derivatives and the main cationic components (H⁺, Na⁺, Mg²⁺ and Ca²⁺) of natural fluids." *The Journal of Chemical Thermodynamics*, Academic Press, 123, 117–127.
- Bunton, C. A., Fuller, N. A., Perry, S. G., and Shiner, V. J. (1963). "The Hydrolysis of Carboxylic Anhydrides. Part III. Reactions in Initially Neutral Solution." *Journal of the Chemical Society*, 2918–2926.
- Callura, J. C., Perkins, K. M., Noack, C. W., Washburn, N. R., Dzombak, D. A., and Karamalidis, A. K. (2018). "Selective adsorption of rare earth elements onto functionalized silica particles." *Green Chemistry*, The Royal Society of Chemistry, 20(7), 1515–1526.
- Charlton, S. R., and Parkhurst, D. L. (2011). "Modules based on the geochemical model PHREEQC for use in scripting and programming languages." *Computers & Geosciences*, 37, 1653–1663.
- Choppin, G. R., Goedken, M. P., and Gritmon, T. F. (1977). "THE COMPLEXATION OF

LANTHANIDES BY AMINOCARBOXYLATE LIGANDS--II THERMODYNAMIC PARAMETERS." *Journal of Inorganic and Nuclear Chemistry*, 39(11), 2025–2030.

Clark, C. E., Harto, C. B., Sullivan, J. L., and Wang, M. Q. (2010). *Water Use in the Development and Operation of Geothermal Power Plants*.

Davris, P., Balomenos, E., Panias, D., and Paspaliaris, I. (2016). "Selective leaching of rare earth elements from bauxite residue (red mud), using a functionalized hydrophobic ionic liquid." *Hydrometallurgy*, 164, 125–135.

Dow Water Solutions DOWEX™ Ion Exchange Resins Product Information Catalog. (2018). .

Dupont, D., Brullot, W., Bloemen, M., Verbiest, T., and Binnemans, K. (2014). "Selective uptake of rare earths from aqueous solutions by EDTA-functionalized magnetic and nonmagnetic nanoparticles." *ACS applied materials & interfaces*, American Chemical Society, 6(7), 4980–8.

Dutta, T., Kim, K.-H., Uchimiya, M., Kwon, E. E., Jeon, B.-H., Deep, A., and Yun, S.-T. (2016). "Global demand for rare earth resources and strategies for green mining." *Environmental Research*, 150, 182–190.

Fryxell, G. E., Mattigod, S. V., Lin, Y., Wu, H., Fiskum, S., Parker, K., Zheng, F., Yantasee, W., Zemanian, T. S., Addleman, R. S., Liu, J., Kemner, K., Kelly, S., and Feng, X. (2007). "Design and synthesis of self-assembled monolayers on mesoporous supports (SAMMS): The importance of ligand posture in functional nanomaterials." *Journal of Materials Chemistry*, 17(28), 2863.

Fryxell, G. E., Wu, H., Lin, Y., Shaw, W. J., Birnbaum, J. C., Linehan, J. C., Nie, Z., Kemner, K., and Kelly, S. (2004). "Lanthanide selective sorbents: self-assembled monolayers on mesoporous supports (SAMMS)." *Journal of Materials Chemistry*, The Royal Society of Chemistry, 14(22), 3356.

Galhoum, A. A., Hassan, K. M., Desouky, O. A., Masoud, A. M., Akashi, T., Sakai, Y., and Guibal, E. (2017). "Aspartic acid grafting on cellulose and chitosan for enhanced Nd(III) sorption." *Reactive and Functional Polymers*, 113, 13–22.

Galhoum, A. A., Mahfouz, M. G., Abdel-Rehem, S. T., Gomaa, N. A., Atia, A. A., Vincent, T., and Guibal, E. (2015). "Diethylenetriamine-functionalized chitosan magnetic nano-based particles for the sorption of rare earth metal ions [Nd(III), Dy(III) and Yb(III)]." *Cellulose*, Springer Netherlands, 22(4), 2589–2605.

Van Gosen, B. S., Verplanck, P. L., Seal II, R. R., Long, K. R., and Gambogi, J. (2017). *Rare-earth elements, chap. O of Critical mineral resources of the United States-Economic and environmental geology and prospects for future supply. U.S. Geological Survey Professional Paper 1802*, (K. J. Schulz, J. DeYoung John H., R. R. Seal II, and D. C. Bradley, eds.), Reston, VA.

Grimes, T. S., and Nash, K. L. (2014). "Acid Dissociation Constants and Rare Earth Stability Constants for DTPA." *Journal of Solution Chemistry*, Springer US, 43(2), 298–313.

Gritmon, T. F., Goedken, M. P., and Choppin, G. R. (1977). "The complexation of lanthanides by

- aminocarboxylate ligands—I.” *Journal of Inorganic and Nuclear Chemistry*, 39(11), 2021–2023.
- Hoogerstraete, T. Vander, Wellens, S., Verachtert, K., and Binnemans, K. (2013). “Removal of transition metals from rare earths by solvent extraction with an undiluted phosphonium ionic liquid: separations relevant to rare-earth magnet recycling.” *Green Chemistry*, 15(4), 919–927.
- Hossain, K. Z., and Mercier, L. (2002). “Intraframework Metal Ion Adsorption in Ligand-Functionalized Mesoporous Silica.” *Advanced Materials*, WILEY-VCH Verlag, 14(15), 1053.
- Hu, Y., Drouin, E., Larivière, D., Kleitz, F., and Fontaine, F.-G. (2017). “Highly Efficient and Selective Recovery of Rare Earth Elements Using Mesoporous Silica Functionalized by Preorganized Chelating Ligands.” *ACS Applied Materials & Interfaces*, American Chemical Society, 9(44), 38584–38593.
- Hu, Y., Florek, J., Larivière, D., Fontaine, F.-G., and Kleitz, F. (2018). “Recent Advances in the Separation of Rare Earth Elements Using Mesoporous Hybrid Materials.” *The Chemical Record*, Wiley-Blackwell, 18, 1–17.
- Iftekhar, S., Ramasamy, D. L., Srivastava, V., Asif, M. B., and Sillanpää, M. (2018). “Understanding the factors affecting the adsorption of Lanthanum using different adsorbents: A critical review.” *Chemosphere*, Pergamon, 204, 413–430.
- Inoue, K., Ohto, K., Yoshizuka, K., Yamaguchi, T., and Tanaka, T. (1997). “Adsorption of Lead(II) Ion on Complexed Types of Chemically Modified Chitosan.” *Bulletin of The Chemical Society of Japan*, 70, 2443–2447.
- Jin, T., Yuan, W., Xue, Y., Wei, H., Zhang, C., and Li, K. (2017). “Co-modified MCM-41 as an effective adsorbent for levofloxacin removal from aqueous solution: optimization of process parameters, isotherm, and thermodynamic studies.” *Environmental Science and Pollution Research*.
- Juere, E., Florek, J., Lariviere, D., Kim, K., and Kleitz, F. (2016). “Support effects in rare earth element separation using diglycolamide-functionalized mesoporous silica.” *New Journal of Chemistry*, The Royal Society of Chemistry.
- Karamalidis, A., Washburn, N. R., Noack, C. W., Perkins, K., and Dzombak, D. A. (2017). “Functionalized Adsorbents for the Recovery of Rare Earth Elements from Aqueous Media.” United States of America.
- Kim, D., Powell, L. E., Delmau, L. H., Peterson, E. S., Herchenroeder, J., and Bhave, R. R. (2015). “Selective Extraction of Rare Earth Elements from Permanent Magnet Scraps with Membrane Solvent Extraction.” *Environmental Science & Technology*, American Chemical Society, 49(16), 9452–9459.
- Krishnamurthy, N., and Gupta, C. K. (2004). *Extractive metallurgy of rare earths*. CRC press.
- Kumari, A., Panda, R., Rajesh Kumar, J., Yoo, K., and Lee, J. Y. (2016). “Review on hydrometallurgical recovery of rare earth metals.” *Hydrometallurgy*, 165, 2–26.

- Lee, J. C. K., and Wen, Z. (2016). "Rare Earths from Mines to Metals: Comparing Environmental Impacts from China's Main Production Pathways." *Journal of Industrial Ecology*, 21(5), 1277–1290.
- Lewis, A. J., Palmer, M. R., Sturchio, N. C., and Kemp, A. J. (1997). "The rare earth element geochemistry of acid-sulphate and acid-sulphate-chloride geothermal systems from Yellowstone National Park, Wyoming, USA." *Geochimica et Cosmochimica Acta*, 61(4), 695–706.
- Liu, Y., and Naidu, R. (2014). "Hidden values in bauxite residue (red mud): Recovery of metals." *Waste Management*, 34(12), 2662–2673.
- Mahfouz, M. G., Galhoum, A. A., Gomaa, N. A., Abdel-Rehem, S. S., Atia, A. A., Vincent, T., and Guibal, E. (2015). "Uranium extraction using magnetic nano-based particles of diethylenetriamine-functionalized chitosan: Equilibrium and kinetic studies." *Chemical Engineering Journal*, Elsevier, 262, 198–209.
- Mateescu, A., Gabriel, C., Raptis, R. G., Baran, P., and Salifoglou, A. (2007). "pH – Specific synthesis, spectroscopic, and structural characterization of an assembly of species between Co(II) and N,N-bis(phosphonomethyl)glycine. Gaining insight into metal-ion phosphonate interactions in aqueous Co(II)–organophosphonate systems." *Inorganica Chimica Acta*, Elsevier, 360(2), 638–648.
- Mehta, D., and Hawley, M. C. (1969). "WALL EFFECT IN PACKED COLUMNS DEVENDRA MEHTA1 AND." *Industrial & Engineering Chemistry Process Design and Development*, UTC, 8(2), 280–282.
- Menelaou, M., Daskalakis, M., Mateescu, A., Raptopoulou, C. P., Terzis, A., Mateescu, C., Tangoulis, V., Jakusch, T., Kiss, T., and Salifoglou, A. (2011). "In depth investigation of the synthesis, structural, and spectroscopic characterization of a high pH binary Co(II)-N,N-bis(phosphonomethyl)glycine species. Association with aqueous speciation studies of binary Co(II)-(carboxy)phosphonate systems." *Polyhedron*, Pergamon, 30(2), 427–437.
- Menelaou, M., Mateescu, A., and Salifoglou, A. (2009). "Structural speciation of the binary Co(II)-phosphonate system." *Journal of Agroalimentary Processes and Technologies*, 15(2), 191–194.
- "N,N-Bis(phosphonomethyl)glycine ≥98.0% (T) | Sigma-Aldrich." (n.d.). <<https://www.sigmaaldrich.com/catalog/product/aldrich/15149?lang=en®ion=US>> (May 6, 2018).
- Nagib, S., Inoue, K., Yamaguchi, T., and Tamaru, T. (1999). "Recovery of Ni from a large excess of Al generated from spent hydrodesulfurization catalyst using picolylamine type chelating resin and complexane types of chemically modified chitosan." *Hydrometallurgy*, 51(1), 73–85.
- Nash, K. L. (1997). "F-Element complexation by diphosphonate ligands." *Journal of Alloys and Compounds*, 249(1), 33–40.
- Nash, K. L., Brigham, D., Shehee, T. C., and Martin, A. (2012). "The kinetics of lanthanide complexation by EDTA and DTPA in lactate media." *Dalton Transactions*, The Royal Society

of Chemistry, 41(48), 14547.

- Noack, C. W., Dzombak, D. A., and Karamalidis, A. K. (2014). "Rare Earth Element Distributions and Trends in Natural Waters with a Focus on Groundwater." *Environmental Science & Technology*, American Chemical Society, 48(8), 4317–4326.
- Noack, C. W., Perkins, K. M., Callura, J. C., Washburn, N. R., Dzombak, D. A., and Karamalidis, A. K. (2016). "Effects of Ligand Chemistry and Geometry on Rare Earth Element Partitioning from Saline Solutions to Functionalized Adsorbents." *ACS Sustainable Chemistry & Engineering*, American Chemical Society, 4(11), 6115–6124.
- Park, D. M., Reed, D. W., Yung, M. C., Eslamimanesh, A., Lencka, M. M., Anderko, A., Fujita, Y., Riman, R. E., Navrotsky, A., and Jiao, Y. (2016). "Bioadsorption of Rare Earth Elements through Cell Surface Display of Lanthanide Binding Tags." *Environmental Science & Technology*, American Chemical Society, 50(5), 2735–2742.
- Parkhurst, D. L., and Appelo, C. A. J. (2013). "Description of input and examples for PHREEQC version 3—A computer program for speciation, batch-reaction, one-dimensional transport, and inverse geochemical calculations." *U.S. Geological Survey Techniques and Methods, Book 6, Chap. A43*, available only at <https://pubs.usgs.gov/tm/06/a43/>, 497.
- Paul-Roth, C., and Raymond, K. N. (1995). "Amide Functional Group Contribution to the Stability of Gadolinium(III) Complexes: DTPA Derivatives." *Inorg. Chem*, 34, 1408–1412.
- Paulick, H., and Machacek, E. (2017). "The global rare earth element exploration boom: An analysis of resources outside of China and discussion of development perspectives." *Resources Policy*, 52, 134–153.
- Pearson, R. G. (1963). "Hard and Soft Acids and Bases." *Journal of the American Chemical Society*, American Chemical Society, 85(22), 3533–3539.
- Pérez-Quintanilla, D., Hierro, I. del, Fajardo, M., and Sierra, I. (2006). "2-Mercaptothiazoline modified mesoporous silica for mercury removal from aqueous media." *Journal of Hazardous Materials*, 134(1), 245–256.
- Polido Legaria, E., Samouhos, M., Kessler, V. G., and Seisenbaeva, G. A. (2017). "Toward Molecular Recognition of REEs: Comparative Analysis of Hybrid Nanoadsorbents with the Different Complexonate Ligands EDTA, DTPA, and TTHA." *Inorganic Chemistry*, 56(22), 13938–13948.
- Popov, K., Rönkkömäki, H., and Lajunen, L. H. J. (2001). "Critical evaluation of stability constants of phosphonic acids (IUPAC Technical Report)." *Pure and Applied Chemistry*, De Gruyter, 73(10), 1641–1677.
- R Core Team. (2017). "R: A Language and Environment for Statistical Computing."
- Ramasamy, D. L., Wojtuś, A., Repo, E., Kalliola, S., Srivastava, V., and Sillanpää, M. (2017). "Ligand immobilized novel hybrid adsorbents for rare earth elements (REE) re- moval from waste water: Assessing the feasibility of using APTES functional- ized silica in the hybridization process with chitosan Ligand immobilized novel hybrid adsorbents for." *Chemical Engineering Journal*.

- Repo, E., Warchol, J. K., Kurniawan, T. A., and Sillanpää, M. (2010). "Adsorption of Co(II) and Ni(II) by EDTA- and/or DTPA-modified chitosan: Kinetic and equilibrium modeling." *Chemical Engineering Journal*, 161, 73–82.
- Roosen, J., and Binnemans, K. (2014). "Adsorption and chromatographic separation of rare earths with EDTA- and DTPA-functionalized chitosan biopolymers." *J. Mater. Chem. A*, The Royal Society of Chemistry, 2(5), 1530–1540.
- Sanada, T., Takamatsu, N., and Yoshiike, Y. (2006). "Geochemical interpretation of long-term variations in rare earth element concentrations in acidic hot spring waters from the Tamagawa geothermal area, Japan." *Geothermics*, 35(2), 141–155.
- Sherry, A. D., Cacheris, W. P., and Kuan, K.-T. (1988). "Stability constants for Gd³⁺ binding to model DTPA-conjugates and DTPA-proteins: Implications for their use as magnetic resonance contrast agents." *Magnetic Resonance in Medicine*, Wiley-Blackwell, 8(2), 180–190.
- Smith, Y. R., Bhattacharyya, D., Willhard, T., and Misra, M. (2016). "Adsorption of Aqueous Rare Earth Elements using Carbon Black Derived from Recycled Tires." *Chemical Engineering Journal*, 296, 102–111.
- De Stefano, C., Foti, C., Giuffrè, O., and Milea, D. (2016). "Complexation of Hg²⁺, CH₃Hg⁺, Sn²⁺ and (CH₃)₂Sn²⁺ with phosphonic NTA derivatives." *New Journal of Chemistry*, 40(2), 1443–1453.
- Stewart, B. W., Capo, R. C., Hedin, B. C., and Hedin, R. S. (2017). "Rare earth element resources in coal mine drainage and treatment precipitates in the Appalachian Basin, USA." *International Journal of Coal Geology*, 169, 28–39.
- Sun, Z. H. I., Cao, H., Xiao, Y., Sietsma, J., Jin, W., Agterhuis, H., and Yang, Y. (2017). "Towards sustainability for recovery of critical metals from electronic waste – the hydrochemistry processes." *ACS Sustainable Chemistry & Engineering*, 5(1), 21–40.
- Taggart, R. K., Hower, J. C., Dwyer, G. S., and Hsu-Kim, H. (2016). "Trends in the Rare Earth Element Content of U.S.-Based Coal Combustion Fly Ashes." *Environmental Science & Technology*, 50(11), 5919–5926.
- Thakur, P., Conca, J. L., Dodge, C. J., Francis, A. J., and Choppin, G. R. (2013). "Complexation thermodynamics and structural studies of trivalent actinide and lanthanide complexes with DTPA, MS-325 and HMDTPA." *Radiochimica Acta*, OLDENBOURG VERLAG, MUNICH.
- Thomas, J. M. (1961). "The Existence of Endothermic Adsorption." *Journal of Chemical Education*, 38(3), 138–139.
- Tian, G., Martin, L. R., Zhang, Z., and Rao, L. (2011). "Thermodynamic, Spectroscopic, and Computational Studies of Lanthanide Complexation with Diethylenetriaminepentaacetic Acid: Temperature Effect and Coordination Modes." *Inorganic Chemistry*, American Chemical Society, 50(7), 3087–3096.
- Turchi, C. S., Akar, S., Cath, T., Vanneste, J., and Geza, M. (2015). *Use of Low-Temperature Geothermal Energy for Desalination in the Western United States*.

- United States Department of Energy. (2010). *U.S. Department of Energy Critical Materials Strategy*.
- United States Environmental Protection Agency. (2012). *Rare Earth Elements: A Review of Production, Processing, Recycling, and Associated Environmental Issues*.
- United States Environmental Protection Agency. (2017). "CompTox Chemistry Dashboard." <<https://comptox.epa.gov/dashboard>> (Nov. 1, 2017).
- Valeur, E., Bradley, M., Specker, E., Keinicke, L., Bradley, M., Carpino, L. A., Henklein, P., Dax, T. G., Hohenthanner, K., Knaus, H.-G., Wenschuh, H., Klose, K., Beyermann, M., and Bienert, M. (2009). "Amide bond formation: beyond the myth of coupling reagents." *Chem. Soc. Rev.*, The Royal Society of Chemistry, 38(2), 606–631.
- Wall, F., Rollat, A., and Pell, R. S. (2017). "Responsible Sourcing of Critical Metals." *ELEMENTS, MINERALOGICAL SOC AMER, CHANTILLY*.
- Wang, W., and Cheng, C. Y. (2011). "Separation and purification of scandium by solvent extraction and related technologies: a review." *Journal of Chemical Technology & Biotechnology*, John Wiley & Sons, Ltd., 86(10), 1237–1246.
- Weber, W. J., and Morris, J. C. (1963). "Kinetics of adsorption on carbon from solution." *Journal of the Sanitary Engineering Division, ASCE*, 89(2), 31–60.
- Weng, Z., Haque, N., Mudd, G. M., and Jowitt, S. M. (2016). "Assessing the energy requirements and global warming potential of the production of rare earth elements." *Journal of Cleaner Production*, 139, 1282–1297.
- Wood, S. A. (2006). "Rare earth element systematics of acidic geothermal waters from the Taupo Volcanic Zone, New Zealand." *Journal of Geochemical Exploration*, 89(1–3), 424–427.
- Wood, S. A., and Shannon, W. M. (2003). "Rare-earth elements in geothermal waters from Oregon, Nevada, and California." *Journal of Solid State Chemistry*, 171(1–2), 246–253.
- Xie, F., Zhang, T. A., Dreisinger, D., and Doyle, F. (2014). "A critical review on solvent extraction of rare earths from aqueous solutions." *Minerals Engineering*, 56, 10–28.
- Yang, G., Chen, H., Qin, H., and Feng, Y. (2014). "Amination of activated carbon for enhancing phenol adsorption: Effect of nitrogen-containing functional groups." *Applied Surface Science*, 293, 299–305.
- Yantasee, W., Fryxell, G. E., Addleman, R. S., Wiacek, R. J., Koonsiripaiboon, V., Pattamakomsan, K., Sukwarotwat, V., Xu, J., and Raymond, K. N. (2009). "Selective removal of lanthanides from natural waters, acidic streams and dialysate." *Journal of Hazardous Materials*, 168(2), 1233–1238.
- Yantasee, W., Lin, Y., Fryxell, G. E., Alford, K. L., Busche, B. J., and Johnson, C. D. (2004). "Selective Removal of Copper(II) from Aqueous Solutions Using Fine-Grained Activated Carbon Functionalized with Amine." *Industrial & Engineering Chemistry Research, American Chemical Society*, 43(11), 2759–2764.

- Zaimes, G. G., Hubler, B. J., Wang, S., and Khanna, V. (2015). "Environmental Life Cycle Perspective on Rare Earth Oxide Production." *ACS Sustainable Chemistry & Engineering*, American Chemical Society, 3(2), 237–244.
- Zhang, C., Zhang, F., Li, L., and Zhang, K. (2016). "Adsorption Rare Earth Metal Ions from Aqueous Solution by Polyamidoamine Dendrimer Functionalized Soy Hull." *Waste and Biomass Valorization*, Springer Netherlands, 7(5), 1211–1219.
- Zhao, F., Repo, E., Meng, Y., Wang, X., Yin, D., and Sillanpää, M. (2016). "An EDTA- β -cyclodextrin material for the adsorption of rare earth elements and its application in preconcentration of rare earth elements in seawater." *Journal of Colloid and Interface Science*, 465, 215–224.
- Zhao, F., Repo, E., Sillanpää, M., Meng, Y., Yin, D., and Tang, W. Z. (2015a). "Green Synthesis of Magnetic EDTA- and/or DTPA-Cross-Linked Chitosan Adsorbents for Highly Efficient Removal of Metals." *Industrial & Engineering Chemistry Research*, American Chemical Society, 54(4), 1271–1281.
- Zhao, F., Repo, E., Yin, D., Meng, Y., Jafari, S., and Sillanpää, M. (2015b). "EDTA-Cross-Linked β -Cyclodextrin: An Environmentally Friendly Bifunctional Adsorbent for Simultaneous Adsorption of Metals and Cationic Dyes." *Environmental Science & Technology*, American Chemical Society, 49(17), 10570–10580.
- Zhou, Q., Yang, H., Yan, C., Luo, W., Li, X., and Zhao, J. (2016). "Synthesis of carboxylic acid functionalized diatomite with a micro-villous surface via UV-induced graft polymerization and its adsorption properties for Lanthanum (III) ions." *Colloids and Surfaces A: Physicochemical and Engineering Aspects*, 501, 9–16.

APPENDIX A

Supporting Information for: Selective Adsorption of Rare Earth Elements onto Functionalized Silica Particles

Table A.1. Standard instrument settings for Agilent 7700x ICP-MS measurements. Oxygen-free grade argon was used as the carrier and dilution gas. Ultra high-purity helium was used in the reaction cell. Tuning solutions purchased from Agilent were diluted 1000:1. Table adapted from Noack, et al. (2016).

	Parameter	Value
Plasma	RF power	1600 W
	Nebulizer pump rate	0.10 rps
	Carrier argon flow rate	0.61 L/min
	Dilution argon flow rate	0.36 L/min
Lenses	Extract 1	0.0 V
	Extract 2	-200.0 V
	Omega bias	-110 V
	Omega lens	9.6 V
	Cell entrance	-110 V
	Cell exit	-150 V
	Deflect	-74.8 V
	Plate bias	-150 V
Octopole reaction cell	Octopole bias	-100.0 V
	Octopole RF	200 V
	He flow rate	10 mL/min
	Energy discrimination	7.0 V
Data acquisition	Replicates	5
	Integration time	0.3 s
Masses monitored	¹⁴⁵ Nd, ¹⁵⁷ Gd, ¹⁶⁵ Ho	
Oxides and doubly charged	¹⁴⁰ Ce ¹⁶ O ⁺ / ¹⁴⁰ Ce	< 2.1%
	¹⁴⁰ Ce ²⁺ / ¹⁴⁰ Ce	< 1.6%

Table A.2. Elemental composition of Great Salt Lake brine. Data provided by the Idaho National Laboratory (sampling location: 40.735287, -112.212512).

Parameter	Unit	Natural C	Parameter	Unit	Natural C	Spiked	Total C
pH	-	7.92	Sc	ug/L	7.15E-03	55.56	55.56
Temp. (Field)	°C	1.8	Y	ug/L	9.64E-02	55.56	55.65
Alkalinity	mg as CaCO ₃	446	La	ug/L	1.60E-01	55.56	55.72
Dissolved O	mg/L	2.7	Ce	ug/L	2.02E-01	55.56	55.76
F	mg/L	<10	Pr	ug/L	3.99E-02	55.56	55.60
Cl	mg/L	85,682	Nd	ug/L	1.56E-01	55.56	55.71
SO ₄	mg/L	10,358	Sm	ug/L	3.07E-02	55.56	55.59
Br	mg/L	51.2	Eu	ug/L	6.21E-03	55.56	55.56
NO ₃	mg/L	<10	Gd	ug/L	3.36E-02	55.56	55.59
Li	mg/L	24	Tb	ug/L	4.00E-03	55.56	55.56
Be	mg/L	0.0352	Dy	ug/L	1.90E-02	55.56	55.57
Na	mg/L	51,330	Ho	ug/L	3.71E-03	55.56	55.56
Mg	mg/L	5,169	Er	ug/L	9.83E-03	55.56	55.57
Al	mg/L	0.328	Tm	ug/L	1.60E-03	55.56	55.56
K	mg/L	4,101	Yb	ug/L	9.08E-03	55.56	55.56
Ca	mg/L	323	Lu	ug/L	1.73E-03	55.56	55.56
SiO ₂ (aq)	mg/L	27.8	Th	ug/L	1.32E-02	55.56	55.57
Ga	mg/L	0.0342	U	ug/L	1.17E+01	55.56	67.23
As	mg/L	0.206					
Se	mg/L	0.213					
Rb	mg/L	4.355					
Sr	mg/L	3.23					
In	mg/L	0.0336					
Cs	mg/L	0.0538					
Ba	mg/L	0.168					
Bi	mg/L	0.0419					

Table A.3. Separation factors for REE/U from experiments performed in Great Salt Lake brines.

Solid	pH	Separation Factors ($\alpha_{\text{REE/U}}$)																
		Sc	Y	La	Ce	Pr	Nd	Sm	Eu	Gd	Tb	Dy	Ho	Er	Tm	Yb	Lu	
Raw Silica	2.63	1.9	0.0	0.0	0.0	0.1	0.0	0.1	0.2	0.0	0.3	0.4	0.3	0.3	0.3	0.2	0.3	
	6.91	0.1	0.0	0.0	0.0	0.0	0.0	0.0	0.0	0.0	0.0	0.0	0.0	0.0	0.1	0.1	0.2	
	7.77	0.1	0.2	0.0	0.1	0.1	0.1	0.1	0.1	0.1	0.1	0.2	0.2	0.3	0.3	0.4	0.6	0.5
Aminated Silica	6.14	0.0	0.0	0.0	0.0	0.0	0.0	0.0	0.0	0.0	0.0	0.0	0.0	0.0	0.0	0.0	0.0	
	8.42	2.8	0.5	0.0	0.3	0.1	0.1	0.2	0.2	0.2	0.4	0.5	0.6	0.7	0.9	1.7	1.3	
	8.99	1.9	0.7	0.4	0.5	0.5	0.5	0.5	0.5	0.5	0.7	0.7	0.8	0.9	0.9	1.4	1.1	
TD-DTPADA	2.31	24.3	58.6	51.7	136.6	200.1	155.1	141.4	101.0	110.0	104.0	102.5	98.7	104.5	104.6	113.6	115.6	
	2.34	24.2	59.7	65.6	170.5	204.8	128.3	125.7	98.0	116.5	104.9	93.8	96.1	98.5	101.3	110.3	110.0	
	2.37	30.3	77.4	53.6	147.9	220.9	210.3	182.1	129.5	157.9	141.9	131.3	138.4	135.1	145.7	147.0	154.2	
	2.45	29.5	81.4	18.0	47.6	108.3	94.1	244.3	178.5	177.3	204.7	203.3	191.1	166.2	210.7	204.8	185.1	
	2.48	27.9	72.5	15.2	42.1	97.6	131.9	218.3	164.8	162.1	192.1	178.0	184.6	183.3	182.0	184.4	173.0	
	2.50	32.2	77.3	17.4	42.7	107.7	142.8	225.2	173.6	169.3	204.1	193.7	197.7	194.1	196.4	206.8	181.9	
	2.68	4.0	24.4	9.0	19.4	34.8	37.2	37.0	29.7	27.2	25.5	22.8	22.4	24.4	26.2	33.0	29.0	
	2.72	5.1	24.1	7.8	17.3	31.4	38.2	38.8	31.4	28.8	27.3	25.1	24.7	25.2	28.1	37.8	30.2	
	7.08	1.5	0.5	0.5	0.4	0.4	0.4	0.3	0.3	0.3	0.3	0.3	0.3	0.4	0.4	0.5	0.6	0.6
	7.21	1.6	0.2	0.3	0.2	0.2	0.2	0.2	0.2	0.2	0.2	0.2	0.2	0.2	0.2	0.3	0.3	0.3
	8.22	4.4	0.7	0.7	0.7	0.5	0.5	0.5	0.5	0.5	0.5	0.5	0.5	0.6	0.7	0.8	1.0	1.1
	8.33	2.2	0.5	0.4	0.5	0.4	0.4	0.4	0.3	0.4	0.4	0.4	0.4	0.4	0.5	0.5	0.6	0.7

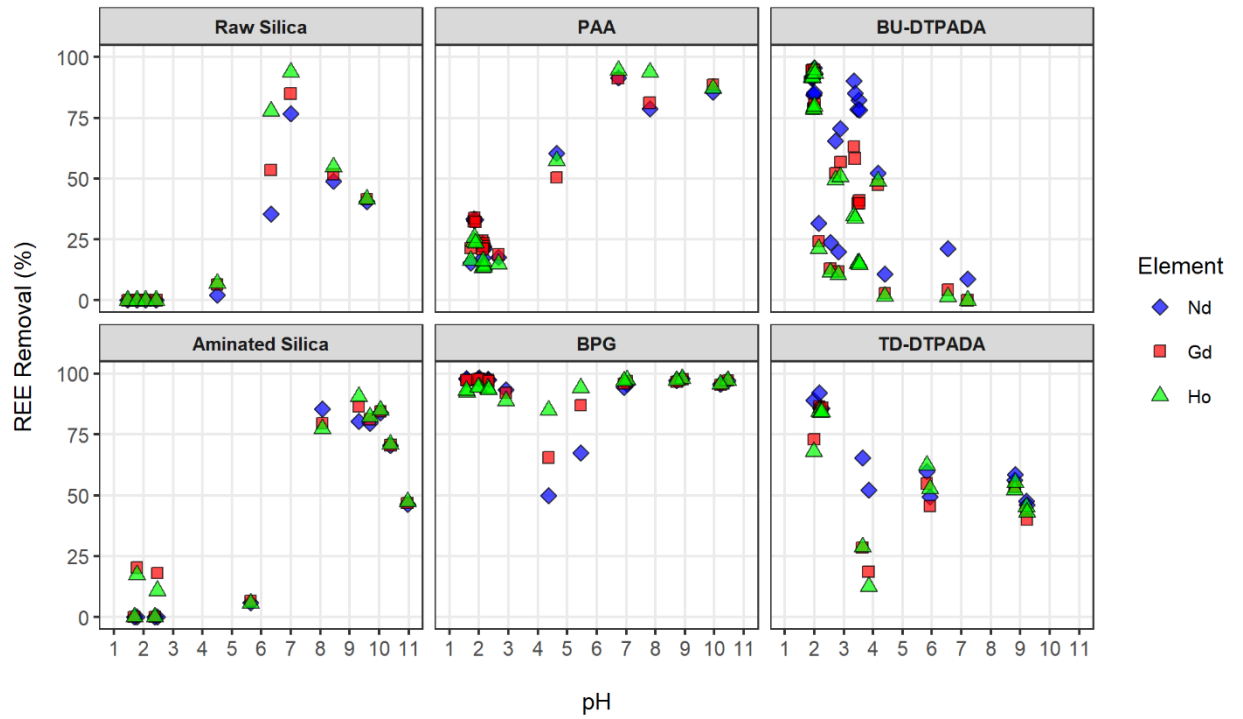


Figure A.1. Full pH edge adsorption dataset for 100 $\mu\text{g/L}$ mixtures of Nd, Gd, and Ho in 0.5M NaCl. Adsorption reactions were performed for 3 hours at $T = 20^\circ\text{C}$, using adsorbent loadings of 10 g/L.

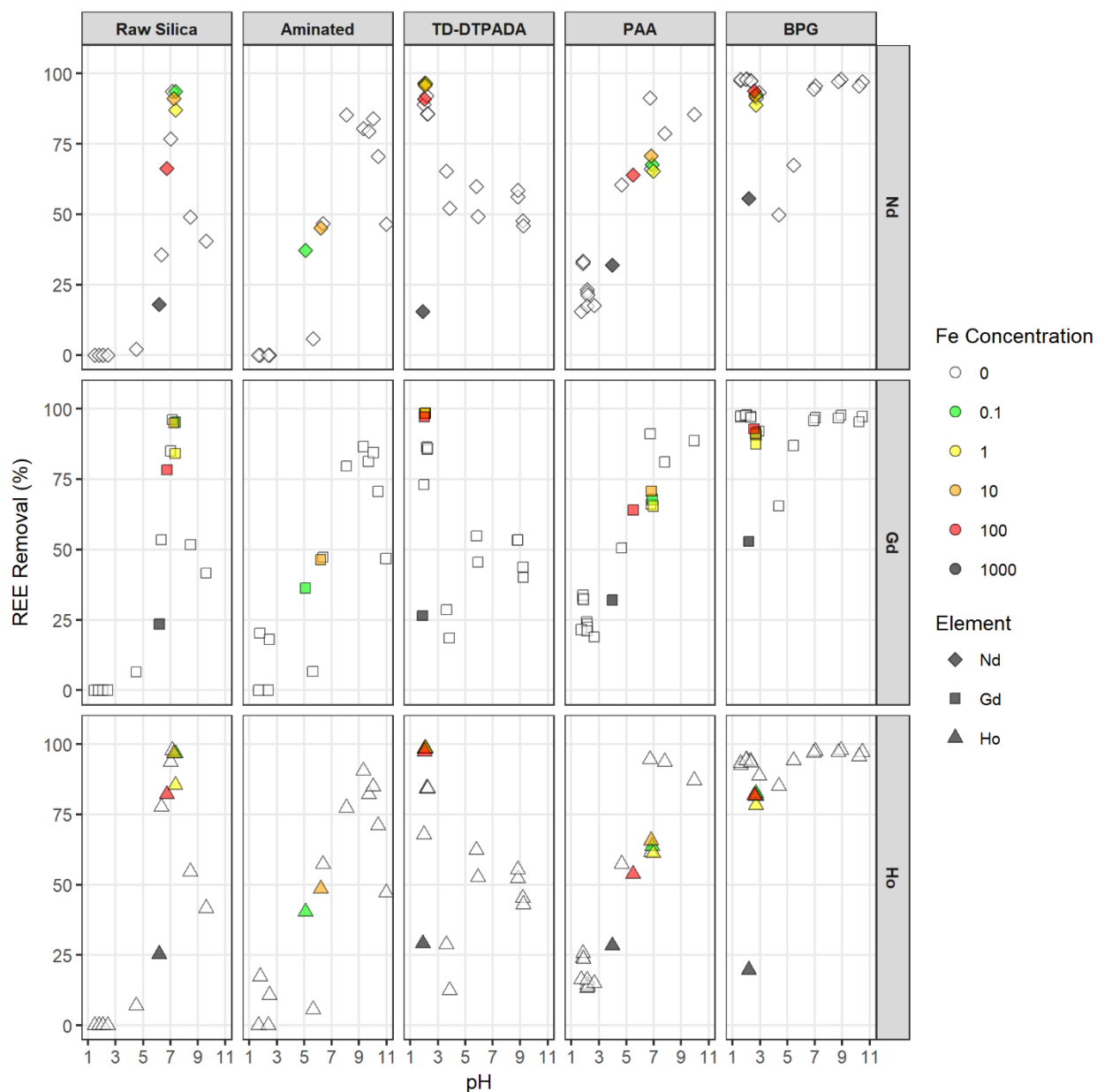


Figure A.2. Adsorption pH trends for 100 $\mu\text{g/L}$ mixtures of Nd, Gd, and Ho in 0.5M NaCl with and without iron. Iron concentrations are denoted by the color of the data points. A single pH value was targeted for each solid for all samples containing Fe, though high concentrations of iron lead to decreased equilibrium pH. Adsorption reactions were performed for 3 hours at $T = 20^\circ\text{C}$, using adsorbent loadings of 10 g/L.

Elution trends for BPG were similar to the TD-DTPADA, with a plateau in recovery observed above 1N (Figure A.3). Overall recovery rates upon elution for REE were relatively low for BPG (maximum of 60% recovered). It is hypothesized that this decrease in elution efficiency may be attributable to residual reactants from the functionalization process, i.e., excess BPG

molecules not covalently bound to the silica support surface remaining on the fresh BPG particle surfaces during the uptake step. These weakly attached compounds would be washed away prior to the elution, carrying with them some complexed REE and thus causing discrepancies between the calculated adsorbed mass and the measured concentrations in elution samples. Subsequent use cycles yielded improved performance and REE recovery, as discussed and shown in Figure 2.8 of the main text.

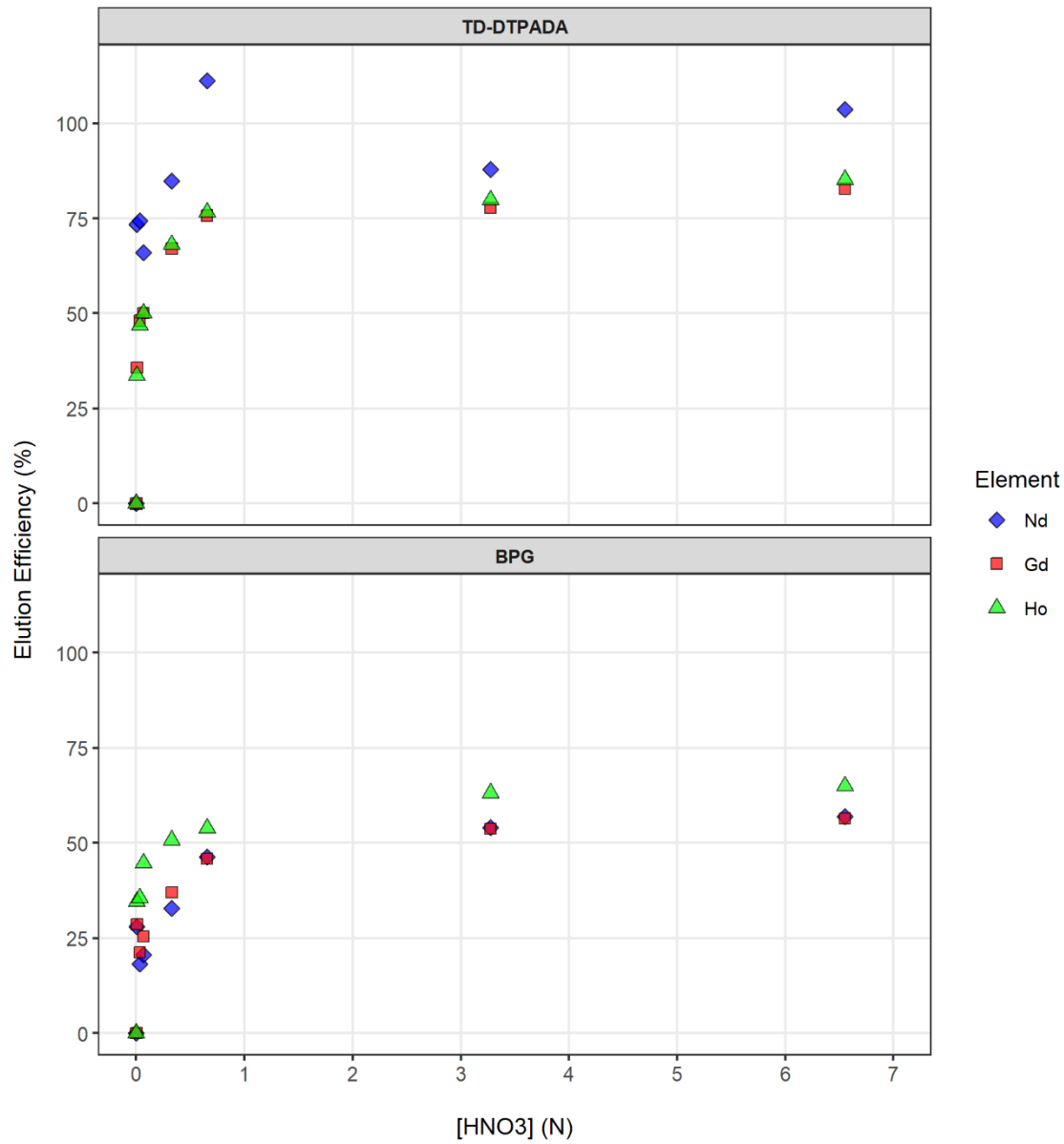
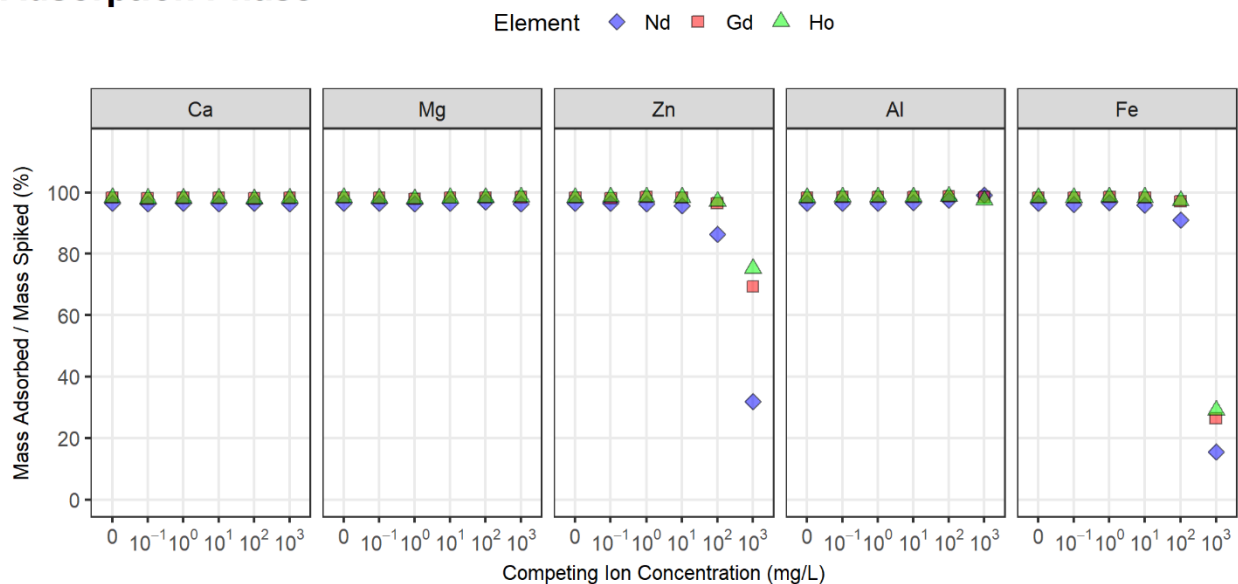


Figure A.3. REE elution efficiency for DTPADA and BPG on silica as a function of nitric acid strength after one use cycle. Adsorption cycles were performed at pH ~1.8.

Adsorption Phase



Elution Phase

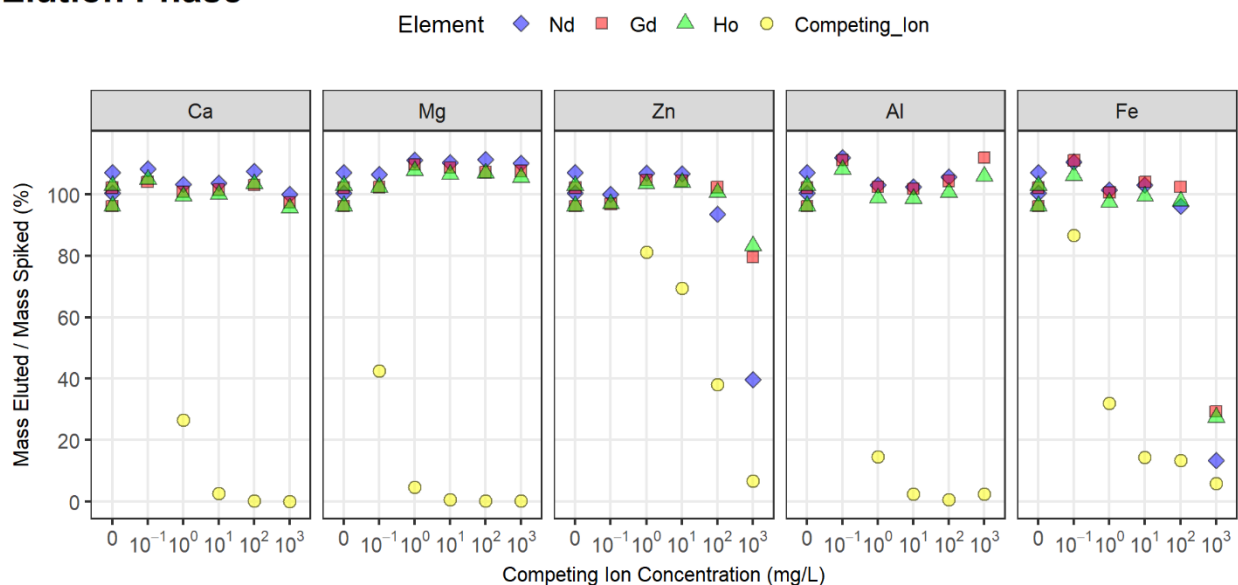


Figure A.4. Ratio of mass eluted to mass spiked for each element eluted from TD-DTPADA particles after competitive adsorption study. Adsorption was conducted at pH ~ 2 and room temperature.

After completion of adsorption reactions for the competition study (10g/L adsorbents in 0.5M NaCl containing 100ppb of each REE + varied concentrations of competing ions), TD-DTPADA adsorbents were separated from solution, rinsed with deionized water, dried overnight, then adsorbed elements were eluted using 0.75N HNO₃. The elution data shown in Figure A.4

confirm the adsorption phase results from Figure 2.4.B of the main text. The low ratio of mass eluted to mass spiked indicates inefficient adsorption of competing ions, particularly in higher concentration ranges, whereas REE uptake was approximately 100% in nearly all samples. This data is summarized in Figure A.5.

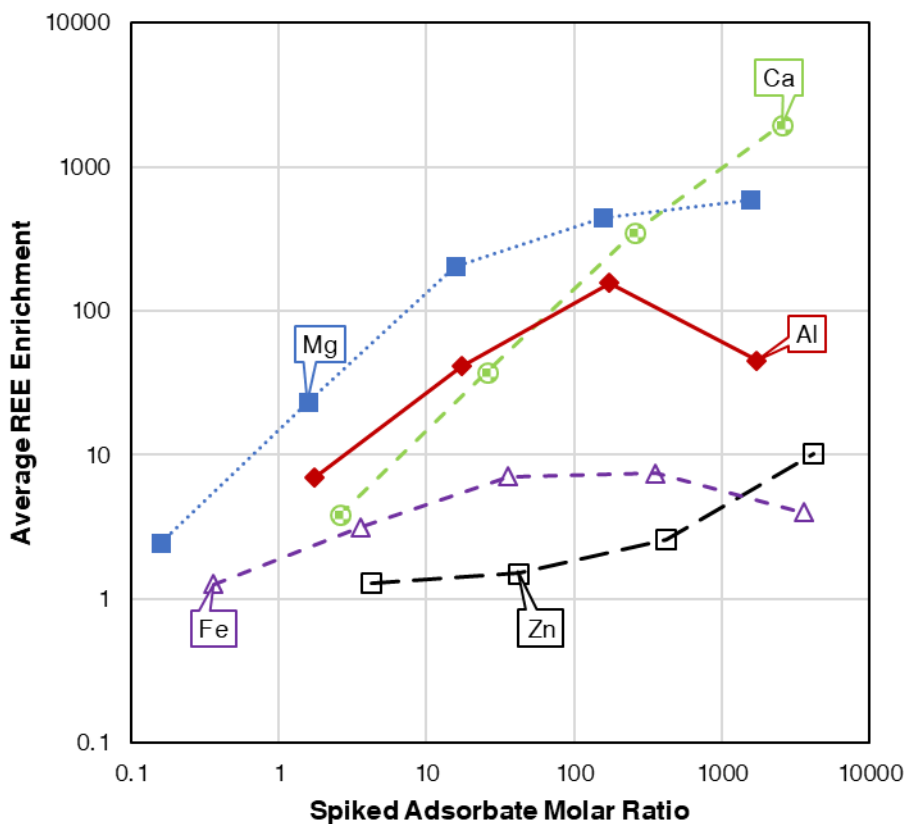


Figure A.5. Enrichment factors for REE relative to competing ions shown as a function of molar ratios of spiked adsorbate concentrations (i.e., x-axis = $[Competing\ Ion]_i / [REE]_i$; adsorbent = TD-DTPADA).

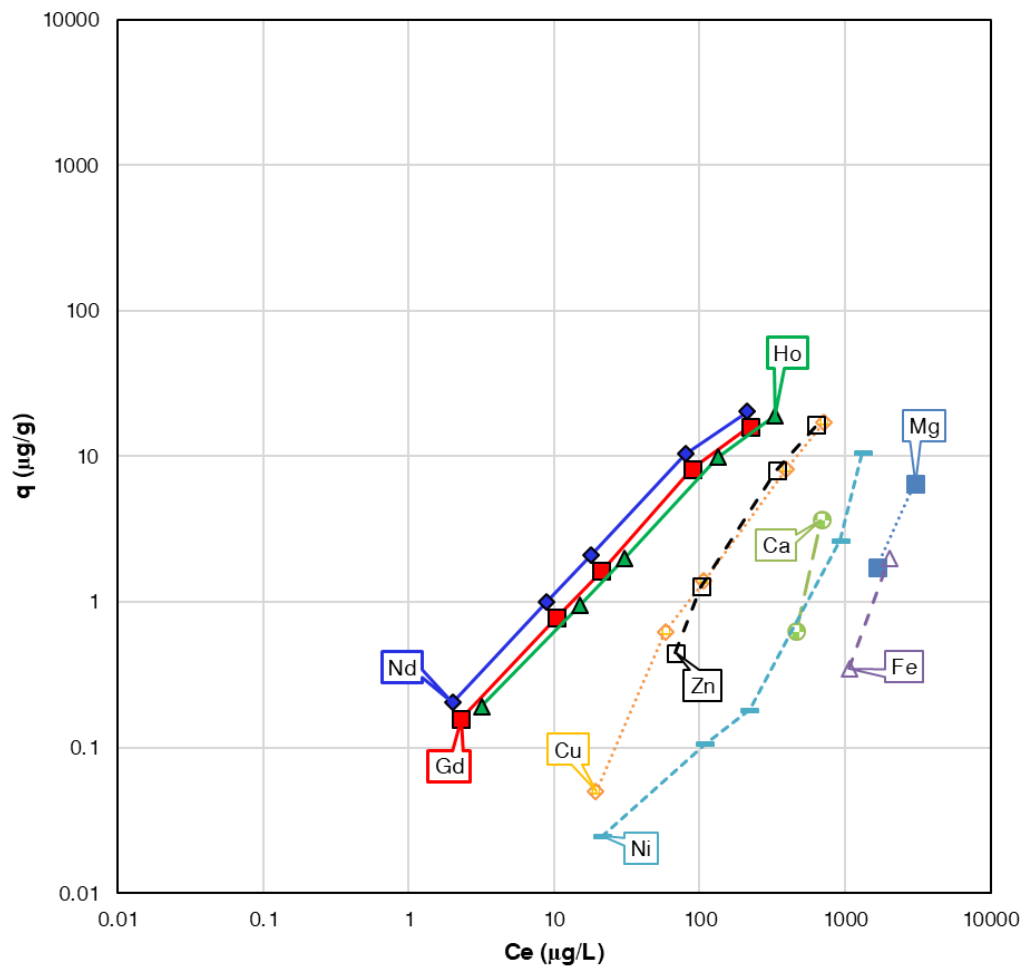


Figure A.6. Competitive isotherm results TD-DTPADA functionalized adsorbents with a mixture of 10 elements (7 competing ions and 3 REE) spiked at equal concentrations on a mass basis. Equilibrium solution-phase concentrations are shown on the x-axis, while the y-axis shows adsorbed concentrations for each element (pH = 2.5, T ~ 20°C).

Table A.4. Separation factors for REE and competing ions from the competitive isotherm study. Adsorbent
 These results are based on elution data from the sorption study.

Average C-spiked (mg/L)	Average Separation Factor ($\alpha_{\text{REE/Competing_Ion}}$)						
	Mg	Al	Ca	Fe	Ni	Cu	Zn
0.02	76.8	44.5	199.3	36.1	15.9	9.5	12.9
0.11	35.1	16.5	41.5	14.0	40.2	12.3	5.0
0.23	38.2	11.8	20.4	20.5	46.6	12.3	4.1
1.15	154.7	42.1	71.8	40.4	32.9	11.0	4.0
2.29	194.4	57.6	71.1	33.0	10.2	6.8	2.9

APPENDIX B

**Supporting Information for: Adsorption Kinetics,
Thermodynamics, and Isotherm Studies for
Functionalized Lanthanide Chelating Resins**

Chelating Ligands and Surface Immobilization

Figure B.1 shows the expected coordination structures for Ln-DTPA complexes both in solution and on the functionalized adsorbents. The bottom right configuration shows the combined influences of binding by the DTPA ligand and residual surface amines.

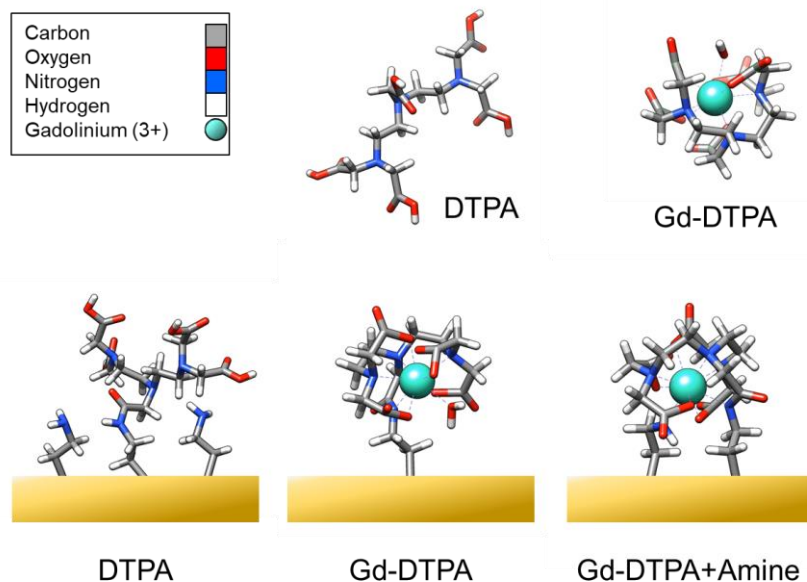


Figure B.1. Lanthanide complex coordination by solution phase and surface-tethered DTPA molecules. Structures for surface complexed REE inferred from literature-reported conformations of REE-DTPA complexes in solution phase (Thakur et al. 2013).

XPS Analysis

Table B.1. Elemental composition of functionalized adsorbents and aminated support.

Functional Group (Element %)									
Ligand	C-C, C=C	C-N	C=O	C(=O)-O	N-H	N-X=O*	NO ₃	O	P
Amine	48.95	16.89	5.49	0.87	5.39	1.71	1.80	18.80	0.08
PAA	49.05	16.11	5.23	1.22	4.82	1.98	1.30	19.50	0.52
BPG	47.48	17.71	5.00	1.21	4.34	2.05	1.32	19.60	0.68
DTPADA	37.63	23.99	6.64	3.14	6.03	1.96	0.92	19.50	0.22
Concentration (mmol/g)									
Ligand	C-C, C=C	C-N	C=O	C(=O)-O	N-H	N-X=O*	NO ₃	O	P
Amine	37.80	13.05	4.24	0.67	4.16	1.32	1.39	14.52	0.06
PAA	37.12	12.19	3.96	0.92	3.65	1.50	0.99	14.76	0.39
BPG	35.94	13.40	3.78	0.92	3.28	1.55	1.00	14.83	0.51
DTPADA	28.92	18.44	5.10	2.41	4.63	1.50	0.70	14.99	0.17

*X = C or P

Sample calculations for ligand concentrations are provided in the following text. Phosphorous was used as an indicator of ligand attachment for PAA (1 P molecule per ligand) and BPG (2 P per ligand), and carboxyl groups were used to identify DTPA attachment (4 x C(=O)-O per surface-bound ligand, since one carboxyl group is occupied by the amide bond with the resin surface). Background values from the aminated support were subtracted from the ligand-functionalized concentrations during calculations. These results were confirmed by calculating ligand loading based on amine conversion efficiency using amine concentrations provided by the resin supplier. Results in the main text refer to the 'amine conversion' calculated values. Direct conversion of XPS surface concentration results to bulk concentrations of ligand on the resins may introduce a degree of error since XPS is only capable of measuring elemental content of a thin surface film. It should be noted, however, that ligand concentrations were nearly identical with both calculation methods, as shown in Table B.2.

Ligand Concentration Sample Calculations for PAA – ‘Bulk Concentration’ Method

$$\text{Mass \%} = \frac{\text{Element \%} \times \text{Element M.W.}}{\sum \text{Element \%} \times \text{Element M.W.}} = \frac{(0.52) \times \frac{31g P}{mol P}}{\left(71.6 \times \frac{12g C}{mol C}\right) + \left(8.1 \times \frac{14g N}{mol N}\right) + \left(19.5 \times \frac{16g O}{mol O}\right) + \left(0.52 \times \frac{31g P}{mol P}\right)}$$

$$= 1.22\%$$

$$\text{Ligand Concentration} = \frac{\left(\frac{\text{Mass \%}}{\text{M.W.}}\right)_{\text{PAA-Functionalized Resin}} - \left(\frac{\text{Mass \%}}{\text{M.W.}}\right)_{\text{Aminated Support}}}{\text{Moles Element} / \text{Ligand}}$$

$$= \frac{(0.0122 - 0.00191)}{\frac{31g P}{mol P} \times \frac{1mol P}{mol PAA}} = 3.3 \times 10^{-4} \frac{\text{mol PAA}}{\text{g Resin}}$$

Sample Calculations for PAA – ‘Amine Conversion’ Method

$$\text{Amine Conversion} = \frac{\%P_{\text{PAA-Functionalized Resin}} - \%P_{\text{Aminated Support}}}{\%NH_{\text{Aminated Support}} \times \frac{1mol P}{1mol PAA}}$$

$$= \frac{0.52 - 0.08}{5.49} = 8\%$$

$$\text{Ligand Concentration} = \text{Amine Concentration}_{\text{Aminated Support}} \times \text{Amine Conversion}$$

$$= 4.0 \frac{\text{mmol}}{\text{g}} \times 8\% = 3.3 \times 10^{-4} \frac{\text{mol PAA}}{\text{g Resin}}$$

Table B.2. Summary of ligand concentration calculations using two different methods.

Ligand	Ligand Concentration (mmol/g)	
	Bulk Concentration Method	Amine Conversion Method
Amine	4.16	4.00*
PAA	0.33	0.33
BPG	0.23	0.22
DTPADA	0.44	0.42

*Provided by resin manufacturer

Maximum Theoretical Ligand Loading Calculations

Ligand concentrations on the resin particle surfaces are theoretically limited by steric effects and by attachment sites (i.e., amine groups). Maximum concentrations based on one-to-one ligand-to-amine attachment would be approximately 4 mmol/g. The maximum packing density based on steric effects can be approximated using molar volume for each ligand (75 cm³/g for PAA, 135 cm³/g for BPG, and 245 cm³/g for DTPADA) and surface area for the raw support (~15 m²/g) (United States Environmental Protection Agency 2017). Sample calculations for BPG – assuming spherical ligand configurations – are shown below. Maximum sterically-limited ligand concentrations are 7.0x10³ mol/g (PAA), 4.7x10³ mol/g (BPG), and 3.2x10³ mol/g (DTPADA). These concentrations are significantly higher than those measured by XPS, as well as the amine-limited theoretical maxima, which suggests that attachment efficiency is hindered by other factors.

$$\text{Ligand Radius} = r = (\text{Molar Volume} \times \frac{3}{4} \div \pi)^{1/3} = 3.18 \frac{\text{cm}}{\text{mol}}$$

$$\text{Ligand Area} = \pi r^2 = 32 \frac{\text{cm}^2}{\text{mol}} = 3.2 \times 10^{-3} \frac{\text{m}^2}{\text{mol}}$$

$$\text{Max Ligand Concentration} = \frac{\text{Resin Surface Area}}{\text{Ligand Area}} = 4.7 \times 10^3 \frac{\text{mol}}{\text{g}}$$

Table B.3. Ligand concentrations from varied functionalization parameters (calculated using bulk concentration method).

Particle	Treatment	Ligand Concentration (mmol/g)	Ligand Density (mmol/m ²)	Improvement from Standard Method
PAA	Standard	1.60	0.126	-
	40°C	1.81	0.142	+13%
	72Hr	1.46	0.115	-8%
BPG	Standard	0.62	0.077	-
	40°C	0.80	0.100	+30%
	72Hr	0.73	0.091	+18%
DTPADA	Standard	0.22	0.020	-
	40°C	0.27	0.024	+20%
	72Hr	0.33	0.029	+48%

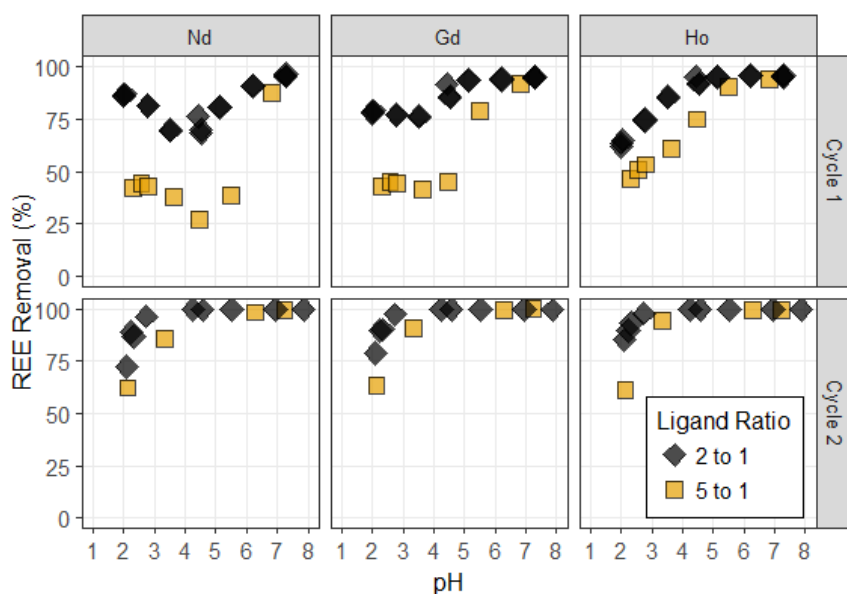


Figure B.2. Effect of molar ratio of ligand to surface amines used in synthesis on adsorbent performance (Ligand = BPG; [NaCl] = 0.5M; [REE] = 0.1 mg/L each; Reaction Time = 24 hours; Reaction Temperature = 20°C).

Lanthanide and Ligand Speciation Modeling

Chemical speciation modeling was performed using the PHREEQC software developed by the U.S. Geological Survey (Charlton and Parkhurst 2011; Parkhurst and Appelo 2013) and implemented in the R programming language (R Core Team 2017). The following figures represent equilibrium fractions for each dissolved species at 25°C using thermodynamic data from the Lawrence Livermore National Laboratory database (llnl.dat). Precipitation of hydroxide ($\text{Ln}(\text{OH})_3$) species is indicated by gray shaded regions (Figure B.3 and Figure B.4). Elements are shown individually for clarity but were modeled as mixtures. Ligand speciation curves were also developed using literature values for dissociation constants (Gritmon et al. 1977; “N,N-Bis(phosphonomethyl)glycine $\geq 98.0\%$ (T) | Sigma-Aldrich” n.d.; Nash 1997), which are presented as reference values in Table 3.2 of the main text (Figure B.5).

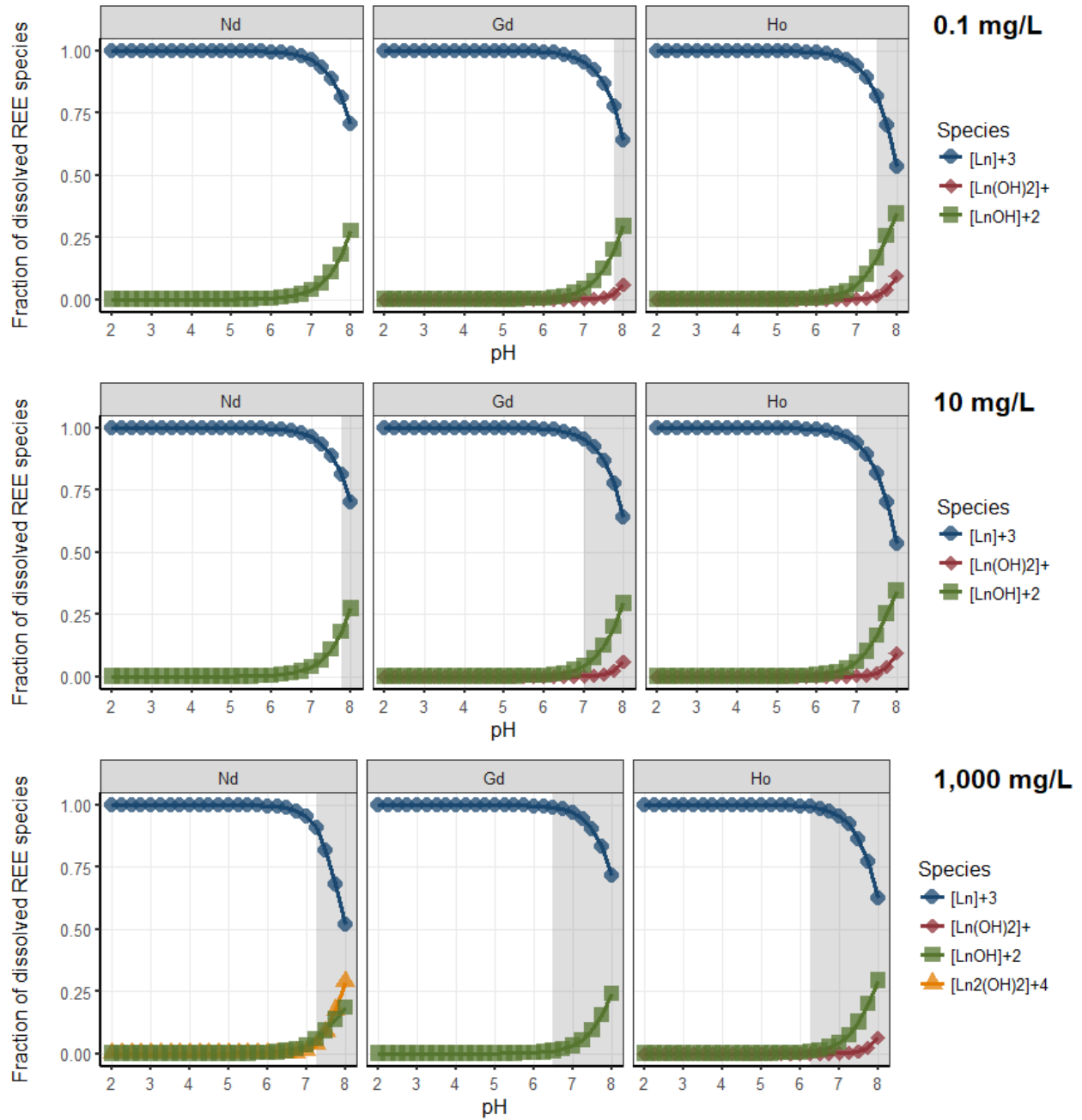


Figure B.3. Calculated equilibrium speciation of lanthanides (Nd, Gd, and Ho at 0.1-1,000 mg/L each) in pure water ($I = 0$) across the pH range of interest for this study. Grey shaded regions indicate potential precipitation of REE.

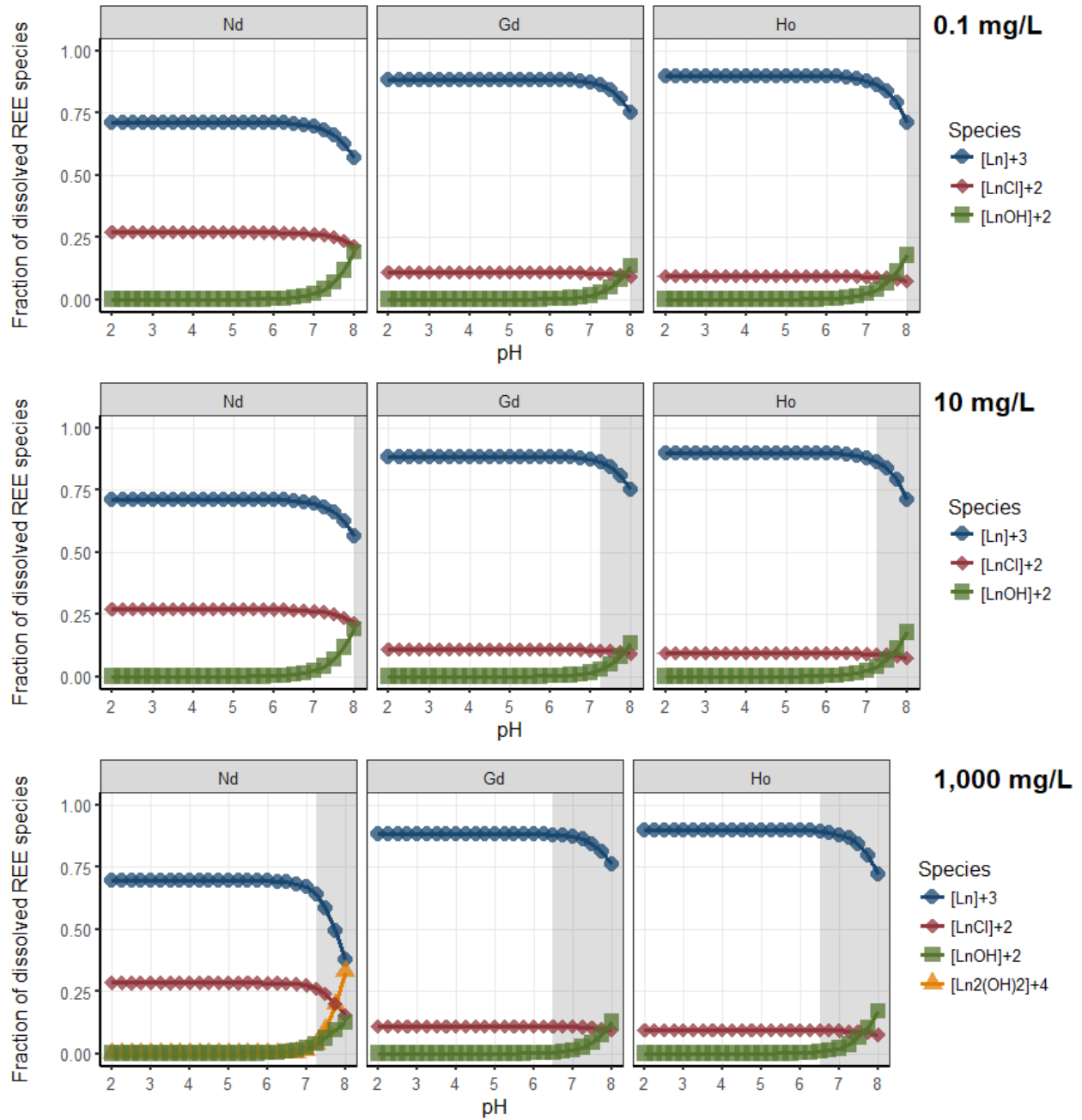


Figure B.4. Calculated equilibrium speciation of lanthanides in solutions containing REE (Nd, Gd, and Ho at 0.1-1,000 mg/L each) and 0.5M NaCl. Note that the species listed are different from Figure B.3 due to the presence of chlorides. Grey shaded regions indicate potential precipitation of REE.

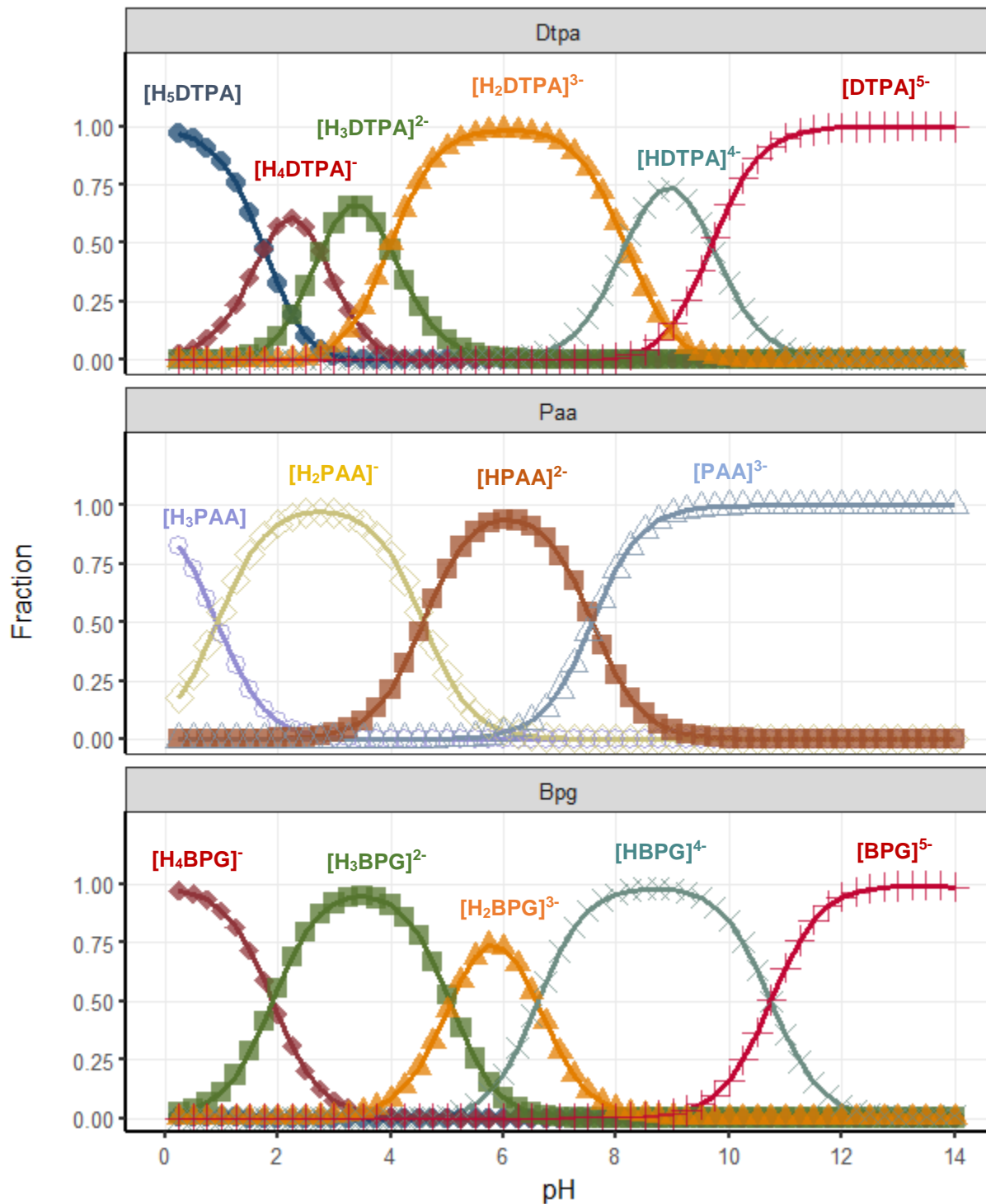


Figure B.5. Calculated equilibrium speciation of DTPA, PAA, and BPG ligands as a function of pH in solution with $I = 0.5M$.

Complexation Modeling for REE with Solution-Phase Ligands

Complexation of dissolved lanthanides was also modeled for the DTPA and PAA ligands, assuming solution-phase behavior. Literature values for ligand pK_A and stability constants were used to determine ligand speciation and equilibrium complex concentrations (DTPA (Grimes and Nash 2014); PAA (Nash 1997)). Since Ln-PAA stability constants for the REE studied in this research were not available, the value for Eu was used to model Nd-PAA, Gd-PAA, and Ho-PAA complexes. Representative concentrations were calculated to be 4.4 mmol-DTPA/L and 3.3 mmol-PAA/L based on experimental adsorbent loadings (10 g/L), sample volumes (10 mL), and XPS data (0.44 mmol-DTPADA/g and 0.33 mmol-PAA/g). Elements are shown individually for clarity but were modeled as mixtures.

DTPA complexes were modeled using LnDTPA^{2-} and LnHDTPA^- species, since these have been reported in the literature as the primary chelating species (Grimes and Nash 2014). PAA complexes were modeled using LnHPAA^+ , $\text{Ln}(\text{H}_2\text{PAA})_2^+$, and $\text{Ln}(\text{HPAA})_2^-$ species, though most of the complexation is attributable to the species with ligand to metal ratios of 2:1 (Nash 1997).

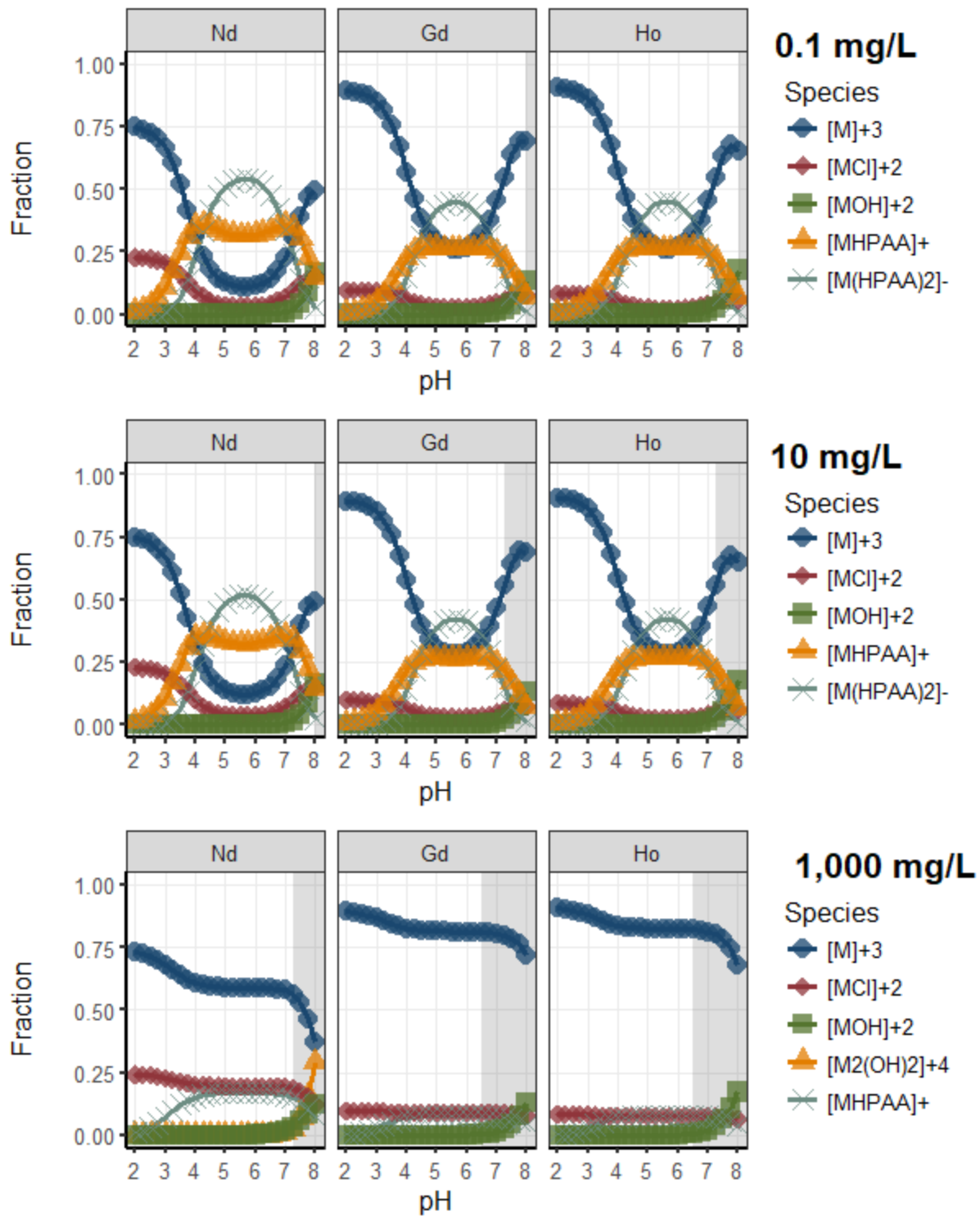


Figure B.6. Modeled complexation of lanthanides (Nd, Gd, and Ho at 0.1-1,000 mg/L each) by solution phase DTPA (4.4 mmol/L) in 0.5M NaCl. Note that colors and shapes for species are different in 1,000 mg/L plots.

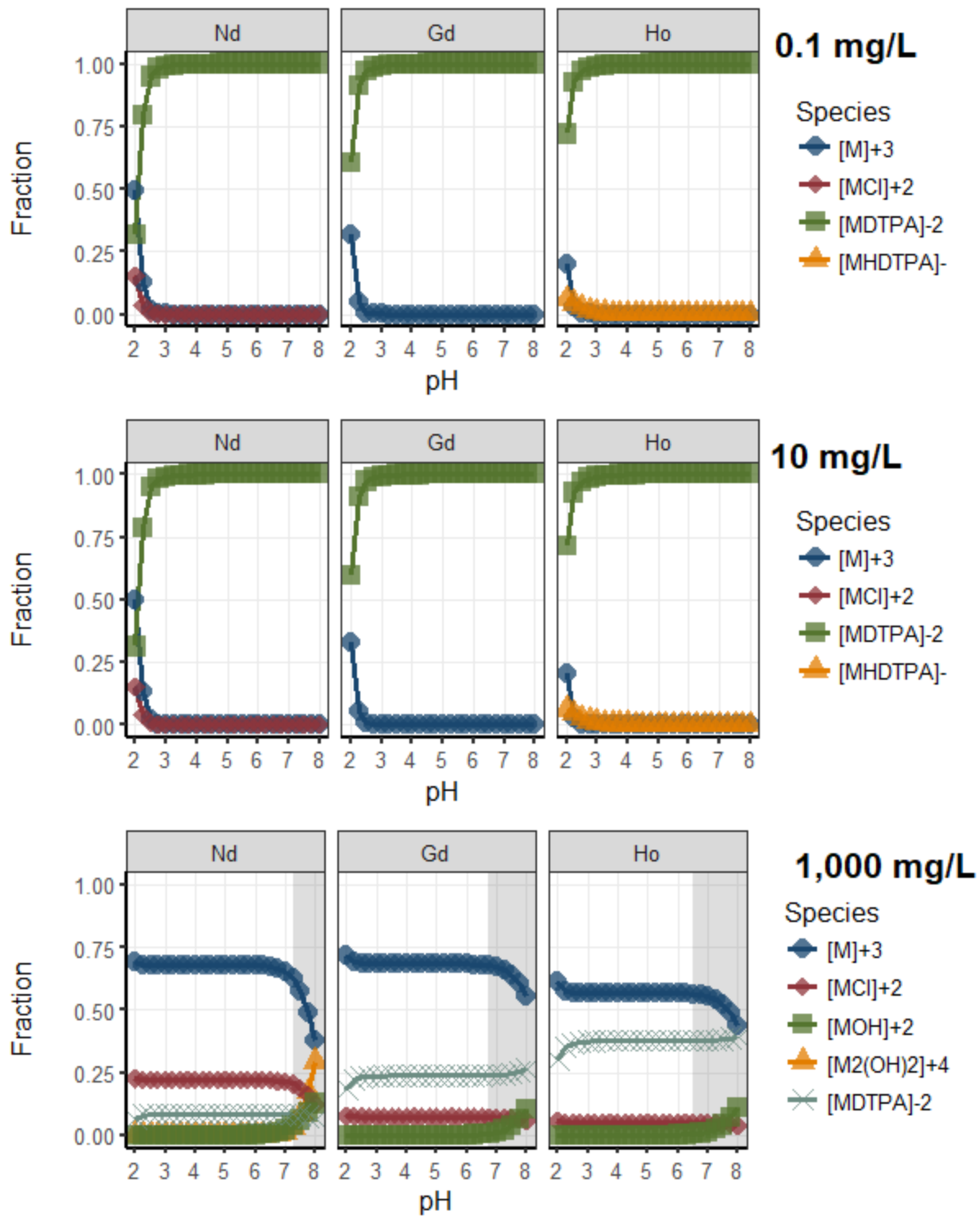


Figure B.7. Modeled complexation of lanthanides (Nd, Gd, and Ho at 0.1-1,000 mg/L each) by solution phase PAA (3.3 mmol/L) in 0.5M NaCl. Note that colors and shapes for species are different in 1,000 mg/L plots.

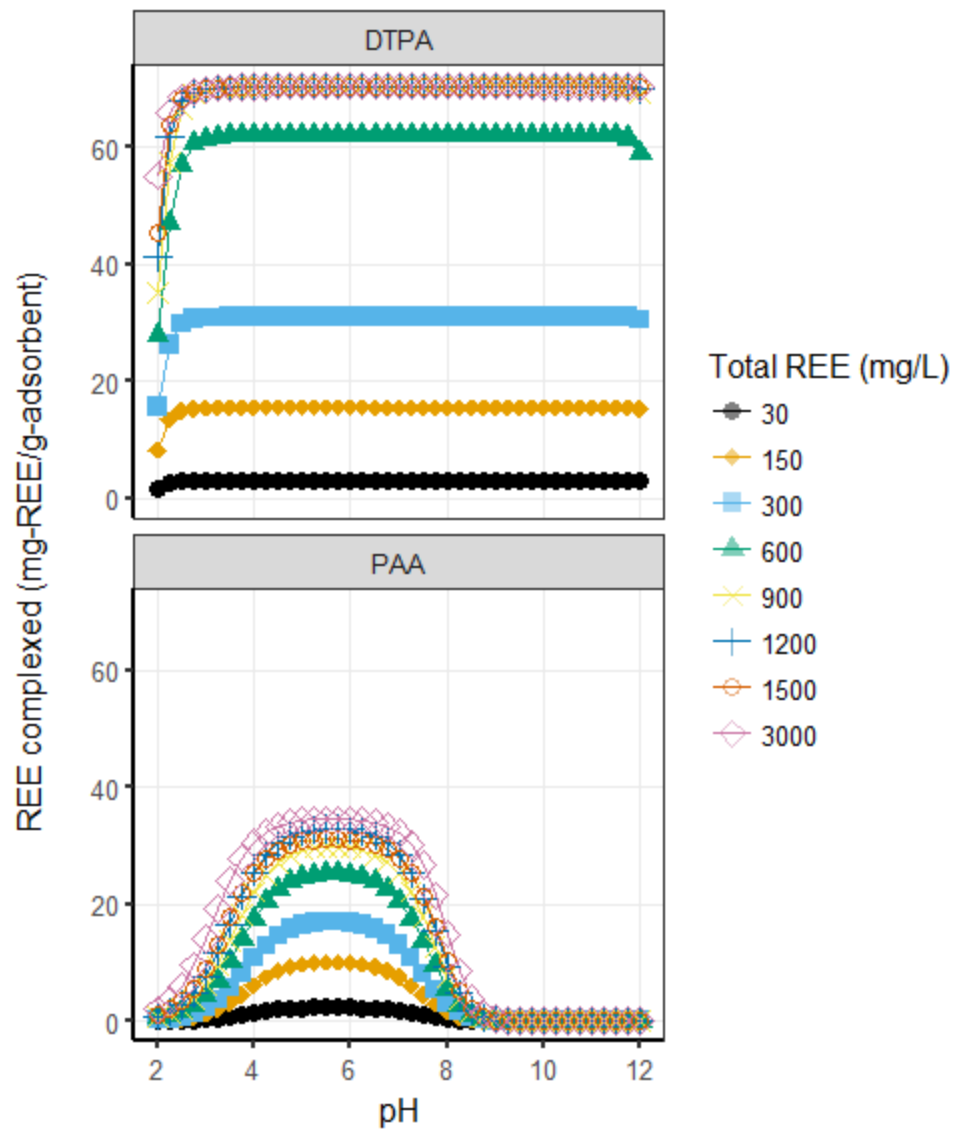


Figure B.8. Summary of modeled complexation by DTPA (4.4 mmol/L) or PAA (3.3 mmol/L) as a function of solution pH in 0.5M NaCl solutions assuming liquid phase ligand behavior.

Isotherm Analysis and Support Comparison

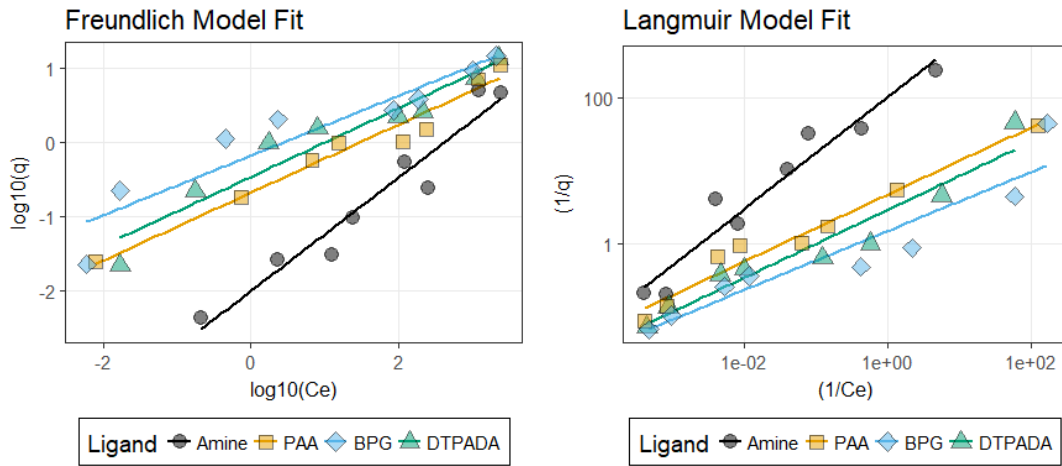


Figure B.9. Linearized Freundlich and Langmuir isotherm model fitting to experimental results for total REE equilibrium adsorption on functionalized adsorbents and aminated resin supports ($I = 0.5M$ NaCl).

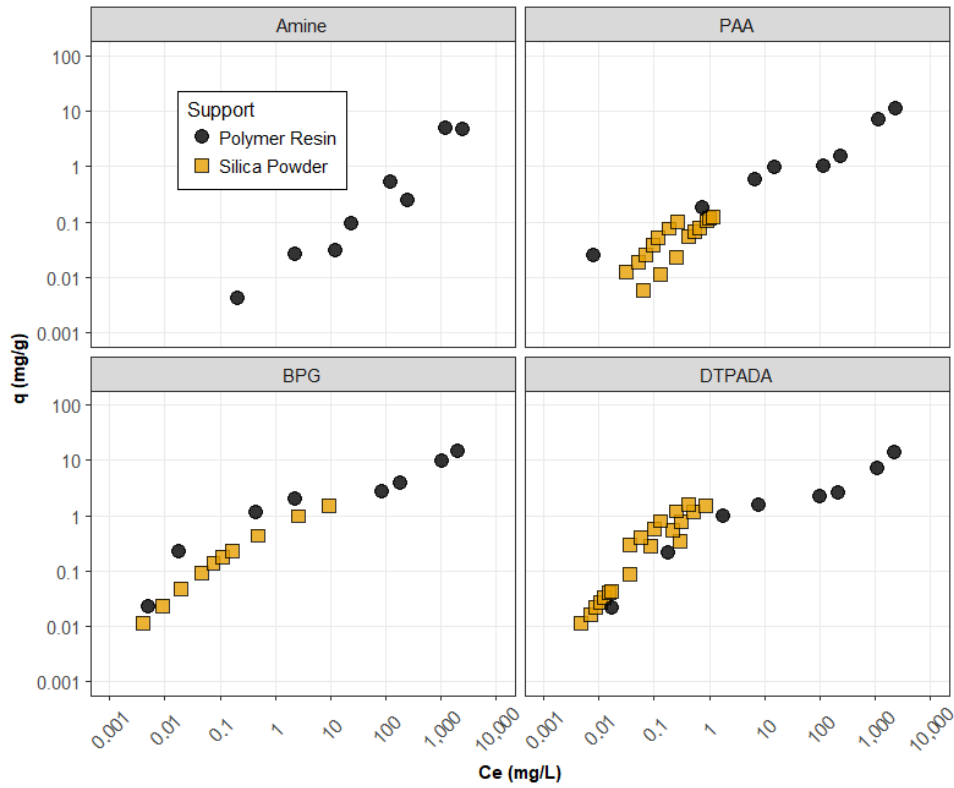


Figure B.10. Log-log isotherm plot for total REE (Nd, Gd, and Ho) adsorption on functionalized silica particles ($d \sim 0.1mm$) and polymer resins ($d \sim 0.6mm$).

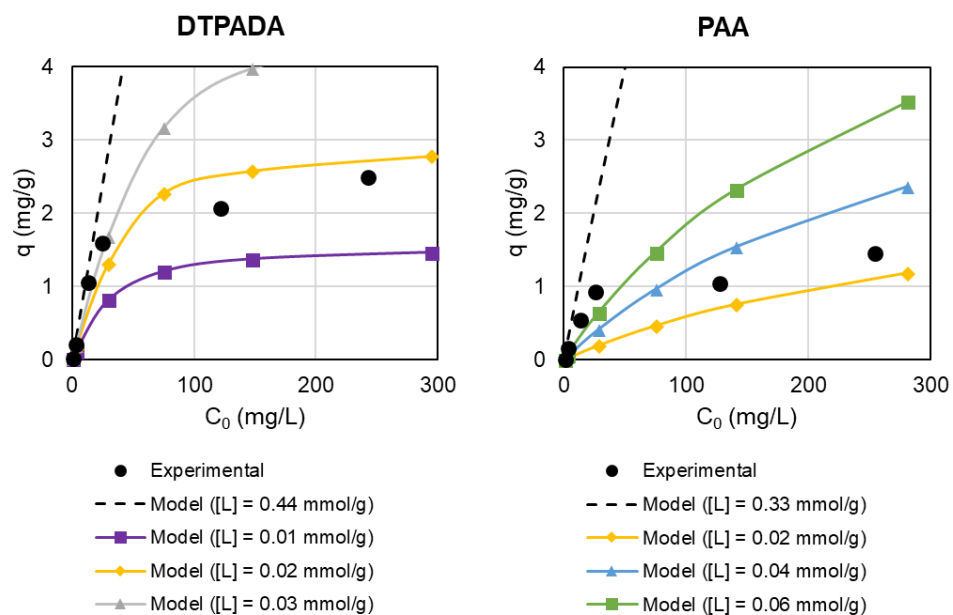


Figure B.11. Total REE (Nd, Gd, and Ho) adsorption (y-axis) as a function of initial total concentration (x-axis). Experimental adsorption data from isotherms are compared to solution-phase ligand binding models using a variety of ligand concentrations (0.01-0.44 mmol/L) for 0.5M NaCl solutions.

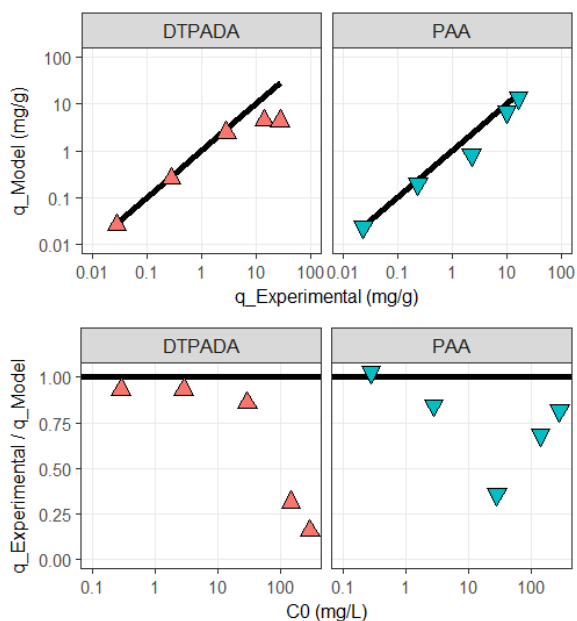


Figure B.12. Comparison of solution-phase model predictions for total REE (Nd, Gd, and Ho) complexation with experimental data for adsorption of REE on functionalized adsorbents. Solid black lines indicate 1:1 correspondence of experimental adsorption data to the solution-phase model predictions for REE complexation. Points are shown as experimentally measured $q_{\text{Experimental}}$ or calculated q_{Model} using a solution-phase model for an equivalent ligand concentration (i.e., [ligand in solution] = [ligand on resins]; [PAA] = 0.33 mmol/g; [DTPA] = 0.44 mmol/g).

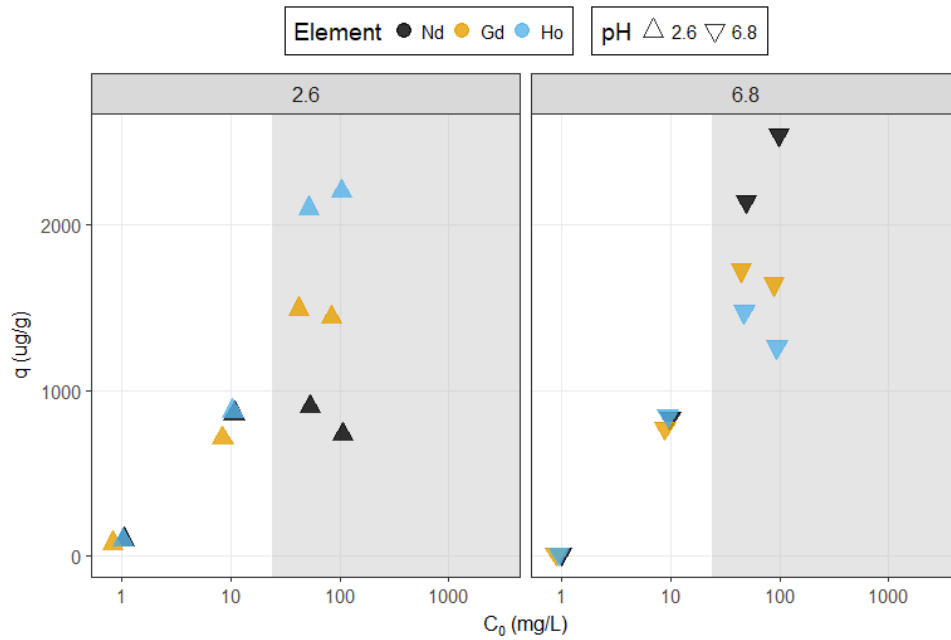


Figure B.13. Individual REE element data from Figure 3.6.B of the main text. Shown as adsorbed concentration vs. spiked concentration for each REE, with the shaded regions indicating likely saturation of surface DTPA.

Thermodynamic Model Fitting

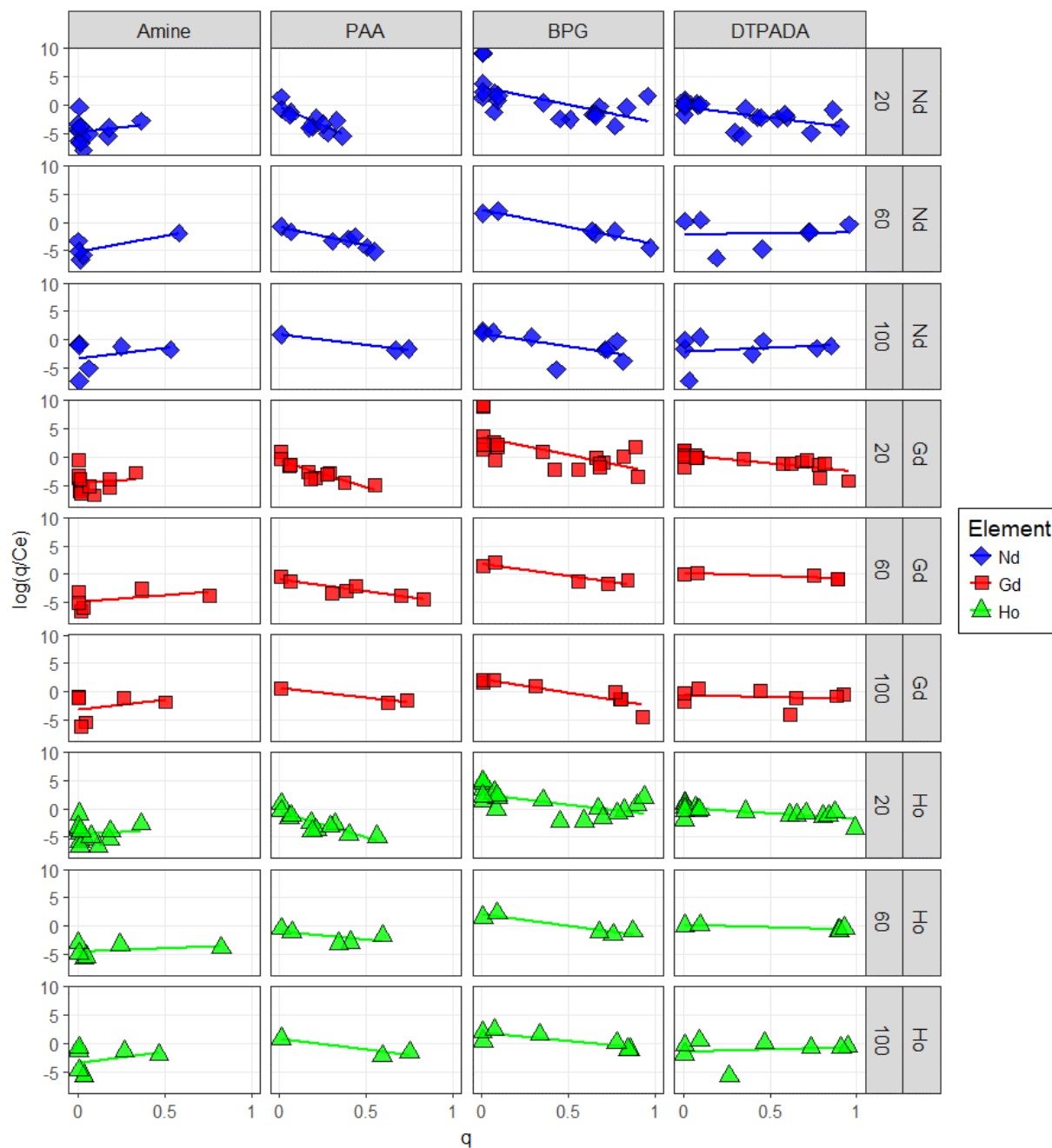


Figure B.14. Thermodynamic model fitting of REE equilibrium adsorption data which shows $\ln(q/C_e)$ [L/g] vs. q [mg/g]. Results are organized by ligand (columns) and reaction temperature/element (rows, temperature units = °C). Y-intercepts from this plot were used to calculate $\ln(K_0)$ and ΔG° values presented in Table 3.4 of the main text.

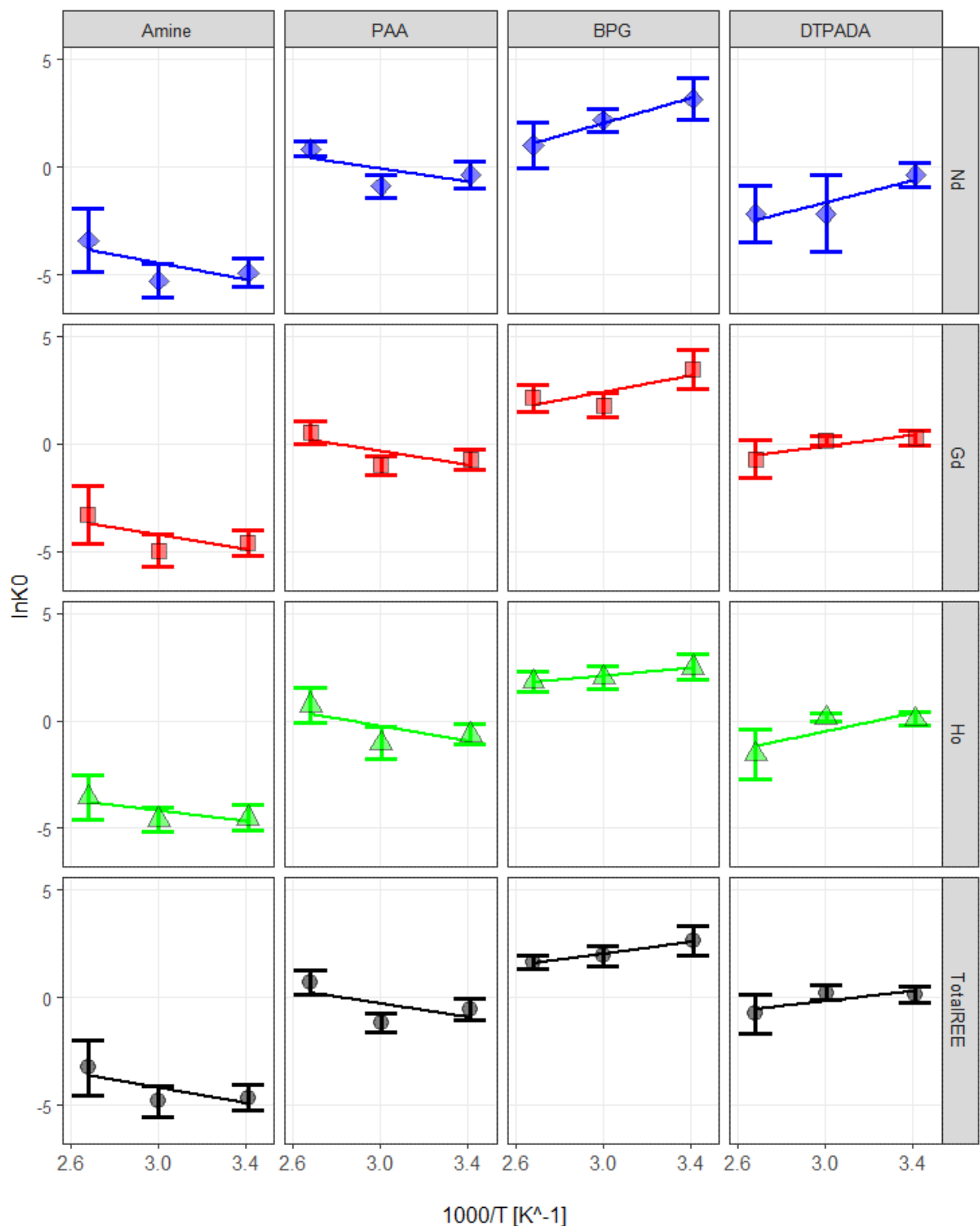


Figure B.15. Van't Hoff plot used to calculate entropy and enthalpy values for adsorption of REE mixtures in sodium chloride solutions (0.5M NaCl) at different temperatures. Results are organized by ligand (columns) and element (rows). Data points shown here represent the y-intercepts from Figure B.14. Error bars show standard error for each series.

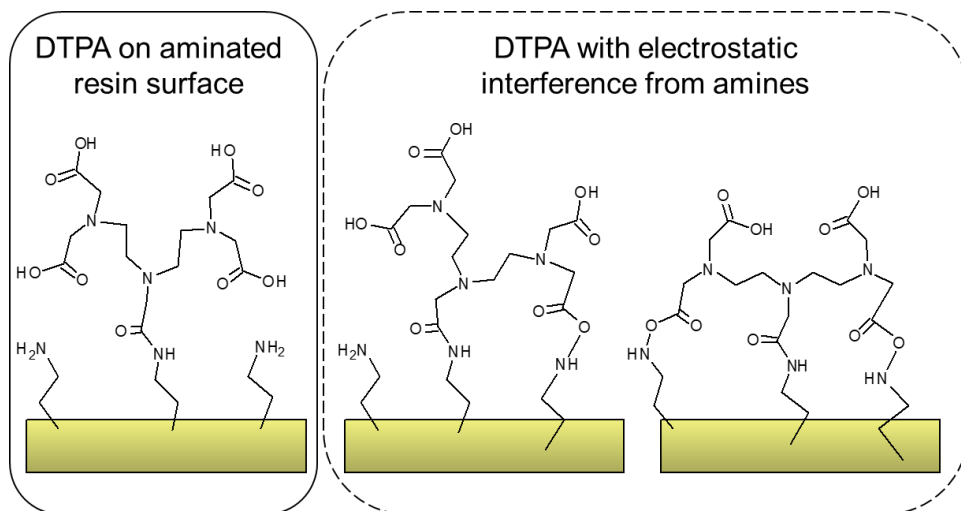


Figure B.16. Potential structures of surface-bound DTPA ligands, shown with and without electrostatic interference from amines. Note that amines will be protonated (i.e., NH_3^+) below pH ~ 9.3 .

APPENDIX C

Supporting Information for: Recovery of Rare Earth Elements with Ligand-Functionalized Polymers in Fixed-Bed Adsorption Columns

Metal Speciation for Selectivity Tests

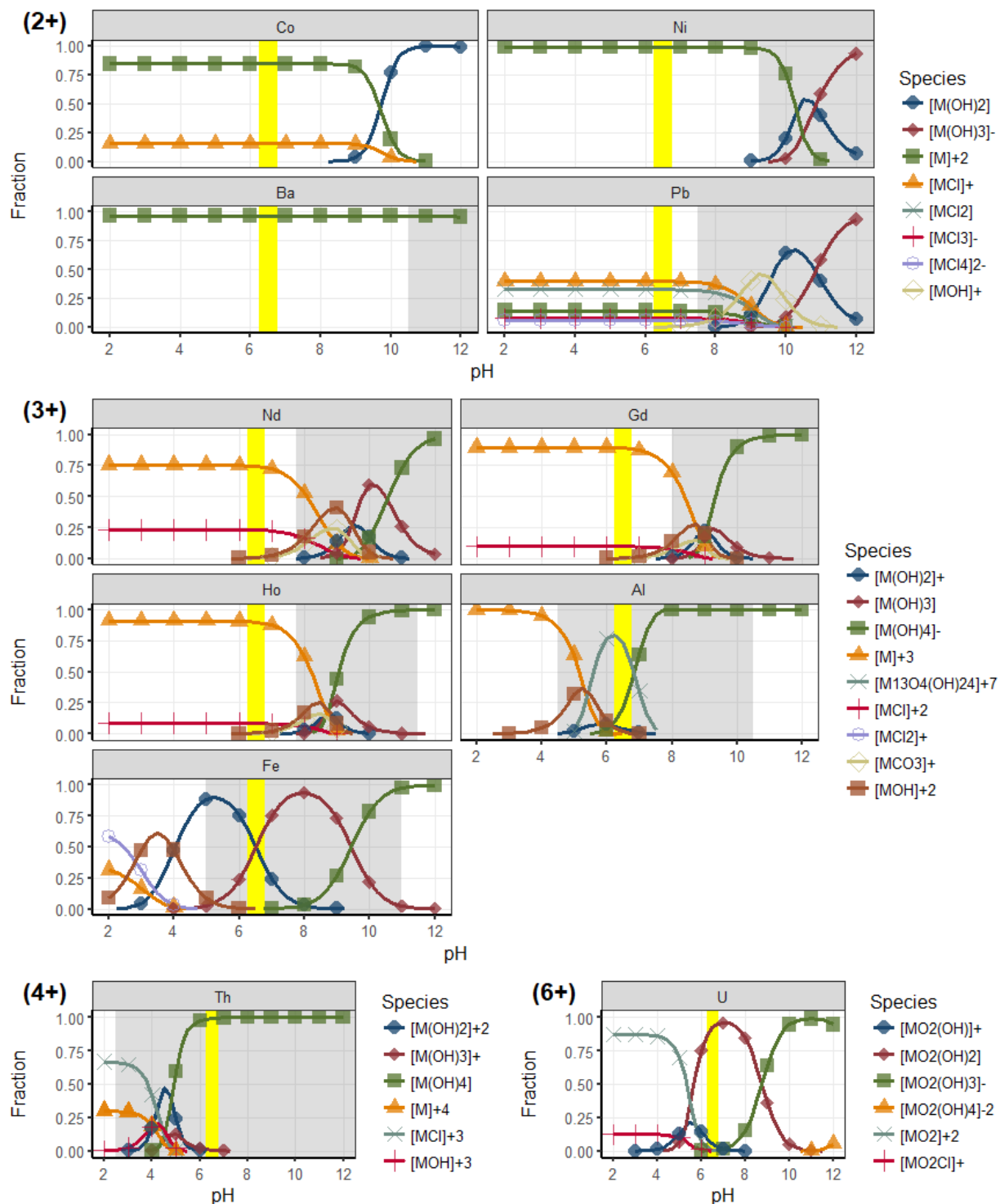


Figure C.1. Speciation of metals in complex mixture used in batch and column experiments calculated with PHREEQC. Metals are separated by valence of the predominant species. Gray shaded regions show potential pH regions of precipitation, and the yellow bar indicates the experimental pH used in this research. (Metal concentrations = 1 mg/L each; I = 0.5M NaCl)

Adsorption and Recovery from Competitive Isotherms

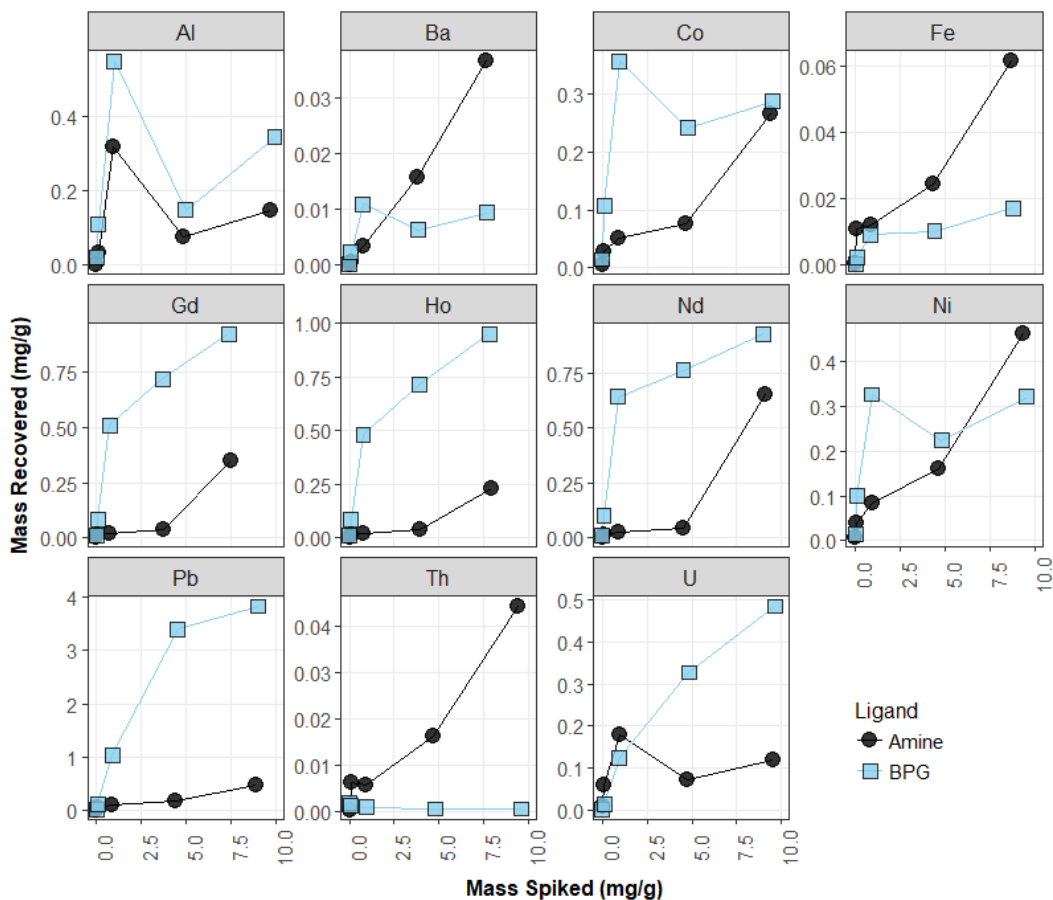


Figure C.2. Metal recovery for each metal in Group D from Figure 4.9 of the main text. Y-axes are different for each plot.

Elution data for Group D was transformed to show separation factors (α) for average REE over each metal, according to Equation C.1. Separation factors in this form capture the efficiency of the entire extraction process, as both the adsorption and elution phases are accounted for. The separation factors are summarized in Table C.1.

$$\alpha = \frac{(C_{e_Elution}/C_{e_Adsorption})_{REE}}{(C_{e_Elution}/C_{e_Adsorption})_{Competing\ Metal}} \quad (C.1)$$

Table C.1. Separation factors for REE (average of Nd, Gd, and Ho) over other metals from the Group D competitive isotherm. Calculated from adsorption and elution data. Values highlighted in red indicate selectivity for the competing metal over REE, while blue or white cells show favorable REE separation (darker blue = greater REE selectivity relative to the competing metal).

Ligand	C _i (mg/L)	Average REE Separation Factor ($\alpha_{\text{REE/Competing_Metal}}$)							
		Al	Fe	Co	Ni	Ba	Pb	Th	U
Amine	1	0.5	1.4	0.5	0.3	28.4	0.2	2.6	0.2
	10	0.1	2.4	0.5	0.3	16.1	0.3	5.0	0.1
	50	0.6	1.9	0.6	0.3	2.3	0.2	2.7	0.6
	100	3.5	8.0	1.9	1.0	10.6	0.9	10.1	3.7
BPG	1	1.1	171.2	1.2	1.6	203.1	0.2	415.6	6.3
	10	1.3	121.4	2.5	2.9	159.5	0.2	1,274.2	5.2
	50	7.2	99.7	4.2	4.5	127.5	0.1	1,897.8	2.5
	100	3.9	75.4	4.4	3.8	102.6	0.2	2,382.4	2.2

Table C.2. Summary of adsorption results for each metal in the multi-element column test with Group D from Figure 4.10 of the main text. Values for the REE are highlighted in yellow.

Element	MW	Resin Adsorption Results					
		Amine			BPG-Functionalized		
		ug/g	umol/g	Breakthrough	ug/g	umol/g	Breakthrough
Co	58.93	86	1.45	100%	202	3.43	100%
Ni	58.69	53	0.90	100%	203	3.46	100%
Ba	137.33	0	0.00	100%	13	0.10	100%
Nd	144.24	30	0.21	100%	749	5.20	91%
Gd	157.25	55	0.35	100%	755	4.80	80%
Ho	164.93	97	0.59	100%	856	5.19	67%
Pb	207.20	95	0.46	100%	1058	5.11	29%
Th	232.04	40	0.17	0%	58	0.25	0%
U	238.03	266	1.12	3%	388	1.63	0%

Mass Transfer Zone Calculations

By studying adsorbent properties and making a few assumptions about the packing of a fixed-bed adsorption column, it is possible to calculate properties of the Mass Transfer Zone for adsorption from a given flow regime. Spherical packing of adsorbent particles within a column typically falls within predictable ranges; a commonly value used to represent the packing density (ρ) with random close packing of uniform spheres in a fixed volume is 0.64, though values over 0.7 may be achieved with agitation (An and Li 2013). This value assumes that all particles have the same diameter and density. For the column system used in these experiments, the bed volume was 0.82 cm^3 , so assuming a packing density of 0.64 the particles occupied approximately 0.52 cm^3 . This value includes both the adsorbent surface and the pore space. Total pore volume for the BPG-functionalized resin was $\sim 60 \text{ cm}^3/\text{kg}$ (Table 3.1 of the main text) and the mass of adsorbent in the bed was $\sim 300 \text{ mg}$ (Table 4.1 of the main text). Fluid superficial velocity (u) is related to the volumetric flow rate and column size and a suitable value was found to be approximately 0.4 m/hour for the BPG-functionalized resins (Section 4.3.1 of the main text). Bed depth (Z) for this system was 4.98 cm and the empty bed contact time (EBCT) was 8 minutes. Calculations for the column void fraction (ϵ), fluid velocity (v), and water residence time (T_w) within the column based on these values are shown below in Equations C.2-C.6.

$$\text{Bed Volume} = 0.82 \text{ cm}^3 = V_{\text{adsorbent}} + V_{\text{void}} = V_{\text{adsorbent}} + (1 - 0.64) \times 0.82 \text{ cm}^3 \quad (\text{C.2})$$

$$V_{\text{adsorbent}} = (V_{\text{bulk}} + V_{\text{pore}}) = 0.52 \text{ cm}^3 \rightarrow V_{\text{pore}} = \frac{60 \text{ cm}^3}{\text{kg}} \times 0.0003 \text{ kg} = 0.018 \text{ cm}^3 \quad (\text{C.3})$$

$$\epsilon = \frac{V_{\text{pore}} + V_{\text{void}}}{\text{Bed Volume}} = \frac{0.018 \text{ cm}^3 + 0.30 \text{ cm}^3}{0.82 \text{ cm}^3} = 0.39 \quad (\text{C.4})$$

$$v = \frac{u}{\epsilon} = \frac{0.4 \text{ m/hour}}{0.39} = 1.03 \text{ m/hour} \quad (\text{C.5})$$

$$T_w = \frac{Z\varepsilon}{v} = \frac{4.98 \text{ cm} \times 0.39}{103 \text{ cm/hour}} \times \frac{3600 \text{ seconds}}{\text{hour}} = 174 \text{ seconds} \quad (\text{C.6})$$

Adsorbate molecules are moved advectively by fluid flow and their transport is slowed down by interaction with the adsorbent particle surfaces. The rate of adsorbate transport is reflected through the Mass Transfer Zone velocity (v_{MTZ}) as shown in Equation C.7, where q_i^* is the adsorbed concentration in equilibrium with C_i and A_R is the column's cross-sectional area (Benjamin and Lawler 2013). The values for q_i^* are 1.75 mg/g ($C_e = 0.3$ mg/L total REE (Nd+Gd+Ho)), 2.81 mg/g ($C_e = 3$ mg/L), and 2.99 mg/g ($C_e = 30$ mg/L), as calculated from the Langmuir parameters for BPG-functionalized resins presented in Table 3.5 of the main text. Bulk density within the column (ρ_B) for these experiments was ~ 370 mg/cm³.

$$v_{MTZ} = \frac{QC_i}{C_i \varepsilon A_R + q_i^* \rho_B A_R} \quad (\text{C.7})$$

Substituting the values for C_i and q_i^* at each influent concentration from Figure 4.7 of the main text reveals that the MTZ speed for each condition is 1.08 mm/min ($C_i = 0.3$ mg/L total REE), 1.09 mm/min (3 mg/L), and 1.22 mm/min (30 mg/L). Therefore, the MTZ is expected to move through the column $\sim 13\%$ faster at influent concentrations of 30 mg/L total REE than 0.3 mg/L. The length of the mass transfer zone can be determined by its velocity and the time it takes for effluent concentrations to increase from 10% breakthrough (t_{10}) to 90% breakthrough (t_{90}). Values for $t_{90}-t_{10}$ were 20,000 minutes for 0.1 mg/L, 6,850 minutes for 1 mg/L, or 950 minutes for 10 mg/L. Thus, the length of the MTZ for each concentration was 2,160 cm (0.1 mg/L), 749 cm (1 mg/L), and 116 cm (10 mg/L).

Column Scaling Calculations

Fixed-bed adsorption column sizing based on target flow rate and influent composition can be calculated from volumetric flow rate (Q), influent concentration (C_i), and desired treatment time (t) using the adsorption capacity (q_i^*) in equilibrium with the influent concentration and equations shown below. REE capacity for the BPG-functionalized resins was modeled using Langmuir adsorption isotherm parameters at $C_i < 100$ mg/L ($q_{\text{Max}} = 3.01$ mg/g, $K_L = 4.658$ L/g; Table 3.5 of the main text). Table C.3 summarizes required column size for a single column packed with BPG-functionalized resins in a range of conditions based on these calculations. Note that the required diameter in high flow conditions may be excessively high for a single column and could be achieved by operating multiple smaller columns in parallel.

$$\text{Cross Sectional Area } (A_R) = \frac{Q}{u} \quad (\text{C.8})$$

$$\text{Column Diameter } (D) = 2 \times \sqrt{\frac{A_R}{\pi}} \quad (\text{C.9})$$

$$\rho_{\text{bulk}} = \frac{300 \text{ mg}}{0.82 \text{ cm}^3} \text{ (from experiments)} = 370 \frac{\text{kg}}{\text{m}^3} \quad (\text{C.10})$$

$$q_i^* = \frac{q_{\text{Max}} K_L C_e}{1 + K_L C_e} \quad (\text{C.11})$$

$$\text{Mass of Adsorbate Needed } (M) = \frac{t \times Q \times C_i}{q_{\text{max}}} \quad (\text{C.12})$$

$$\text{Volume of Adsorbate Needed} = \frac{M}{\rho_{\text{bulk}}} \quad (\text{C.13})$$

Table C.3. Fixed-bed adsorption column sizing table for BPG-functionalized resins. Assumes 0.4 m/hour superficial velocity and Langmuir adsorption parameters for the resin ($q_{Max} = 3 \text{ mg/g}$; $K_L = 4.657 \text{ L/g}$).

Online Time ^a (days)	Flow Rate (m ³ /day)	C _i (mg/L)	q _i (mg/g)	Adsorbent Mass (kg)	Column Diameter ^b (m)	Minimum Column Length (m)	REE Adsorbed (g)
1	1	0.1	0.96	0.1	0.36	0.00	0.1
		1	2.48	0.4	0.36	0.01	1.0
		10	2.95	3.4	0.36	0.09	10.0
	10	0.1	0.96	1.0	1.15	0.00	1.0
		1	2.48	4.0	1.15	0.01	10.0
		10	2.95	33.9	1.15	0.09	100.0
	100	0.1	0.96	10.5	3.64	0.00	10.0
		1	2.48	40.4	3.64	0.01	100.0
		10	2.95	339.4	3.64	0.09	1,000.0
1,000	0.1	0.96	104.5	11.52	0.00	100.0	
	1	2.48	403.5	11.52	0.01	1,000.0	
	10	2.95	3,393.6	11.52	0.09	10,000.0	
7	1	0.1	0.96	0.7	0.36	0.02	0.7
		1	2.48	2.8	0.36	0.07	7.0
		10	2.95	23.8	0.36	0.62	70.0
	10	0.1	0.96	7.3	1.15	0.02	7.0
		1	2.48	28.2	1.15	0.07	70.0
		10	2.95	237.6	1.15	0.62	700.0
	100	0.1	0.96	73.2	3.64	0.02	70.0
		1	2.48	282.5	3.64	0.07	700.0
		10	2.95	2,375.5	3.64	0.62	7,000.0
1,000	0.1	0.96	731.8	11.52	0.02	700.0	
	1	2.48	2,824.8	11.52	0.07	7,000.0	
	10	2.95	23,755.1	11.52	0.62	70,000.0	
30	1	0.1	0.96	3.1	0.36	0.08	3.0
		1	2.48	12.1	0.36	0.31	30.0
		10	2.95	101.8	0.36	2.64	300.0
	10	0.1	0.96	31.4	1.15	0.08	30.0
		1	2.48	121.1	1.15	0.31	300.0
		10	2.95	1,018.1	1.15	2.64	3,000.0
	100	0.1	0.96	313.6	3.64	0.08	300.0
		1	2.48	1,210.6	3.64	0.31	3,000.0
		10	2.95	10,180.7	3.64	2.64	30,000.0
1,000	0.1	0.96	3,136.4	11.52	0.08	3,000.0	
	1	2.48	12,106.5	11.52	0.31	30,000.0	
	10	2.95	101,807.5	11.52	2.64	300,000.0	

^a Time of operation before replacing or regenerating the column.

^b Diameter of a single column with the required surface area to meet superficial velocity requirements. Actual column configuration may require multiple small columns operating in-parallel, rather than a single large column.